STUDIES ON A METAL UPTAKE PROTEIN FROM *CANDIDATUS* LIBERIBACTER ASIATICUS

Ph.D. THESIS

by

NIDHI SHARMA

DEPARTMENT OF BIOTECHNOLOGY
INDIAN INSTITUTE OF TECHNOLOGY ROORKEE
ROORKEE - 247 667 (INDIA)
MAY, 2015

STUDIES ON A METAL UPTAKE PROTEIN FROM *CANDIDATUS* LIBERIBACTER ASIATICUS

A THESIS

Submitted in partial fulfilment of the requirements for the award of the degree of

DOCTOR OF PHILOSOPHY

in

BIOTECHNOLOGY

by

NIDHI SHARMA

DEPARTMENT OF BIOTECHNOLOGY
INDIAN INSTITUTE OF TECHNOLOGY ROORKEE
ROORKEE - 247 667 (INDIA)
MAY, 2015

INDIAN INSTITUTE OF TECHNOLOGY ROORKEE
ROORKEE

CANDIDATE'S DECLARATION

I hereby certify that the work which is being presented in the thesis entitled, **"STUDIES ON A METAL UPTAKE PROTEIN FROM *CANDIDATUS* LIBERIBACTER ASIATICUS"** in partial fulfilment of the requirements for the award of the degree of Doctor of Philosophy and submitted in the Department of Biotechnology of the Indian Institute of Technology Roorkee, Roorkee is an authentic record of my own work carried out during the period from December, 2009 to May, 2015 under the supervision of Dr. Ashwani Kumar Sharma, Associate professor, Department of Biotechnology, Indian Institute of Technology Roorkee, Roorkee.

The matter presented in this thesis has not been submitted by me for the award of any other degree to this or any other institute.

(NIDHI SHARMA)

This is to certify that the above statement made by the candidate is correct to the best of my knowledge.

Dated: **(Ashwani Kumar Sharma)**
(Supervisor)

The PhD Viva-Voce Examination of **Ms. Nidhi Sharma**, Research Scholar has been held on…….

Chairman SRC **External Examiner**

This is to certify that the student has made all the corrections in the thesis.

Supervisor **Head of the Department**

ABSTRACT

Metal ion uptake and sequestration is critical for bacterial survival and growth in the environment as well as within various hosts. Transition metals such as manganese, zinc, and iron play an important role as enzyme co-factors for a number of biological processes including DNA replication, protein synthesis, respiration, cell wall synthesis and neutralization of reactive oxygen species. Metal deficiencies greatly inhibit the growth of microorganisms. Therefore, inhibition of metal uptake can serve as a possible strategy towards developing antibacterial agents against the pathogenic bacteria.

Citrus Huanglongbing (HLB) is an extremely destructive, fast-spreading disease of citrus which causes severe economic losses worldwide. The disease is caused by phloem-limited, unculturable, Gram-negative α-proteobacteria *Candidatus* Liberibacter spp. Three species known are '*Candidtaus* Liberibacter asiaticus' (CLas), '*Ca*. L. africanus', and '*Ca*. L. americanus'. CLas is considered to be the most devastating species and is transmitted by Asian citrus psyllid, *Diaphorina citri*. Almost all citrus plants are susceptible to HLB and to date, there is no established cure for this century-old and yet, newly emerging disease. HLB is mainly identifies by blotchy mottling with green patches on leaves. Infected shoots are undersized, and the branches slowly die due to disease progress. Fruit from infected trees may be small and irregular, with deprived coloration. HLB seriously effects the citrus industry by reducing the lifespan of the trees and diminishing fruit yield as well fruit quality. The symptoms of HLB have been associated with those of zinc deficiency and it has been reported that CLas infection significantly reduces levels of zinc and several other mineral nutrients.

Proteins are large biological molecules which perform various functions within living organisms including metabolic reactions catalysis, DNA replication, cell signaling, and transport of molecules from one location to another. In course of time, proteins evolve to perform specific functions by changing their primary sequence and hence tertiary structure. Proteins have been classified into various superfamilies on the basis of common ancestry which are further divided into families consisting of evolutionary related protein and subfamilies based on three dimensional structures. ATP binding cassette (ABC) family is one of the largest family, present in all forms of life from prokaryotes to humans, includes several hundred different membrane transport proteins. These proteins transport a variety of substrates

including ions, sugars, amino acids, phospholipids, cholesterol, peptides, polysaccharides, proteins and other ligands. The metal ions like Zn^{2+}, Mn^{2+} and Fe^{2+} are also transported across membranes through ABC transport systems. The bacterial ABC-type transport systems comprise of three components that are: a solute-binding protein (SBP) found in the periplasm in Gram-negative bacteria or linked to the cytoplasmic membrane in Gram-positive bacteria, trans-membrane permease and nucleotide-binding protein (ATPase). The solute binding proteins which are involved in uptake of divalent metal ions zinc, manganese and iron belongs to the Cluster A-I family of substrate binding proteins.

The Znu system, a member of ABC transporter family, is critical for survival and pathogenesis of CLas. Two homologues of this system have been identified in CLas. It has been reported that only first ZnuABC gene cluster is functional and able to complement Δznu *Escherichia coli* and Δznu *Sinorhizobium meliloti* strains. In the present work, a periplasmic solute binding protein from second of the two gene clusters of Znu system (CLas-ZnuA2) have been characterized by bioinformatics analysis and other biophysical techniques which include X-ray crystallography, surface plasmon resonance (SPR) and circular dichriosm (CD).

The thesis has been divided into four chapters. **Chapter 1** reviews the literature describing about bacterial ABC permeases and their mechanisms of substrate translocation, the structure and mechanism of metal binding and release of Cluster A-I proteins and their role in virulence of pathogenic bacteria. The chapter also describes about history of HLB disease, host range, evolutionary relationships between CLas and other related bacteria, detection and genome analysis of CLas and its virulence mechanism and hitherto controls strategies.

Chapter 2 describes the materials used and methods adopted for the present work. The CLas-ZnuA2 gene has been cloned in pET 28c expression vector. The recombinant protein has been produced in *E. coli* and purified to homogeneity by affinity and size exclusion chromatography methods. The multiple sequence alignment and phylogenetic analysis of CLas-ZnuA2 and other related proteins has been done. The CD experiments of the protein in metal-free state as well as in presence of different concentration of metal ions have been carried out at different temperatures and the effect of different metals on the thermal stability of protein has been elucidated. The SPR experiments have been performed to elucidate the binding affinity of the protein towards different metal ions. The crystallization of the purified protein was

performed and the crystal structure was determined in metal-free, intermediate and Mn^{2+} and Zn^{2+} bound states.

Chapter 3 describes the results obtained in the present work. The sequence similarity search showed that CLas-ZnuA2 shares significant sequence similarity with Cluster A-I proteins which are involved in uptake of divalent metal ions (Mn/Fe/Zn) in PDB database. The phylogenetic analysis of proteins present in PDB database showed that CLas-ZnuA2 clusters with Mn-specific proteins. Multiple sequence alignment revealed presence of conserved metal binding residues His39, His106, Glu172 and Asp247 specific for Mn/Fe binding. The CD studies showed that metal bound states of CLas-ZnuA2 are more thermally stable than metal-free state. The SPR studies showed that CLas-ZnuA2 have almost equal order of affinity for Mn^{2+} and Zn^{2+}. The three dimensional structure of CLas-ZnuA2 in metal-free state, intermediate state and metal bound states showed the presence of similar fold like other related Cluster A-I proteins containing two α/β domains connected by a rigid linker helix. One unique feature is presence of curved linker helix in all states of CLas-ZnuA2 due to the presence of a proline residue within linker helix. This Pro was found to be absent in other reported related structures, however closely related proteins in non-reduntant database possess the Pro in linker helix. The major difference observed in metal-free and metal-bound states was the position of loop hosting His39 which was moved outside and side chain of His39 was flipped away in metal-free state while in metal-bound states this loop was moved inside and His39 side chain was flipped towards the metal ion. In intermediate state, this loop and thus His39 occupies similar position like metal-free state having occupancy of 0.8 and metal ion was present with half occupancy. Also metal ion was not in ideal coordination distances from other three metal binding residues. The Mn^{2+} and Zn^{2+} bound structures are almost similar with some variations in the intra-molecular interactions. Both Mn^{2+} and Zn^{2+} coordinate pentavalently with square pyramidal geometry rather than ideal octahedral and tetrahedral geometry respectively. The coordination chemistry observed is different from tetrahedral geometry for Mn^{2+} and Zn^{2+} ions observed in other Mn-specific SBPs.

Chapter 4 includes the discussion. The comparison of CLas-ZnuA2 structure in three states showed that metal binding and release is facilitated by a large displacement along with a change in orientation of the side chain for one of the metal binding residue (His39) flipped away from metal binding site in metal-free form. The sequence and structure of CLas-ZnuA2

has been compared with metal-free and metal-bound states of related proteins and unique mechanism of metal binding and release has been proposed which is different from other related Mn-specific metal binding proteins. The crystal structure captured in intermediate state of metal binding revealed the changes in conformation and interaction of the loop hosting His39 during the metal binding. A rigid body movement of C-domain along with partial unfolding of linker helix at its C-terminal during metal binding, as reported for PsaA, a Mn-binding protein from *Streptococcus pneumonia*, was not observed in CLas-ZnuA2. The present results suggested that despite showing maximum sequence identity to the Mn/Fe-specific SBPs, the mechanistic resemblance of CLas-ZnuA2 seems to be closer to Zn-specific SBPs of Cluster A-I family. In conclusion, CLas-ZnuA2 protein shows unique features and has been diverged from related Cluster A-I proteins to adopt different mechanism of metal binding achieved by single amino acid change possessing Pro in linker helix due to which it might be involved in transport of both Mn^{2+} and Zn^{2+} ions depending upon the requirement of bacteria.

LIST OF PUBLICATIONS

1. **Nidhi Sharma,** Purushotham Selvakumar, Sumit Bhose, Dilip Kumar Ghosh, Pravindra Kumar, Ashwani Kumar Sharma. Crystal Structure of a periplasmic solute binding protein in metal-free, intermediate and metal-bound states from *Candidatus* Liberibacter asiaticus. (2015) *J Struct Biol* 189:184-194
2. Purushotham Selvakumar, **Nidhi Sharma**, Prabhat Pratap Singh Tomar, Pravindra Kumar, Ashwani Kumar Sharma. Structural insights into the aggregation behavior of *Murraya koenigii* miraculin-like protein below pH 7.5. (2014) *Proteins* 82:830-840.
3. Purushotham Selvakumar, Deepankar Gahloth, Prabhat Pratap Singh Tomar, **Nidhi Sharma**, Ashwani Kumar Sharma. Molecular evolution of Miraculin-like proteins in soybean Kunitz super-family. (2012) *J Mol Evol* 73:369-379.
4. **Nidhi Sharma**, Purushotham Selvakumar, Ashwani Kumar Sharma. A Proline kink in linker helix and imperfect metal coordination geometry in CLas-ZnuA2 rescues bacteria from possible zinc toxicity. (Manuscript under preparation)

WORKSHOPS/CONFERENCE ATTENDED AND POSTER/ORAL PRESENTATION

1. Attended **Indo-US conference** on "**Recent advances in Structural Biology and Drug Discovery**" held in Department of Biotechnology, IIT Roorkee, India from October 9-11, 2014 and presented poster entitled "Crystal Structure Of a Periplasmic Solute Binding Protein at 1.63 Å Resolution from *Candidatus* Liberibacter asiaticus".
2. Attended "**7th Asian Biophysics Association Symposium and Annual Meeting of the Indian Biophysical Society"** held in All Indian Institute of Medical Sciences, New Delhi, India from January 30-2 February, 2011 and presented poster entitled 'Bioinformatics analysis of two distinct Miraculin-like proteins from *Citrus reticulata'*.
3. Attended "**42nd National Seminar on Crystallography"** held in Jawaharlal Nehru University, New Delhi, India from November 21-23, 2013 and presented work entitled 'Characterization and preliminary X-ray diffraction studies of a metal binding protein from *Candidatus* Liberibacter asiaticus'.

ACKNOWLEDGEMENT

Throughout my graduate studies I have looked forward to writing the acknowledgement section of thesis to mark an end of a process. Now that the time has come, I feel overwhelmed with gratitude to realize the number of faculty, friends, family, philosophers and guides who have supported my decisions, encouraged my ideas, given me strength, and shared many experiences through the process. Because this thesis owes its gratitude to many, I now also find it the most challenging section to write! With mixed feelings of nostalgia, happiness, gratitude and a certain sense of sadness at the journey's end, I offer my acknowledgements:

At this moment of accomplishment, first of all I am indebted to express my heartfelt thanks to my venerable supervisor Dr. Ashwani Kumar Sharma for his expert guidance, outstanding advice, encouraging attitude and critical comments that made difficult task simple. His encouragement, supervision and support from the preliminary to the concluding level enabled me to develop and understand the subject. This work would not have been possible without his constant guidance and rock solid support at every step from almost past five and half years. He is a mentor who not only supported academically but also emotionally through the rough road to finish this thesis and gave me moral support that I needed during the difficult time. I have learnt a lot from his wisdom and experience, both professionally and personally. I thank him for his patience, kind nature, for many fruitful discussions and also for rectifying my mistakes.

I would like to express my sincere thanks towards Dr. Pravindra Kumar for providing Macromolecular Crystallographic Unit facilities. I am courteous to him for his unwavering help and support during structure solution. I am indebted to him for his valuable advice, constant encouragement and precious time without which this work was a very difficult task.

I feel overwhelmed in thanking to Prof. Partha Roy (present), Prof. R. Prasad and Prof. Ritu Barthwal (Former) Head, Department of Biotechnology for providing necessary facilities, support and cooperation in the Department. I would also like to acknowledge Dr. Ramesh Chandra Head, Institute Instrumentation Center for providing IIC facilities. I would also like to express my sincere thanks to the members of my research committee Dr. R.P. Singh (SRC chairman) Department of Biotechnology, Dr. R. Prasad (internal expert) Department of Biotechnology and Dr. R. K. Peddinti (external expert) Department of chemistry for their intellectual suggestions, prudent admonitions and immense concern throughout my research period. I am courteous to Prof. G. S. Randhawa, Chairman DRC, Department of Biotechnology for his support and encouragement.

Here I take this opportunity to convey my sincere regards, gratitude and special thanks to all faculty members of Department of Biotechnology, IIT Roorkee, for their constant encouragement and support during my research work. I am so indebted to them for providing me necessary help time to time in the form of valuable advice or assistance in handling the instruments.

I would also like to extend my gratitude towards Dr. Shailly Tomar for her precious suggestions especially for SPR experiments. I feel really blessed to have an opportunity to learn from her. I would like to express my sincere gratitude and special thanks to Dr. Dilip Ghosh for kind help towards my research work by proving genomic DNA, without which this work would not have been possible. I would like to express my sincere thanks towards Dr S. Karthikeyan for his generous help in data collection at X-ray facility, IMTECH, Chandigarh. I gratefully acknowledge the help provided by Ms. Ritika, Mr. Sumit, Mr. Ashish and Ms. Manali for their help and support during this work.

I am obliged to my labmates Dr. Girijesh Patel, Dr. Selva kumar, Mr. Prabhat Tomar, Mr. Bibekananda kar, Ms. Anamika Singh, Ms. Preeti Verma, Ms. Gunjan Saini, Mr. Pranav Kumar and Mr. Vishvajeet Shandilya for their honest efforts, friendly attitude and assistance while working in lab. Very special thanks are due to my labmates as well as my friends Ms. Gunjan and Ms. Preeti for wonderful assistance, motivation and support whenever and wherever required and for providing pleasurable laboratory atmosphere and nice time during this research work. I would like to acknowledge my sincere thanks to Dr. Selva Kumar for his wise input at each step of this work. I thank him for raising critical questions and lending me a receptive ear. I am forever grateful for his unwavering support and belief in my abilities.

I would like to thank my loving friends, Dr. Sonali Dhinwal, Dr. Rajbala Yadav and Ms. Anamika Singh who have always been there for me and without whom I could not imagine surviving this journey. Through all my good and bad times during my thesis, these people were with me all the time and helped me in every way. I consider myself truly fortunate to consider as close friends, Ms. Aarti Sharma, Ms. Kumkum Bharti and Ms. Reenu, Padam, in whose wisdom I have found my source of comfort and strength. They have always been there for me at each unexpected turn, and when I have needed someone to lean on. Thank you all for always being there for me and helping me to accomplish this massive task comfortably. I am thanking all for the good time, days filled with pleasure, cherished memories and the feelings that I will always treasure.

I would like to thank Dr. Preeti. Dr. Satya Tapas, Dr. Shivendra Singh, Dr. Pramod, Mr. Pradeep, Dr. Megha Aggarwal, Ms. Manju Narwal, Mr. Harvijay Singh, Mr. Vijay Sharma, Ms. Anchal Sharma, Ms. Neha Singh, Mrs. Monu Batra, Ms. Pooja Kesari, Ms. Ramanjeet Kaur, Ms. Benazir Fatma and Ms. Anjali Malik, for their sincere cooperation and efforts. They contributed well for the accomplishment of the studies included in the thesis. My special thanks to Dr. Aditya Dev, Mr. Rajesh Sharma, Mr. Rajat Mudgal and Mr. Madhusudan for providing a hand of help and assistance in various instrumentation operations.

I must acknowledge as well the many other friends and colleagues specifically Dr. Swati Srivastava, Dr. Shilpi aggarwal, Dr. Saroj, Dr. Megha, Ms. Shweta Tripathi, Dr. Shilpi Kumari, Dr. Swati Verma, Dr. Rajni, Ms. Varinder, Ms. Priyanka, Mr. Rajat, Dr. Meenu, Dr. Nidhi, Ms. Ankita, Ms. Supriya, Ms.

Sandhya, Mr. Ashish, Mr. Hrishikesh, Mr. Virendra and Mr. Sujeet for their love and support throughout this journey. They made my Roorkee stay full with fun, colorful and unforgettable.

I am also grateful to the Institute Sports Club as well as the Institute Hospital. Both helped me in maintaining physical fitness so that I could accomplish my studies contained in this thesis. I also appreciate the help from The Department Library. In recognition of all the help and support, I would like to mention all the technical and office staff of the Biotechnology Department in particular Mr. Ved Pal Singh Saini, Mr. Subhash Jain, Mr. Yogeendra Walthare, Mrs. Shashi Prabha, Mr. Lokesh, Mrs. Surita, Mr Anuj, Mr. Rajesh, Mr. Anil, Mr. Padam and Mr. Pradeep.

My deepest sense of gratitude goes to my parents for their unconditional love, support and immeasurable strength. My parents have always been there when I needed them, especially my mother. I would not have finished this dissertation without her support and encouragement. This is as much her labor of love as it is mine. I feel at a loss to find words to thank her for all she has done. I would have never been able to begin my journey from home, and come this far without the support and love of my brother Mr. Aditya Sharma. He encouraged me to pursue my research work and inspired me to achieve the targets. He always stands firmly behind me and provide resources to carry out my studies. He was the core inspiration to reach at great height and comfort when I occasionally falter. Without him this thesis would have been a distant dream. My deep appreciation goes to my admirable and esteemed sister-in-law Mrs. Bhavna Sharma who always encouraged me to move forward and meet the challenges held high in everything I try. I thank her for her love, affection and sincere prayers. Thank you all for everything so far. I would like to delightfully mention the company of the little ones of my family; apple of my eyes, my nephews Kushagra and Kushal for giving me immense pleasure even in the distressed hours of my research period. I would like to express my heartfelt gratitude to my family. None of this would have been possible without the love and the patience of my family. They have cherished with me every great moment and supported me whenever I needed it.

I would like to thank everybody who directly or indirectly helped me in the successful completion of this thesis, as well as expressing my apology that I could not mention personally every one.

Beyond all these, I thank almighty God for blessing me and keeping me strong and calm during all good and hard times throughout my life.

Finally, I would like to thank Council of Scientific & Industrial Research (CSIR), New Delhi, India for financial assistance as JRF and SRF.

(Nidhi Sharma)

CONTENTS

Page No.

CHAPTER 2

MATERIALS AND METHODS

CHAPTER 4

DISCUSSION

LIST OF FIGURES

LIST OF TABLES

LIST OF ABBREVIATIONS USED

˚C	Degree Centigrade
Å	Angstrom
ABC	ATP-binding cassette
B-factor	Debye-Waller factor/Temperature factor
bp	Base pair
CD	Circular dichroism
CLas	*Candidatus* Liberibacter asiaticus
Da	Daltons
DNA	Deoxyribose nucleic acid
dNTPs	Deoxy nucleotide tri phosphates
E. coli	Escherichia coli
EDTA	Ethylenediaminetetracetic acid
e.g.	For example
et al.	et alia
Fe	iron
g	Gram
h	Hours
H-bond	Hydrogen bond
HEPES	2-[4-(2-hydroxyethyl) piperazin-1-yl] ethanesulfonic acid
HLB	Huanlongbing
IITR	Indian Institute of Technology Roorkee
IPTG	Isopropyl β-D-thiogalactoside
K	Kelvin
kDa	Kilo Daltons
LB	Luria Bertani
M	Molar
mg	milligram
min	Minute
ml	millilitre
mM	millimolar

Mn	Manganese
$MnCl_2$	manganese chloride
NaCl	Sodium Chloride
NCBI	National Center for Biotechnology Information
Nde	Neisseria denitrificans
Ni-NTA	Nickel-nitrilotriacetic acid
nm	Nanometer
NMR	Nuclear magnetic resonance
NRCC	National Research Centre for Citrus
PCR	Polymerase chain reaction
PDB	Protein Data Bank
Pvt Ltd	Private Limited
rDNA	ribosomal deoxyribose nucleic acid
R-factor	Residual-factor
RNA	Ribose nucleic acid
rpm	Revolutions per minute
RU	response unit
s	Seconds
SBP	Solute binding protein
SDS-PAGE	Sodium dodecyl sulfate polyacrylamide gel electrophoresis
SPR	surface plasmon resonance
TEV	tobacco etch virus
USA	United States of America
UV	ultra-violet
Xho	Xanthomonas holcicola
Zn	Zinc
$ZnCl_2$	zinc chloride
α	Alpha
β	Beta
γ	Gamma
µg	Microgram
µl	Microlitre

Introduction

Proteins are basic biological macromolecules that have important functional role in all living cells. They also make the major structural ingredient of living organisms. The functional versatility of proteins is due to their structural diversity. Interaction of proteins with other biomolecules depends on their three dimensional structure and nature of amino acid side chains. Proteins can be found as single molecule or made up of several units which perform different functions. Structure of protein also depends on different physiological conditions like temperature, pH, salt concentration that ultimately affects the function of protein. Cofactors also play roles on the quaternary structures and dynamics among the different oligomeric states. Proteins form different inter and intra molecular bond like electrostatic, hydrophobic, van der Waals forces and hydrogen bonding. These bonds play important role in protein structure and activity, when the mutations occurs the position of the interaction changes and lead to structural and functional changes in proteins. Some proteins require metal ions for stability of their structure as well as function, these ions can be within the protein or taken from their physiological environment. Proteins play important roles in various processes like defense (e.g. antibodies), transport of other molecules (e.g. hemoglobin), reaction catalysis (enzymes), regulatory role (hormones), structural role (e.g. collagen and elastin) and gene regulation by maintaining chromosome structure. Apart from proteins, other factors also contribute in innate host defenses such as reactive nitrogen species [22]. In microorganisms, various proteins are involved for adaption to changes in environments by signal transduction [170, 171, 246]. Over a long period of time, proteins evolve in terms of sequence through mutation and selection and therefore in structure to perform different biological functions [197].

Metal ion uptake and sequestration is critical for bacterial survival and growth in the environment as well as within various hosts. Transition metals such as manganese, zinc, and iron play an important role as enzyme co-factors for a number of biological processes. Manganese is a metal cofactor involved in a wide range of enzymatic processes including phosphorylation, hydrolysis, carbon metabolism, decarboxylation and oxidative stress response. Zinc has critical structural and/or catalytic roles in all major classes of enzymes and in transcription and replication factors. Iron is essential for the growth of organisms because of the requirement for iron as a cofactor in many important proteins that mediate processes as diverse as oxygen and electron transport, energy production and DNA synthesis. Therefore, for

pathogenic organisms, these metal ions are important determinants of survival and virulence. In bacteria, metal ions are transported by various transporters across the cell membranes. One of the transport systems facilitating metal ion transport across membrane is ATP-binding cassette-type (ABC-type) transport system. The ABC-type transport systems comprise of three components; a solute-binding protein (SBP) found in the periplasm in Gram-negative bacteria or linked to the cytoplasmic membrane in Gram-positive bacteria, a trans-membrane permease and a nucleotide-binding protein (ATPase). The SBPs which transport divalent metal ions belong to the Cluster A-I family which includes zinc, manganese and iron transporters.

Citrus Huanglongbing (HLB) is an extremely destructive, fast-spreading disease of citrus which causes severe economic losses worldwide. The disease is caused by phloem-limited, unculturable, Gram-negative bacteria *Candidatus* Liberibacter spp. Three species of 'Ca. Liberibacter' known are '*Ca*. L. asiaticus', '*Ca*. L. africanus', and '*Ca*. L. americanus'. *Ca*. L. asiaticus (CLas) is considered to be the most devastating species and is transmitted by Asian citrus psyllid, *Diaphorina citri*. CLas encodes two ZnuABC homologous systems, out of which only one system is functional and able to complement Δznu *Escherichia coli* and Δznu *Sinorhizobium meliloti* strains. Therefore second homologous ZnuABC cluster might be involved in transport Mn^{2+} or Fe^{2+} ions. Earlier in our lab a miraculin like protein from *Murraya koenigii* (MKMLP), a member of rutaceae family, has been characterized [65, 195, 196, 201, 202]. Recently, remarkable up-regulation of MLPs was observed at different stages of HLB disease development [57].

In present work, we have cloned, expressed and purified a periplasmic solute binding protein from second of the two homologous gene clusters of Znu system (CLas-ZnuA2) in CLas. The bioinformatics analysis has been performed using various tools. The biochemical and biophysical characterization of CLas-ZnuA2 have been done by various techniques including circular dichroism and surface plasmon resonance in order to determine binding affinities and stability of CLas-ZnuA2 upon binding of different metal ions. We have also determined high resolution crystal structures in metal-free, intermediate and metal-bound states (Mn^{2+} and Zn^{2+}). The comparison of CLas-ZnuA2 structures with related metal-free open and metal-bound closed forms of structures showed a unique mechanism for metal binding and release. This is the first report of a crystal structure of cluster A-I SBP from a plant pathogen[198].

1.1. ABC Transporters

1.1.1. Introduction

ATP-binding cassette (ABC) transporters are well-known among living organisms from prokaryotes to human representing one of the largest protein families [102, 151]. These transporters are observed in all species and are related evolutionarily. Nevertheless, they are functionally different performing roles in a variety of important cellular functions including translocation of various substrates across membranes such as metabolic products, lipids and sterols, and drugs [152, 180].

Bacterial ABC permeases (complex of ABC transporter and solute binding protein) facilitate the unidirectional transbilayer movement of extracytosolic cargoes into the cytoplasm against their concentration gradient by the coupling of ATP hydrolysis [90]. Typically ABC transporters consists of a conserved four-domain architecture with two nucleotide-binding domains (NBDs) located in the cytoplasm which are connected to the translocation pore formed by the two trans-membrane domains (TMDs) [39]. NBD binds and hydrolyzes ATP to supply energy for the import and export of a broad range of substrates [241]. The NBD contains two highly conserved motifs, the Walker A and Walker B motifs which organize together for ATP binding. NBD also contain the consensus signature sequence motif LSGGQ/R/KQR highly conserved and specific to the ABC superfamily. This sequence is situated N-terminal with respect to the Walker B motif and is also called the linker peptide or C motif. Conversely, TMDs exhibit low sequence identities and are structurally diverse. TMDs can be classified into type I or II, based on the number of transmembrane helices (usually 5 or 10 per TMD, respectively) [137]. Type I TMDs are commonly involved in the transport of ions, carbohydrates and other moderately small cargoes, while type II TMDs are responsible for transport of relatively larger cargoes like metal chelates, haem and vitamin B12 [44, 77].

Bacterial importers characteristically include periplasmic solute-binding proteins (SBPs) that bind to incoming substrates and deliver them to the TMD in the inner membrane of gram-negative bacteria. Import across the outer membrane may be facilitated by outer membrane proteins (OMPs) such as porins. The importers of gram-positive bacteria, which lack periplasm or outer membrane, contain proteins corresponding to the substrate-binding proteins

anchored to the exterior of the cell via lipid groups. SBPs are believed to be responsible for affinity and specificity of the importers along with directionality as they are absent in exporters.

1.1.2. Mechanism of substrate translocation by ABC transporters

Based on available structural and biochemical data from various systems, the suggested mechanism for substrate translocation across the membrane is as follows [165] (Figure 1.1). In the resting state, the substrate-binding site of permease is observed in an inward-facing orientation and the cytosolic NBDs are located apart from each other [175]. When a loaded SBP interacts with the inward-facing permease, the NBDs come together [92]. ATP binding to the NBDs induces a sequence of conformational changes in all components of the translocation machinery. ATP-bound NBDs form a catalytic site for ATP hydrolysis due to conformational changes which activate the permease to adopt an outward-facing conformation. This reorientation of the TMDs is associated with the opening of the SBP, which delivers the cargo to the permease [165]. Subsequent ATP hydrolysis leads to the permease to adopt its inward-facing conformation and the substrate is now available to diffuse to the cytoplasm [105, 141, 166] (Figure 1.1).

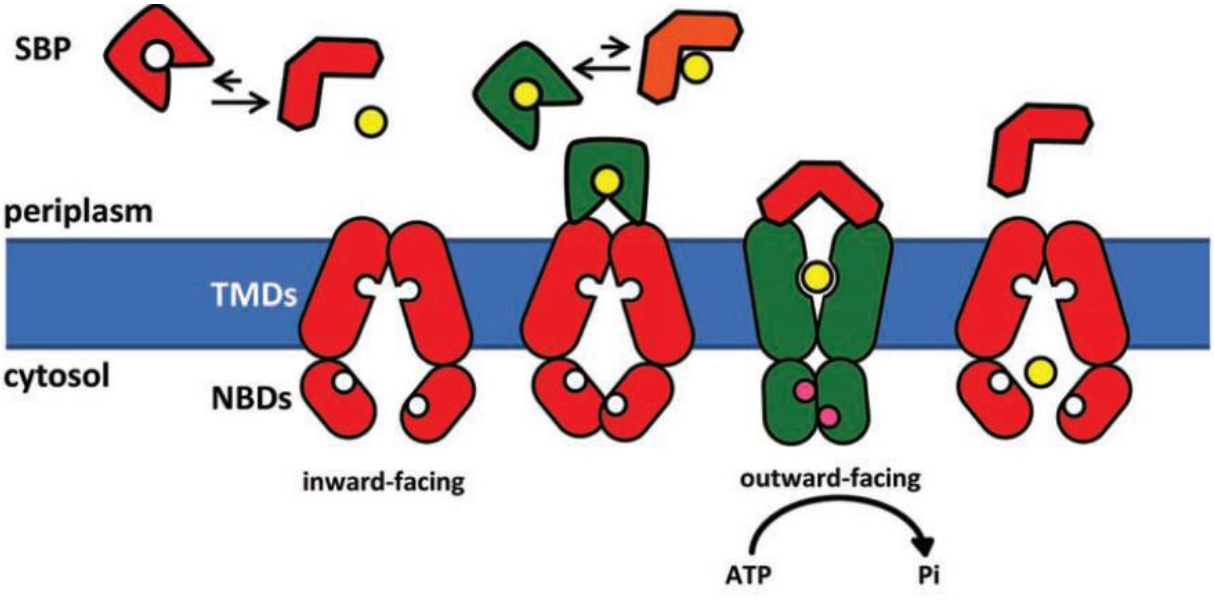

Figure 1.1: General mechanism for substrate transport by SBP-dependent ATP-binding cassette transporters across the membrane of Gram-negative bacteria.

Substrate (yellow circle) binding shifts the equilibrium of the SBP from the open (red) to the closed (green) conformation, which interacts with the resting, inward-facing TMD (red). Substrate-bound SBP interaction with the permease imparts the two NBDs to come close together. ATP binding (pink circle) to NBDs triggers conformational changes in each component of the solute translocation machinery, which opens the SBP and delivers the substrate into the outward-facing TMDs (green). Hydrolysis of ATP restores the system to its resting state and facilitates the transport of the substrate into the cytoplasm. [142]

SBPs are responsible for the molecular recognition and binding of extracellular cargoes and determine the specificity of their cognate ABC transporters thereby playing an important role in the translocation process [47]. The disruption of SBP-dependent ABC transport systems may facilitate a novel therapeutic strategy against pathogenic bacteria because of their integral role in cell signaling and pathogenesis.

1.1.3. Substrate-binding proteins and their role in virulence

1.1.3.1. Substrate-Binding Proteins

Prokaryotic SBPs facilitate the ABC-transporter-mediated translocation of various solutes ranging from small molecules such as metal ions to large complex molecules like vitamins and metal chelates [177]. Consequently, SBPs display high specificity for their cargo-substrates and exhibit low sequence identity (<20%) from functionally unrelated ABC permeases [17]. However, all SBPs show a conserved fold comprising of two α/β domains connected by a linker region (Figure 1.2). The substrate-binding site for SBPs is situated in the cleft between the two α/β domains [178]. Most SBPs have a flexible linker region that acts like a hinge which allows the protein to function in a "Venus flytrap" manner [144] (Figure 1.2). On the basis of the available structural data for SBPs the behavior of these proteins in solution could be explained. In the absence of substrate, the two α/β domains may be freely moved as rigid bodies around the hinge region in an open unliganded conformation. The availability of substrate changes the conformation to the closed-liganded state facilitating the substrate trapping between the two α/β domains [177, 211]. Structural data for SBPs in ligand-bound and ligand-free forms suggest that the extent of movement of the two α/β domains alters noticeably among SBPs from different clusters. For example, in LivJ, an amino acid-binding protein, the

α/β domains rotate ~60° upon substrate binding [216] in contrast to the slight or no movement of the α/β domains of Cluster A-I proteins upon binding to metal ions [124, 240] (Figure 1.2). In the absence of substrate, SBPs switch between open-unliganded and closed-unliganded apo conformations, with the former being the predominant state [211].

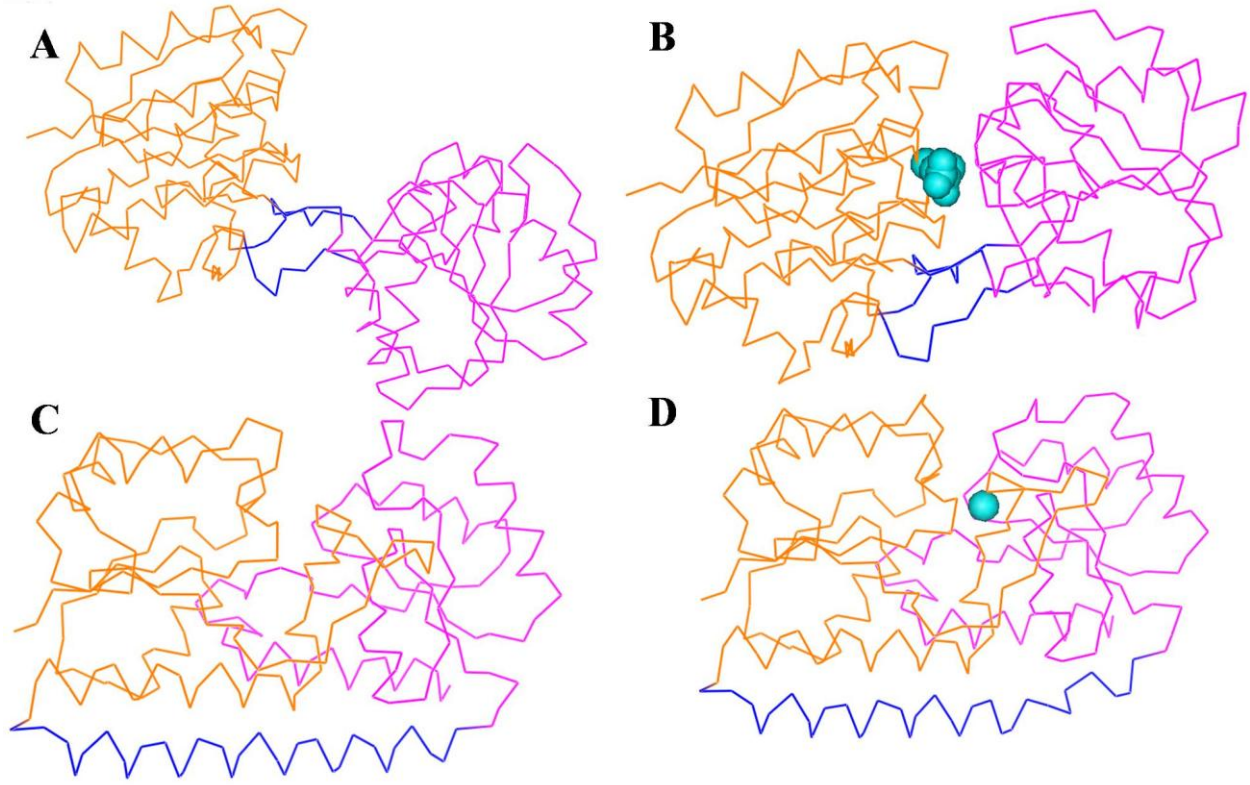

Figure 1.2: Open and closed conformations of prokaryotic SBPs. A) and **B)** represents the open and closed conformation of LivJ respectively. The binding of substrate (spheres) promotes the rotation of around 60° of the N-terminal (orange) and C-terminal (magenta) domains around a flexible linking region (blue). **C)** and **D)** represents the open and closed conformation of PsaA respectively where very less domain movement of around 13° is observed upon metal binding.

SBPs have been classified into 6 different Clusters (A-F) on the basis of their conserved scaffold [17] (Table 1.1). Cluster A-I involves the SBPs which are involved in transport of divalent metal ions.

Table 1.1: Classification of substrate binding proteins as given by Ronnie P.A. Berntsson *et al*.

Clusters		**Types of substrates**
A	I	Divalent metal ions
	II	Siderophores
B		Carbohydrates, Leu, Ile, Val, Autoinducer-2, Natriuretic peptide
C		Di- and oligopeptides, Arg, cellobiose, nickel
D	I	Carbohydrates
	II	Putrescine, thiamine
	III	Tetrahedral oxyanions
	IV	Iron ions
E		Sialic acid, 2-keto acids, ectoine, pyroglutamic acid
F	I	Trigonal planar anions
	II	Methionine
	III	Compatible solutes
	IV	Amino acids

1.1.3.2. Structures of Cluster A-I SBPs and metal specificity

Most Cluster A-I proteins preferentially bind to specific divalent metal ions with high affinities, but some Cluster A-I proteins bind to more than one metal with similar affinities [89, 124]. The first crystal structure of Cluster A-I SBP member was determined for PsaA from *Streptococcus pneumonia* [122] in Zn(II) bound form although physiologically this protein binds to Mn(II). Hitherto, Cluster A-I protein structures are available for receptors involved in the transport of transition metals Zn(II), Mn(II), and Fe(II) (Table 1.2). The differences in their 3d-orbital occupancies of these transition metals make them act rather differently from each other. Mn(II) and Fe(II) have partially filled 3d-orbital and prefer “hard” ligands, like oxygen atoms present in carboxylate groups in side chains of aspartate and glutamate. These metals prefer ligand coordination number of 6 with octahedral coordination geometry. In contrast, Zn(II) has complete 3d orbital and favors “soft” ligands such as the amide group of histidine residues. The preferred coordination number of Zn(II) for ligands is 4 with a tetrahedral coordination geometry [85, 172]. The specificity of metal ion in Cluster A-I proteins is considered to be a result of the particular coordination chemistry preferred by individual metal-binding sites. However, most Cluster A-I proteins bind to multiple divalent metal ions *in vitro*.

Table 1.2: List of available Cluster A-I SBP structures and observed metal-coordinating residues.

Protein	Metal	Metal-coordination site				PDB ID(s)	Organism(s)	Ref.
ZnuA	Zn(II)	Glu59	His60	His143	His207	2osv, 2ogw, 2ps0, 2prs	*Escherichia coli*	[31, 128, 240]
		Glu59	His140	His147	His211	2xy4, 2xqv	*Salmonella enterica*	[97]
		H_2O	His83	His179	His243	1pq4, 2ov3	*Synechocystis 6803*	[12, 234]
	Co(II)	Glu59	His60	His143	His207	2ps9	*E. coli*	[240]
	Apo					2ps3, 2xh8, 2ov1	*E. coli, S. enterica, Synechocystis 6803*	[97, 234, 240]
Lbp	Zn(II)	His66	His142	His206	Glu281	3gi1, 3hjt	*Streptococcus pyogenes, Streptococcus agalactiae*	[134, 135]
AdcAII	Zn(II)	His71	His147	His211	Glu286	3cx3	*Streptococcus pneumoniae*	[138]
TroA	Zn(II)	His68	His133	His199	Asp279	1toa, 3mfq	*Treponema pallidum, Streptococcus suis*	[124, 247]
	Apo					1k0f	*T. pallidum*	[125]
MntC	Mn(II)	His89	His154	Glu220	Asp295	1xvl, 3ujp	*Synechocystis 6803*	[2, 104, 185]
	Zn(II)	His50	His123	Glu189	Asp264	4k3v	*Staphylococcus aureus*	[76]
		His50	His123	Glu189	Asp264	4nno	*S. aureus*	[3]
	Apo	His50	His123	Glu189	Asp264	4nnp	*S.aureus*	[3]
PsaA	Mn(II)	His67	His139	Glu205	Asp280	3ztt	*S. pneumoniae*	[150]
	Zn(II)	His67	His139	Glu205	Asp280	1psz	*S. pneumoniae*	[122]
	Cd(II)	His67	His139	Glu205	Asp280	4utp	*S. pneumoniae*	[15]
	Apo	His67	His139	Glu205	Asp280	3zk7	*S. pneumoniae*	[38]
MtsA	Fe(II)	His67	His139	Glu205	Asp280	3hh8	*S. pyogenes*	[209]
SitA	Mn(II)	His64	His137	Glu203	Asp278	4oxr	*Staphylococcus pseudintermedius*	[1]
	Zn(II)	His64	His137	Glu203	Asp278	4oxqA	*S. pseudintermedius*	[1]
	Apo	His64	His137	Glu203	Asp278	4oxqB	*S. pseudintermedius*	[1]
Pden 1597	Zn(II)	His61	His138	His204	Asp279	4xrv	*Paracoccus denitrificans*	[84]

In Cluster A-I proteins, four positions are responsible for coordinating the metal ion. Usually, the similar types of ligands are present in three of these places: two Nε2 atoms from extremely conserved histidine residues and a carboxylate group from an aspartate or a glutamate residue. The fourth position is thought to play the central role in receptor-metal ion specificity. For Zn(II) specific SBPs, this position is occupied by the "soft" Nε2 atom of a histidine residue while a carboxylate group of a glutamate residue is present for Mn(II) and Fe(II) binding SBPs.

Recently, a discrepancy to this metal ion-binding mode has been observed in the ZnuA structure from *Salmonella enterica,* a Zn(II) binding SBP. In the Zn(II)-bound structure of *Salmonella enterica* ZnuA, one of the metal ligands is contributed by the Nε2 atom from a histidine residue present in the histidine-rich loop unique to ZnuA homologs [97]. In addition, *E. coli* ZnuA has a second Zn(II) atom bound to a histidine residue near to the histidine-rich loop, but absent in the primary metal-binding site [240]. These structures suggest the presence of a low affinity, secondary metal-binding site in ZnuA, which might play a role in translocation of Zn(II) in and out of the high-affinity primary metal-binding site [12, 240]. Although the physiological role of the histidine-rich loop in ZnuA-like SBPs is not yet clear, it has also been suggested to play a regulatory role in ZnuA-like proteins, functioning as a sensor for high Zn(II) concentrations [97].

1.1.3.3. Mechanism of metal binding and release

The available three-dimensional structures of cluster A-I SBPs, both in metal-free and metal-bound states, have revealed differences in the mechanism of metal binding and release. In Zn(II) binding SBPs, metal binding and release is mainly accomplished through local conformational changes without the involvement of any significant change in relative domain movements and the linker helix. In the case of *Trepanoma pallidum* TroA and *Synechocystis* ZnuA SBPs metal binding site remains identical in apo and bound state with only minor flipping of side chains was observed whereas in *E. coli* ZnuA the loop displacement is also observed. However, in Mn(II) binding SBPs *Staphylococcus aureus* Mntc and PsaA flipping of metal binding residues along with a rigid body movement of C-domain and partial unfolding of linker helix at its C-terminal is observed. Available data from solution studies such as secondary structure changes detected by circular dichroism (CD), perturbation of chemical

shifts by NMR along with calorimetry data support the idea that the structure of Cluster A-I SBPs experiences some rearrangements upon metal-binding [43, 150, 206, 238, 240, 247].

1.1.3.4. Role of Cluster A-I SBPs in virulence

Pathogenic bacteria secrete many virulence factors including proteins to invade host immune system contributing in the pathogenicity and also some toxins for disease development [21, 45, 52, 62, 66, 78, 82, 86, 103, 112, 158, 190, 204]. The transition row metal ions acquirement is crucial for bacterial colonization and virulence and Cluster A-I SBPs have an essential role in this process [127]. Mn(II) is a metal cofactor playing role in a broad range of enzymatic processes such as phosphorylation, hydrolysis, carbon metabolism, decarboxylation and oxidative stress response [169, 184]. ABC permeases which transport Mn(II) have been identified in almost all pathogenic bacteria. The Mn(II)-ABC permease of *S. pneumoniae*, consists of the Cluster A-I SBP PsaA and the ABC transporter PsaBC, is required for virulence, although not necessary for growth [147, 150]. The requirement of Mn(II) for proliferation and virulence has also been reported in other pathogenic bacteria such as *S. pyogenes, S. mutans*, *S. suis*, *Neisseria gonorrhoeae,* and *S. aureus* [93, 101, 131, 168, 193]. Iron has key role in a wide range of process including respiration, photosynthesis and nitrogen fixation. MtsABC has been shown to be important for manganese and iron transport, oxidative stress resistance and virulence of *S. pyogenes* [101]. Zn(II) play significant structural and/or catalytic roles in all classes of enzymes and has function in transcription and replication factors [6, 36]. Consequently, acquisition of Zn *in vivo* is important for determining virulence in numerous pathogenic bacteria. The Zn(II)-ABC permease of *S. pneumoniae* is vital for colonization of the host environment [14, 35]. ABC permease ZnuABC mediated Zn(II) acquisition is also involved in the virulence of *E. coli* O157:H7 [64], *E. coli* CFT073 [81, 186], *Listeria monocytogenes*, and *Salmonella enterica* [5, 26].

PsaA has been proposed to be a candidate protein target for antimicrobial development. Recently, novel pneumococcal PsaA inhibitors have been identified using fragment-based drug design approaches [11]. PsaA binds to Mn^{2+} reversibly and Zn^{2+} irreversibly, therefore extracellular Zn^{2+} inhibits the acquisition of the essential metal Mn^{2+} by competing for binding to PsaA irreversibly and exploited by the host defense mechanism to inhibit the bacterial growth [38, 150]. Recently, structure-based functional studies identified an antibody fragment

FabC1 which sterically blocks a structurally conserved surface of *Staphyloccus aureaus* MntC. This blockage prevents interaction of MntC with the MntB membrane importer thereby increasing *S. aureus* sensitivity to oxidative stress forming the basis for ABC importer inhibition by an engineered antibody fragment [3].

1.2. Citrus Huanglongbing

1.2.1. Introduction

India occupies sixth rank in the production of citrus fruit in the world whereas citrus industry is third largest fruit industry in India after mango and banana. So citrus occupies an important place in the horticultural wealth and economy of India. Other countries which are major producers of citrus fruit include Spain, USA, Israel, Morocco, South Africa, Japan, Brazil, Turkey and Cuba. Citrus fruits originated in the tropical and sub tropical regions of South East Asia, particularly India and China. The native place of many citrus species is the North East India. Citrus fruits are of particular interest because of its refreshing juice and high content of vitamin C. Of the various types of citrus fruits grown in India, orange (santra or mandarin), sweet orange (mosambi, malta or satgudi) and lime/lemon are of commercial importance. In India, citrus fruits are mainly produced in Maharashtra, Andhra Pradesh, Punjab, Karnataka, Uttaranchal, Bihar, Orissa, Assam and Gujarat.

Huanglongbing (HLB) is considered as one of the oldest diseases in citrus. It has been identified mainly in East Asia for over a century and has not been observed in Americas till recent times. It presents an exceptional challenge in newly infected citrus producing areas. It is a highly destructive disease of citrus, caused by endogenous, Gram-negative, unculturable, phloem sieve-tube restricted α-proteobacteria called Liberibacters, transmitted from one tree to another by grafting or by insect vectors called citrus psyllids. Practically all commercial citrus species and cultivars are sensitive, regardless of rootstocks. HLB is mainly identified by blotchy mottling with green pathches on leaves. Infected shoots are undersized, and the branches slowly die due to disease progress. Fruit from infected trees may be small and irregular, with deprived coloration (Figure 1.3). HLB seriously damages the citrus industry by reducing the lifespan of the trees and diminishing fruit yield as well fruit quality. HLB can hamper the citrus production productive capacity citrus trees, with losses of 30 to 100% [8].

For HLB, only control is the prevention of the trees from becoming infected. Therefore, HLB is presumably the most serious disease for citrus industry worldwide including India. It presents an unprecedented challenge in newly infected citrus production areas and represents a dangerous threat to the areas still free from the disease.

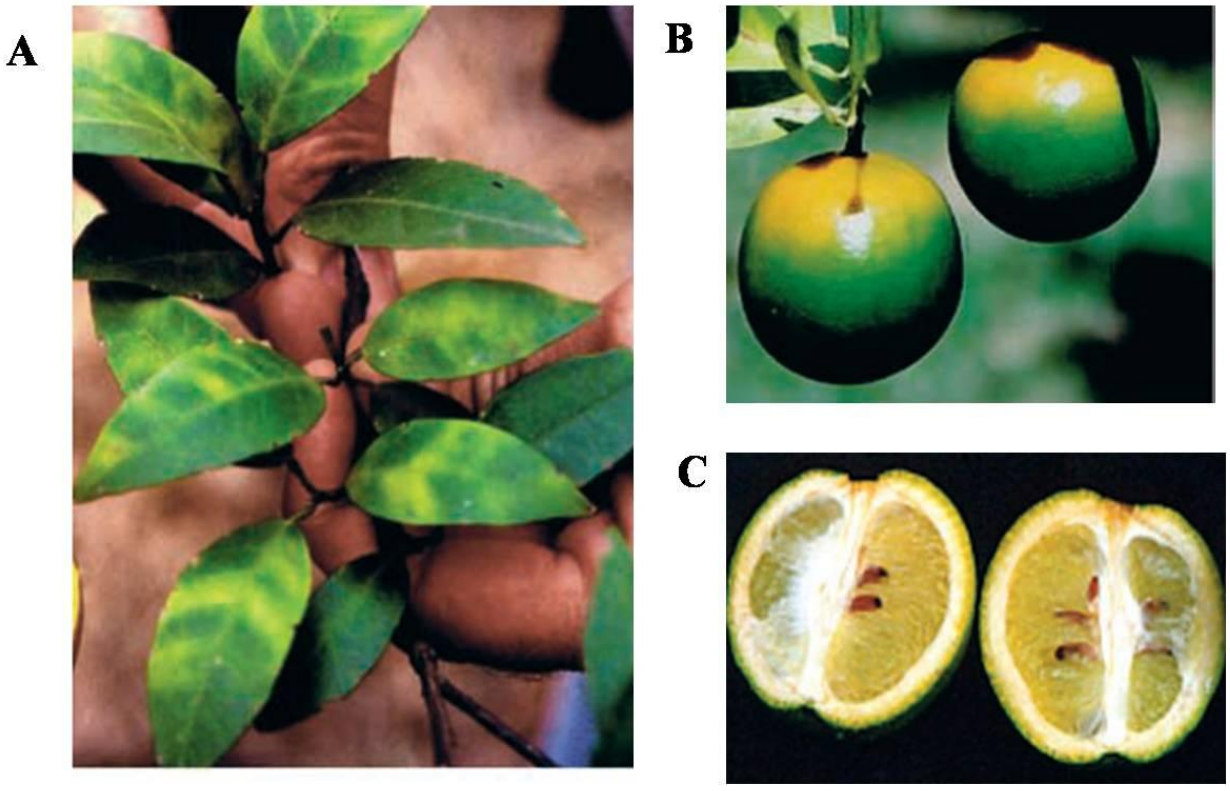

Figure 1.3: Symptoms of HLB in infected citrus plants. A) Blotchy mottle-affected sweet orange leaves. **B)** Fruit colour inversion; lower fruit normal, upper fruit with colour inversion. **C)** HLB-affected sweet orange. [25]

Three types of HLB associated species known are *Candidatus* Liberibacter asiaticus (CLas) (Asia, North America, and Brazil), *Candidatus* Liberibacter africanus (CLaf) (Africa) and *Candidatus* Liberibacter americanus (CLam) (Brazil) [212]. The CLas and CLam are heat tolerant and naturally transmitted by the Asian citrus psyllid (ASP) *Diaphorina citri* Kuwayama (Hemiptera: Psyllidae) which is also heat tolerant whereas CLaf is heat sensitive

and vectored by heat sensitive African citrus psyllid *Trioza erytreae* (Del Guercio) (Hemiptera: Triozidae) [83].

1.2.2. History and geographical distribution

1.2.2.1. China: Huanglongbing

In 1919, Reinking first reported "yellow shoot" of citrus while examining diseases of economic plants in southern China which he thought to be of little importance in those days. However, later surveys demonstrated that by 1936 the disease had spread turning out to be a serious trouble. The most extensive work on HLB in southern China was to be conducted from 1941 to 1955 by Lin Kung Hsiang. In the Chaozhou district, the farmers gave the name to the disease as "huang long bing", "huang" meaning yellow, "long" stands for dragon and "bing" standing for disease and hence "yellow dragon disease". The most noteworthy result achieved by Lin was the demonstration that HLB is a graft-transmissible, infectious disease, and neither any physiological disorder such as mineral deficiencies or water logging, nor a soil-borne disease such as nematode infestation or Fusarium infection [94]. Since Lin first demonstrated the graft-transmission nature of HLB and he used the name Huanlongbing for the disease, the International Organization of Citrus Virologists (IOCV) proposed that the official name of the disease to be "Huanglongbing" at the 13th conference of the Organization in Fuzhou (China) in 1995, and this proposal was accepted. Today, HLB is broadly used for the African, American, and Asian forms of the disease.

1.2.2.2. South Africa: Greening

In the western Transvaal, a disease similar to HLB was observed in 1928 with name "yellow shoot" while the name "greening" existed in the eastern Transvaal [163]. Initially it was assumed to be mineral toxicity [227] but in 1965, A.P.D. McClean and P.C.J. Oberholzer, demonstrated that greening was transmissible by graft inoculation [149] as well as by the African citrus psylla, *T. erytreae* [148]. The infectious nature of "greening" was thus established ten years after that of "Huanglongbing".

1.2.2.3. Philippines: Mottle leaf

In 1921, Lee described the disease first and related it to zinc deficiency [123]. The disease became a severe problem in the late 1950s. The symptoms of "mottle leaf" were first compared with those of HLB in China and Taiwan, and "greening" in South Africa by Salibe and Cortez (1968) and Martinez and Wallace (1968) [146, 189]. The major role of the Philippines to HLB was the demonstration in 1967, that "mottle leaf" could be transmitted by the Asian citrus psylla, *Diaphorina citri* [145]. In the same year, in India also it was also reported that HLB could be transmitted by *D. citri* from trees affected by "citrus dieback".

1.2.2.4. India: Citrus Dieback and HLB

Roghoji Bhonsale first observed "citrus dieback" in the 18th Century in the Central Provinces, shortly after the introduction of citrus in India. It was also noticed by Bonavia in 1988 in Assam [20]. Capoor in 1963 that stated citrus plants were acutely suffered from certain disorders resulting in low production, twig dieback, slow death and even sudden wilting [28]. According to Asana (1958), "dieback in citrus is not a specific disease" [7] and similarly, for Capoor (1963), dieback was merely a symptom picture, and many factors were suggested to account for it [28]. In some cases, the major cause was *Citrus Tristeza Virus* (CTV) as clearly proved by the Virus Research Center at Poona [28, 231]. In other cases, HLB might have been involved as certainly the case in the Coorg region, north of Mysore where "the most pronounced symptom of the disease is the characteristic mottling of leaves" according to Asana (1958). Several years later, HLB in mottled Coorg mandarin leaves was confirmed by positive dot blot hybridisation [230] and also members of the 12th conference of the IOCV in India in 1992 observed very severe HLB symptoms on the "Coorg" mandarin trees and other citrus cultivars in Gonicoppal and Chitalli. HLB hypothesis was further supported from the work of Fraser and co-workers [60, 61] which indicated that CTV was not always present in dieback-affected trees. Many of the citrus species affected in India are tolerant to tristeza in other countries. Furthermore, applications of zinc and other minor elements failed to cure the dieback condition, though sometimes minor and momentary improvements were obtained. These observations indicated that HLB might have been involved in dieback, and a survey in all major citrus areas of India was made for "dieback". The most prominent feature of dieback found during the survey, was the fact that, in early stages of the disease, leaf symptoms were often

limited to one or a few limbs. This feature had already been described for "greening" in South Africa by McClean and Oberholzer (1965), and for "Huanglongbing" by [94] in China and it was thus concluded that dieback was "caused by the virus responsible for greening disease of citrus in South Africa" [94, 148, 149]. Eventually, Capoor and co-workers proved the presence of HLB in India after succeeding in transmitting the HLB pathogen by the Asian psylla, *D. citri* at the virus Research Center at Poona [29]. Among the trees positive for HLB, some carried CTV others did not. Finally, in 1971, Bové and coworkers detected the HLB bacterium in a Musambi sweet orange seedling, which had been infected experimentally by *D. citri* nymphs with the "Poona" strain of HLB [24, 119]). Many results on HLB in the Bordeaux laboratory have been obtained with the Poona strain.

1.2.2.5. Indonesia: Phloem necrosis and Vein phloem degeneration

In Indonesia, HLB is called "Vein phloem degeneration" [215]. In an anatomical study of greening-affected sweet orange shoots from South Africa, Schneider (1968) identified localized pockets of necrotic phloem scattered all over the vascular system of mature leaves blocking the translocation stream [192]. Other anatomical aberrations observed were immense accumulation of starch in the plastids, disordered cambial activity with excessive formation of phloem, soon to become necrotic. Leaf mottle symptoms related with HLB are most likely the outcome of these alterations.

1.2.2.6. Thailand: Destruction of citrus by HLB

HLB first emerged in Thailand in the 1960s and was so severe that the time between the beginning of the disease and debilitation of the whole tree was about two years [194]. Roistacher (1996) has emphasized the seriousness of the disease and destruction of citrus due to it in Thailand [182]. Around 10 to 15% of tangerine trees are being destroyed by HLB each year in the northern regions. The disease is also propagated by infected nursery productions besides being spread by *D. citri*.

1.2.2.7. HLB in America

Until recently, America was free of HLB, but symptoms of the disease were recognized in the State of São Paulo, Brasil in March 2004 and in Florida, USA in August 2005, two of the

largest citrus growing regions in the world. After its detection in Florida and State of São Pauloa, it has also been identified in various states including Louisiana, South Carolina, Georgia and very recently, in Texas and California. It has also been identified in Cuba, Belize, Jamaica, Mexico, and some other countries in the Caribbean [233].

1.2.3. Bacterial nature of the HLB agent confirmed by Electron microscopy

By 1967, when the name "HLB" was not up till now used, it became well-known that "greening" could be transmitted by graft inoculation as well as by the two citrus psyllids. These results indicated that the greening causing pathogen was a virus as at that time the only plant agent known to be transmitted in these ways was virus. It became trendy to talk of the "greening virus" and also the term "stubborn virus" came into the literature for the same reasons. In 1967, it was found that mycoplasma like organisms (MLOs) were associated with plant diseases, the previous causes of which were linked to be viruses [48]. Mycoplasmas refer to special bacteria, which lack a cell wall around their single cytoplasmic membrane. Most of the "MLO-diseases" were of the "yellows" type, and their symptoms were similar to those of greening and/or stubborn. Therefore, search for MLOs in greening and stubborn-affected sweet orange leaves was commenced by electron microscopy (EM), initially in Versailles, and later on in Ordeaux, France. In both cases, micro-organisms were spotted in the phloem sieve tubes of symptomatic leaves, but not in healthy leaves. In the stubborn case, the micro-organism was shortly found to be in culture, and turned out to be a new type of mycoplasma named *Spiroplasma citri* with helical morphology and motility [188]. While greening organism could not be obtained in culture and it was also thought to be a mycoplasma initially [119, 120], but the agent was soon found to be enclosed by a 25-nm-thick envelope, much thicker than characteristic mycoplasmas (including *S. citri*) cytoplasmic membrane envelope which is 7 to 10-nm-thick [71, 187]. These observations suggested that the HLB organism contained a bacterial cell wall besides its cytoplasmic membrane. Later on, it was proved that the cell wall was of the Gram negative type, composed of a membrane and a peptidoglycan layer [68]. Thus, the causative agent of HLB was a Gram negative bacterium [69]. Garnier and Bové (1977) showed by EM that HLB bacterium possesses a characteristic, electron-dense layer surrounding the bacterial cell and this suffices for HLB detection. HLB bacterium cell was surrounded by two triple layered membranes, the inner cytoplasmic membrane and the outer membrane, the

inner zone was sometimes rather thicker as more electron dense than the outer zone suggesting a peptidoglycan layer.

Indirect evidence for the Gram negative nature of the HLB bacterium had already been found prior to the EM experiments through studying the effect of penicillin on HLB affected trees [9, 23] where penicillin had a positive effect on HLB-affected citrus while it had no effect on *Spiroplasma citri*-affected citrus because mycoplasmas lacking cell wall are insensitive to penicillin.

Soon after the detection of HLB bacterium by EM in infected sweet orange leaves with South Africa "greening" [119], similar organisms were detected by EM in leaves infected with Reunion "greening", India "dieback", Taiwan "likubin", and Philippines "mottle leaf" [24, 119]. Finally, the HLB bacterium was also seen in *T. erytreae* [153] and in *D. citri* [32]. The HLB bacterium is probably the first walled, sieve tube-restricted bacterium seen in plants.

Figure 1.4: HLB-associated vector Asian citrus psyllid and bacteria *Candidatus* Liberibacter asiaticus (CLas). A) Transmission electron microscopy picture of CLas in the phloem of citrus. **B)** and **C)** Asian citrus psyllid (*Diaphorina citri*) feeding on citrus plants [74].

1.2.4. Nomenclature for HLB Bacterium

The genus "*Candidatus*" is proposed for non-culturable bacteria by Murray and Schleifer [160] and therefore given to HLB bacterium which was assigned as the first member of a new subgroup in the α subdivision of the Proteobacteria based on 16S rDNA sequence comparisons. Afterwards the trivial name "Liberobacter" was substituted by Liberibacter ("liber" for bark and bacter for bacterium) and given to this new subgroup of organisms. Finally, based on temperature sensitivity, DNA hybridizations, genomic properties and serology, the HLB associated *Candidatus* Liberibacters (*Ca.* L.) from Asia, Africa and America were named as *Candidatus* Liberibacter asiaticus, *Candidatus* Liberibacter africanus and *Candidatus* Liberibacter americanus respectively [99].

1.2.5. Host range

Two types of plants are of importance while talking about hosts in HLB: the plant that sustains the psyllid vectors and the plant in which the bacterial pathogen can reproduce. The psyllid vectors have a narrow range of host in comparison to the broad host range of the Liberibacters. [74, 83]

1.2.5.1. Psyllid Hosts

The preferred hosts of *D. citri* are *Murraya paniculata* (Orange jasmine and mock orange) [10] and *Citrus aurantifolia [83]* although it could be able to feed on several citrus species and closely related species. Tsai and Liu [222] found that among *M. paniculata* (orange jasmine), *C. jambhiri* (Rough lemon), *C. aurantium* (sour orange), and *Citrus* × *paradisi* Macfad (grapefruit); the grapefruit was the best host of *D. citri.* Two Florida native *Zanthoxylum* plants, *Zanthoxylum clavahercules* L. and *Z. fagara* (L.) Sarg and *Casimiroa edulis* Llave & Lex may be non-hosts or very poor hosts of the ACP as suggested by Halbert and Manjunath [83] based on greenhouse studies.

1.2.5.2. Hosts of Liberibacters

The present knowledge of the Liberibacter host range is on the basis of symptoms [83]. Most citrus varieties are vulnerable to some level apart from their rootstock [25, 83]. However, one feature of HLB is that in diverse types of citrus, different extent of disease and symptoms

are provoked. Moreover, different isolates of CLas can cause varying degrees of disease in citrus cultivars [220]. The most serious symptoms are discovered on mandarin, sweet orange, tangelo and grapefruit; followed by lemon, rough lemon and sour orange [25, 83, 109, 136, 221]. There is no resistance observed for HLB in citrus species but some species and cultivars were found to have tolerance to some extent. Studies have established the susceptibility of few cultivars to decline more than others [109] like grapefruit was more resistant than sweet orange cultivars. A number of citrus species stayed free of symptoms after heavy inoculum [18] indicating an unambiguous degree of tolerance. Various cultivar such as pummel, kumquat became infected which were formerly resistant to HLB. It was supposed that the variation in host range was because of the evolution of HLB strains for pathogenicity. Several citrus relatives such as *Severinia buxifolia* [41, 95, 96, 179], *Limonia acidissima* L. [95, 109], *Clausena lansium [42, 46]*, and *Toddalia lanceolata* Lam [111], could carry HLB pathogen as reported by various studies.

1.2.5.3. Alternative hosts

M. paniculata is most preferable host of psyllids as confirmed by field observation and laboratory studies; however, it is not yet clear that whether it will serve as alternative host for Liberibacters [95, 140, 232]. Hung *et al*. [95] demonstrated that CLas can multiply in the Chinese box orange (*S. buxifolia*) and the wood apple (*L. acidissima*) but not in the jasmine orange (*M. paniculata*) or the curry leaf. In contrast, some studies reported steady symptoms in *M. paniculata* plants which were inoculated [83]. Some reports [248] also mentioned naturala infection of *M. paniculata*d with CLas in Florida. It was concluded that *M. paniculata* might be able to serve as reservoir host for CLas because it can host CLas for minimum two months and transmission of CLas to the sweet orange might be possible during this period. In the Western Cape Province of South Africa, the symptoms for HLB like blotchy mottle leaves were observed on *Calodendron capense* and therefore infection of a Liberibacter was discovered on this plant. This Liberibacter was characterized as a subspecies “capensis” of CLaf [70].

1.2.5.4. Hosts other than Rutaceae family

In various studies, certain experiments involving inoculation of *Ca.* L. spp. on plants of non-Rutaceae family showed that transmission of all species to periwinkle plants is possible by dodder (Cuscutaceae family) [67]. CLas and CLam efficiently colonize and multiply to a high level within dodder. Thus the use of dodder might facilitates transmission of Liberibacter spp. to citrus [239, 245], non-Rutaceae family plants like periwinkle [67, 87, 242] and numerous solanaceae family plants including tomato [49] and tobacco [67], indicating an wide-ranging physiological host of CLas. Some studies also [55] reported the presence of HLB symptoms such as yellow shoots on *Pithecellobium lucidum,* a non-member of Rutaceae family.

1.2.6. Evolution of *Candidatus* Liberibacter spp.

All *Ca.* L. spp. are a member of the gram-negative α-proteobacteria in the Rhizobiaceae family. Due to limitation of obtaining the bacteria in culture, the classification of the *Ca.* L. spp. is grounded on the 16S rRNA gene sequence and not the conventional methods like morphology, growth, metabolism, enzymatic activity, and DNA-DNA hybridization [110]. Phylogenetic analysis has revealed that CLas is an "early branching member" of Rhizobiaceae with the lengthy branch indicating its fast evolution [50]. The recent findings of *Ca.* L. europaeus and *Ca.* L. solanacearum indicate widespread occurrence of *Ca.* L. spp. in psyllids and their host plants. Recently a bacteria isolated from the hybrid mountain papaya (*Carica stipulate* × *C. pubescens*) affected from bunchy top, has been designated to be the first cultured member of Liberibacter genus and it was named as *Liberibacter crescens [126]*. Fascinatingly, all *Ca.* L. spp. are resides in phloem and transmitted by psyllids, but *L. crescens* resides in the periphery of phloem and it has not been concluded yet that whether it might be transmitted by insects or not [126].

Ca. L. spp. might have evolved from the same ancestor in the Rhizobiaceae family. The bacteria which are closely related to *Ca.* L. spp. have genome sizes in range of 3.4 Mb (*Agrobacterium* sp.), 5.7 Mb (*Agrobacterium tumefaciens*), 6.3 Mb (*Agrobacterium vitis*), 6.5 Mb (*Rhizobium etli*), 6.7 Mb (*Sinorhizobium meliloti*), and 7.3 Mb (*Agrobacterium radiobacter)*. In contrast, the genome size of *Ca.* L. spp. is much-reduced ranging from 1.23

Mb for CLas and 1.26 Mb for *Ca.* L. solanacearum and 1.5 Mb for *L. crescens* [126]. The reduction in genome size and low GC content of CLas and *Ca.* L. solanacearum might be the consequence of steady and nutrient-rich environments and attenuated purifying selection owing to minute population sizes and strong bottleneck effects [155, 157, 235]. The comparison of genome of CLas with other *Rhizobiales* members identified number of conserved microsyntenous orthologous genes (MOGs) [88] which speculates the underlying evolutionary relationships and their importance in host-microbe interactions and their duplication probably helps their ongoing evolution [118]. Studies comparing the gene expression of CLas in planta and in psyllid by quantitative reverse-transcription polymerase chain reaction found that out of the 381 genes, 182 were found to be up-regulated in planta compared to 16 genes up-regulation in psyllid and 183 genes demonstrated no noteworthy variation. This biased gene induction in planta in comparison to psyllid advocates more active state of CLas in planta in comparison to a passive and inactive status in psyllid. Additionally, it has been suggested that CLas might be able to form a biofilm in the psyllid which might be due to either stress or its physical status adjustment for psyllid transmission. No biofilm development has been observed for CLas in planta. Collectively, these evidences indicate the role of psyllids as psyllids for CLas to its definitive plant host. Interestingly, CLas does not possess complete restriction modification system thus it is susceptible to prophage integration, as revealed by the presence of several phage-derived gene sequences within its genome. This could result in a superior rate of evolution in CLas through phage-mediated recombination events [133]. In addition, CLas lacks three proteins involved in DNA replication and repair which are present in *Ca.* L. solanacearum. As a result, it has been proposed that CLas [50] quickly evolves typical of host-restricted symbionts and pathogens due to the eminent genetic drift consequential from both population bottlenecks and relaxed selection on many genes [50, 155].

1.2.7. Detection of HLB

At present, HLB is preliminary detected majorly by examining disease symptoms visually in trees. Suspected samples are sent to diagnostic laboratories for secondary analysis. A number of methodologies have been developed to detect HLB in these samples such as serologic assays, biological assays, electron microscopy, DNA probes, loop mediated isothermal amplification, PCR and real-time PCR [25, 63, 72, 74, 91, 100, 107, 132, 164, 213]. In recent years, HLB diagnosis by real time PCR has become popular because of its sensitivity

and reliability [25, 130, 132, 156] and has been adapted and implemented to screen vast numbers of quarantine specimens which was first developed by Li *et al*. making use of CLas 16S rDNA gene sequence and cytochrome oxidase I as the citrus endogenous gene.

1.2.8. Genome analysis of CLas

In spite of the limitation of culturing CLas thus difficulty in obtaining pure genomic DNA, it has been successfully sequenced providing a basis for the evaluation of the metabolic and functional capabilities of the pathogen [50, 223]. Genomic analysis of CLas has provided helpful insights into the biology and pathogenicity of the HLB pathogen. CLas contains genetic features characteristic to obligate intracellular bacteria [154], such as small genome size (1.23 Mb), low GC content (36.5%), and a significant genome reduction in comparison to other members of the *Rhizobiaceae* family. Genome wide, gene-based phylogeny places CLas within the order *Rhizobiales* closely associated with members of family *Rhizobiaceae.* It has been considered that CLas is an early branch member of the *Rhizobiaceae* family which has evolved much more rapidly typical of host-restricted symbionts or pathogens.

1.2.8.1. Metabolic pathways

CLas contains all 14 genes encoding NADH dehydrogenase subunits [A-N], a key component of the respiratory electron transport chain. However, no homologs were identified corresponding to the terminal stages of oxidative phosphorylation. Likewise, no homologs for the cytochrome bc1 complex, cytochrome c oxidase, the cbb3-type or the cytochrome bd complex have been identified although all four cytochrome O ubiquinol oxidase subunits [I to IV] were identified. The respiratory complex of CLas resembles that of the citrus pathogen *Xylella fastidiosa* [19] which is active only under oxygen-rich conditions [37, 181]. Therefore, lack of key enzymes involved in oxidative phosphorylation and diverse terminal oxidases concludes limited capacity for aerobic respiration in CLas. Several enzymes involved in nitrogen metabolism and glutamate metabolism were identified, suggesting a dependence of CLas on nitrogen metabolism. On the basis of enzymes identified, glycolysis is suggested to be the major pathway for the catabolism of monosaccharides. CLas encodes for an ATP/ADP translocase alongwith ATP synthase, allowing it to both synthesize ATP as well as its uptake from surroundings. Additionally, genes for the tricarboxylic acid (TCA) cycle were identified

in CLas which may enable it to utilize a variety of amino acids as energy sources. CLas contains all enzymes of the pentose phosphate pathway except transaldolase and the full pathways for both purine and pyramidine biosynthesis has been also identified.

1.2.8.2. Transport proteins and types of secretion systems

A total of 137 transport proteins has been identified in CLas out of which 9 proteins belong to the channels/pores class of transporters, 24 proteins are electrochemical potential-driven transporters, 92 proteins are classified under primary active transporters, one belongs to the group translocators class and the remaining 11 proteins can be classified under the incompletely characterized transport systems class of transporters. Of the 92 primary active transporters, 40 are ABC transporters characteristic of α-Proteobacteria with a broad host range but in contrast to intracellular bacteria of a similar size with average of 15 ABC transporters [39]. It is fairly possible that some of these transporters have an effect on virulence, host range, or symptom elicitation, alone or in combination.

1.2.8.3 Secretion systems

In accordance with its intracellular lifestyle neither type III or IV secretion systems or their effectors nor plant cell-wall degradation enzymes such as cellulases, pectinases, xylanases, or endoglucanases which require type II secretion have been identified in CLas. However, all proteins necessary for the first step of the type II secretion system, the general secretory pathway responsible for the export of proteins to the periplasm [176] were identified in the CLas. The genes for pilus formation and flagella biosynthesis were also found in CLas although there are no evidences reported for the same.

Several complete type I secretion systems were present facilitating two major functions. The first function is defensive, involving multidrug efflux and thus protecting the bacterium against toxic environmental chemicals, antibiotics and phytoalexins. The second function is offensive, allowing the secretion of degradative enzymes and offensive effectors like antibiotics or associated with pathogenicity. Offensive enzymes and effectors secreted via the type I system comprise hydrolases (proteases, phosphatases, esterases, nucleases, and glucanases) and a comparatively huge number of protein toxins.

1.2.8.4. Proteome and transcriptome analysis of citrus plants on CLas infection

Using the isobaric tags for relative and absolute quantification (iTRAQ) technique, Fan *et al*., reported significant up-regulation of proteins involved in stress/defense response, such as 4 miraculin-like proteins, chitinase, Cu/Zn superoxide dismutase and lipoxygenase in sweet orange plants (*Citrus sinensis)*[57]. Microarray analysis also revealed up-regulation of stress-related genes including miraculin-like proteins and Cu/Zn superoxide dismutase [57]. Similar results have been reported for grapefruit plants (*Citrus paradisi*) based on protein profiling by 2DE and mass-spectrometry analysis [162]. Microarray studies on sweet orange plants infected by CLam suggested induction of transcripts related to signaling, metabolism and/or stimulus to hormones, stress and pathogenesis, biosynthesis of secondary metabolites and oxidative stress and transcription factors. Also genes associated with the endomembrane system including transcripts encoding three zinc transporters (ZIP1, ZIP4 and ZIP5) and a zinc inducer facilitator (ZIF1) involved in Zn homeostasis and Zn sequestration, were upregulated [143].

1.2.9. Virulence mechanism

In order to design management strategies against CLas and controlling HLB, it is critical to understand the interaction between citrus and CLas and the virulence mechanism employed by CLas. However, due to the complexity in obtaining CLas in culture, limited information is available regarding understanding of virulence mechanism with some promising improvement.

1.2.9.1. Phloem blockage and aberrations

The major cause for development of HLB disease symptom is suggested to be the phloem blockage resulting from plugged sieve pores but not HLB bacterial aggregates [106, 192]. Phloem blockage is due to the large amounts of callose deposition and phloem protein (PP). The callose deposition is confirmed by aniline blue staining while phloem proteins are thought to be involved because the PP2 gene was induced in HLB diseased citrus [106]. Nevertheless, PP2 has been thought to be a host defense response to stop more spread of the pathogen within the sieve tubes. Koh et al. also observed callose deposition in the sieve plates and around plasmodesmata pore units (PPUs) linking companion cells and sieve elements. The callose deposition around PPUs was suggested to be preceded, followed by accumulation of

starch in the chloroplasts. The development of callose around PPUs in infected leaves prevented the symplastic flow of solutes from companion cells into sieve tubes, thereby decreasing the phloem loading efficiency. This blockage is harmful for plants as well as CLas. Consequently, CLas might not be capable of surviving in completely blocked sieve elements [217]. The accumulation of sucrose in infected leaves, which is the main photoassimilate in phloem transported from mature leaves to sink organs, suggests that photoassimilate translocation is disrupted by CLas infection, probably because of phloem blockage [56, 58, 106, 108]. This decreased photoassimilate transportation might be responsible for the tiny, distorted, and inadequately colored fruit containing undeveloped or partially developed seed. Sucrose deficiency has been linked with seized fruit growth [73]. Interestingly, it has been noticed that many genes involved in photosynthesis are repressed presumably due to increased sucrose/glucose levels [4, 56, 106]. The establishment of HLB symptoms was correlated with microscopic aberrations increment including phloem necrosis, enormous accumulation of starch in the plastids, abnormal cambial activity, and excessive phloem development and phloem collapse [106, 192]. As a result, these changes are accountable for the blotchy mottle, yellowing, leatheriness and vein clearing in infected leaves [192].

1.2.9.2. Metabolic imbalances by nutrient depletion

CLas causes host metabolic imbalances by nutrient exhaustion or disturbed transportation resulting in HLB symptoms [50]. The disruption in host cellular metabolic functions might be due to import of host-cell metabolites for growth and development eventually leading to disease appearance. It was suggested that CLas make use of fructose preferentially causing fructose reduction and the glucose accumulation in the infected host tissues [56]. The accumulation of glucose consequently leads to the suppression of enzymes involved in photosynthesis causing HLB symptom development. CLas encodes comparatively low number of genes implicated in the biosynthesis of compounds, which are taken up from the host without much difficulty. Recently, Li et al. [129] identified 14 ABC transporter systems and 7 nontransporting ABC proteins which could be used by the bacterium for importing metabolites and enzyme cofactors to resist organic solvent, heavy metal, and lipid-like drugs, maintaining the composition of the outer membrane and secreting virulence factors. These numerous transporter proteins might play a crucial role to provide necessary nutrients to CLas resulting in a metabolic imbalance in citrus. CLas also encodes an ATP/ADP translocase in

addition to its ATP synthase so that it can utilize the energy source directly from its host, as do other obligate intercellular parasites such as *Rickettsia prowazeki* [50, 226, 236].

1.2.9.3. Hormone

Phytohormones play important role in determining citrus fruit set, productivity, and plant response to pathogen infection [183]. On the basis of comparison between symptomatic and asymptomatic fruits from infected and healthy sweet orange trees, Rosales and Burns found that ethylene production was reduced in infected plants whereas indole-3-acetic acid (IAA) and abscisic acid (ABA) contents in the stylar end, middle section, or stem end of fruit were higher in symptomatic plants [183]. The lower IAA content in symptomatic stem end suggested acceleration in abscission, although ethylene production in the whole fruit is lower contrasting its role in abscission promotion. The content of IAA was higher in the misshapen area in comparison to the normal-growing regions of symptomatic plants. The hypodermal cell size was also enlarged in the analogous regions. Therefore, IAA has been suggested to play important role in development of distorted fruits [183].

1.2.9.4. Suppression or avoidance of plant defense

CLas elicits a delayed defense response plants [106] and this manipulation of defense response is critical for its survival in plant. The reduced genome of CLas and psyllids mediated transmission might facilitate it to avoid pathogen-associated molecular pattern (PAMP)-triggered immunity. Peptidoglycan recognition proteins (PGRPs) are involved in the recognition of PAMP [199, 200]. Additionally, lack of type II plant cell-wall degrading enzymes helps it in inhibition of defense responses based on auto degradation products of the plant cell wall [167]. However, CLas has 57 genes for biogenesis of cell envelope [50], which might function as PAMPs. It has been revealed that a functional *fla* gene is present in CLas which encodes flagellin and hook-associated protein of 452 amino acids that contains the conserved flg22 [249]. Studies suggested that CLas flagellin may act as a PAMP and elicit host plant resistance to the HLB bacteria [249].

Microarray analysis suggested that the CLas infection in citrus does not produce a noteworthy induction of defense-related genes in the early stages [4, 106]. Besides, CLas could further inhibit the host defense. CLas contain a gene encoding a salicylate hydroxylase which

converts salicylic acid (SA) into catechol for resistance suppression [228]. This gene is highly induced in planta in comparison to psyllid. SA has role in plant defenses against pathogens for basal defense, the hypersensitive response and systemic acquired resistance [207]. Salicylate hydroxylase expression in plants demolish plant defenses by degrading SA [229] which could be one of the mechanisms utilized by CLas to avoid plant defense responses [218, 219] in accordance with the down-regulation of defense-related genes in CLas-infected citrus [4, 106].

1.2.9.5. Prophages SC1 and SC2

CLas contains an excision plasmid prophage, SC2 and a chromosomally integrated prophage, SC1 that gets lytic in citrus [245], and might impart in the pathogenicity of CLas. A lytic burst of CLas within phloem cell, mediated through SC1 genes, might elicit an apoptosis cascade, leading to death [59, 106]. SC1 and SC2 also contain many genes for virulence factors that might be reason for the pathogenicity of CLas, for example, i) two peroxidases that might protect CLas against reactive oxygen species ii) two adhesins, which might be useful in transmission by psyllids [245]. However, SC1 and SC2 involvement in the pathogenicity of CLas need to be further investigated.

1.2.9.6. Serralysin and hemolysin

The antimicrobial proteins and peptides production is one of the major defense strategies utilized by a plant in response to infection by pathogenic organisms. CLas encodes a putative type I secretion system (T1SS), serralysin, and its expression was found to be up-regulated in planta in comparison to psyllid [239]. Serralysin is a secreted metalloprotease secreted by a various microorganisms which inactivates antimicrobial proteins and peptides [191]. The upregulation of the serralysin biosynthesis gene in planta suggests that CLas may exploit serralysin to alter the plant defenses, probably by degradation of plant antimicrobial peptides. It also helps in the acquirement of carbon and nitrogen by the proteolysis of host proteins and nutrient uptake [13, 16] further aiding to bacterial survival in hosts. Due to possible challenge in selecting effective antimicrobial peptides against CLas, the serralysin of CLas could be a potential target in screening antimicrobial compounds for controlling HLB.

Hemolysin is produced by animal and insect pathogens which helps in survival of bacteria in plants by various mechanism like cell lysis, necrosis, and apoptosis stimulation

[126]; availing the iron for pathogen [208]; and induction ions, water, and low molecular weight molecules leakage across plant cell [75]. Hemolysin is believed to play a significant role in proteins degradation produced responsible for the defense reaction or uptake of crucial nutrients [114]. Therefore hemolysis production by Clas might also play a significant role in survival of CLas by contributing to nutrient acquisition, ion transfer, and phloem necrosis.

1.2.10. Metabolite signature of CLas infection

Symptoms of HLB include starch accumulation in the leaves and phloem impairment. Studies have reported that the concentration of sugars including fructose, glucose, sucrose, and proline decreases during CLas infection reflecting altered carbohydrate transport. However phenylalanine, histidine, asparagine and limonin concentration is increased during CLas infection in Valencia or Hamlin fruit [34]. In *Citrus sinensis* Valencia fruits, concentration of sucrose is found to be reduced upon CLas infection. Additionally in infected fruits, many amino acids concentration including alanine, arginine, isoleucine, leucine, proline, threonine, and valine is reduced with the exception of increased concentration of phenylalanine, asparagine, and histidine. Ascorbate, citrate, limonin and limonin glucoside concentrations were higher in infected fruits [205]. Micro X-ray fluorescence investigation revealed that that Zn concentration in the phloem of veins in healthy leaves of grapefruit was more than 10 times higher than that in HLB-affected leaves [214].

1.2.11. Control strategies

Currently no control strategies developed to control HLB and stop it from spreading to new citrus-production areas. The only control strategy is to prevent trees from becoming infected by removing the infected tree and minimizing the psyllid population. Recently, combination of penicillin and streptomycin has been demonstrated to be effective in eliminating or suppressing the CLas bacterium providing a therapeutically effective level of control [244]. Also a number of antibiotics such as Ampicillin, Carbenicillin, Penicillin, Cefalexin, Rifampicin and Sulfadimethoxine were found to be highly effective in eliminating or suppressing CLas infection and might be potential candidates for control of citrus HLB [243].

Other approaches for controlling HLB might involve targeting essential proteins for survival and developing inhibitor molecules against them to impair the protein function. Essential proteins of many pathogenic bacteria are potential targets for developing anti-bacterial drugs [79, 80, 98, 115, 116].

1.2.12. ABC transporters in CLas

ABC transporters of CLas may be involved in host metabolic imbalances in infected plants and development of HLB symptoms [50]. Wenlin Li et al. have identified 14 ABC transporter systems and 7 non-transporting ABC proteins in CLas. Out of the 14 ABC systems, 8 are predicted to be involved in uptake of essential nutrients including amino acids, B family vitamins, ions, and lipids [129]. The other six ABC systems are predicted to function as L-amino acid transporter, phosphate transporter, thiamine transporter, choline transporter, zinc transporter, and manganese and iron transporter. Vahling-Armstrong et al. demonstrated that the zinc transport ABC system (*znu*ABC gene cluster #1) of CLas is involved in high-affinity zinc uptake [225]. Their studies showed that both ZnuB and ZnuC genes from CLas were able to complement respectively ΔZnuB and ΔZnuC *Escherichia coli* and *Sinorhizobium meliloti* strains however CLas-ZnuA gene was not able to functionally complement ΔZnuA *E. coli* strain and only partially complement the ΔznuA *S. meliloti* strain. Therefore, this system might contribute to the zinc deficiency associated with HLB-affected trees. Their studies have also shown that the gene cluster of Mn and Fe ABC transport system (*znu*ABC gene cluster #2) was not able to functionally complement *Δznu*ABC *E. coli* and *S. meliloti* strains.

2.1. Materials

All the enzymes used for cloning were purchased from NEB (New England Biolabs). The primers were purchased from BioServe Biotechnologies (India) Pvt Ltd. Plasmid isolation and gel-DNA extraction kits were purchased from Zymo Research. For protein purification, Ni-NTA beads and imidazole were purchased from Sigma Aldrich. Amicon ultra-15 protein concentrators were purchased from Millipore (Bedford, Massachusetts, USA). The crystallization screens and trays were purchased from Hampton Research. All other chemicals were of analytical grade and purchased from commercial sources.

2.2. Sequence analysis

Sequence search was carried out using the BLAST search tool at the NCBI website (www.ncbi.nlm.nih.gov). Putative signal sequence was predicted by SignalP 4.1 server [173]. Multiple sequence alignments were made using Clustal Omega Webserver (http://www.ebi.ac.uk/Tools/msa/clustalo/) taking default parameters and ESPript 3.0. Phylogenetic analysis was done by MEGA 6 program from amino acid alignments using the Maximum Likelihood method based on the JTT matrix-based model [210]. The reliability of the branching was tested by bootstrap statistical analysis (1000 replications).

2.3. Cloning and isolation of CLas-ZnuA2

2.3.1. Cloning of CLas-ZnuA2 gene

2.3.1.1. Genomic DNA

The CLas genomic DNA was isolated from infected citrus plants at NRCC Nagpur. PCR amplification of 1160 bp fragment corresponding to 16S rDNA was carried out using forward primer 1OI 1-5’-GCGCGTATGCAATACGAGCGGCA-3’ and reverse primer OI 2c -5’-GCCTCGCGACTTCGCAACCCAT-3’ to confirm the presence of genomic DNA. PCR conditions were 94°C (4 min), 94°C (1 min)/58°C (1 min)/72°C (1 min) for 30 cycles, followed by 72°C (10 min).

2.3.1.2. PCR amplification of CLas-ZnuA2 gene

Primer set was designed for amplification of CLas-ZnuA2 gene on the basis of sequence present in NCBI database (GenBank accession code ACT57010.1). The oligonucleotide primers ZnuA2F- 5'- AATACATATGACGACACAAAAAAAAGTAGTATT ATCC-3' and ZnuA2R- 5'- AATACTCGAGTCAAAATAAAGTATCCACAATTTTCG-3' containing NdeI and XhoI sites was used to amplify CLas-ZnuA2 gene encoding protein of length 275 amino acid lacking signal sequence. The restriction sites of Nde I and Xho I inside the primer facilitated the cloning into pET-28c vector, where a TEV (tobacco etch virus) protease cleavage site has been added in place of thrombin protease cleavage site. PCR conditions were 94°C (4 min) 94°C (1 min)/58°C (1 min) / 72°C (1 min) for 30 cycles, followed by 72°C (10 min).

2.3.1.3. Elution of DNA from agarose gel

PCR amplicons obtained were purified from 1% agarose gel using a gel elution kit in order for removal of non-incorporated nucleotides and primers. In brief, agarose gel slice containing desired DNA fragment was cut out with clean blade. Gel solubilization buffer was added to the sample contained in a tube and then incubated at 50°C. When the gel was solubilized, complete solution of tube was loaded on to the silica column provided with the kit and centrifuged. The column was washed with the wash buffer twice and eluted with the 50µl of elution solution. The concentration measurement of eluted product was assessed either by measuring optical density on a spectrophotometer.

2.3.1.4. Construction of expression plasmids

Amplified product of CLas-ZnuA2 was cloned into the expression vector pET-28c. The presence of His6 tag and TEV protease cleavage site (MGSSHHHHHHSSENLYFQGHM) for cleavage of His6 tag in recombinant protein, after cloning, facilitated protein purification. Briefly, amplified product and pET-28c vector were digested with the Nde I and Xho I restriction enzymes from NEB (New England Biolabs) according to manufacturers' instructions. The reaction mixture containing restriction digestion enzymes was incubated at 37 °C for three hours. The digested DNA was incubated at 65°C for 10 min for inactivation of

enzymes and then purified by 1% low melting agarose using gel extraction kit as previously described in this chapter.

The ligation of digested CLas-ZnuA2 gene and pET-28c vector was done using T4 DNA ligase (NEB) according to manufactures' instructions. The reaction mixture containing T4 DNA ligase was incubated at 16°C for overnight in Thermocycler. The ligated product was transformed intoXL10-Gold host cells (Agilent Technologies) by heat shock method and plating was done on Luria-Bertani (LB) agar (purchased from HiMedia) plates containing 30 µg/ml of kanamycin and 34 µg/ml of chloramphenicol. Some colonies obtained were picked and inoculated on LB broth (HiMedia) containing 30 µg/ml of kanamycin and 34 µg/ml of chloramphenicol. The plasmids were isolated and presence of insert was verified by PCR using gene specific primers of CLas-ZnuA2 taking isolated plasmids as template and by restriction digestion of isolated plasmids.

2.3.1.5. Sequencing of pET-28c plasmid containing CLas-ZnuA2

The plasmid pET-28c containing CLas-ZnuA2 insert was sequenced for final confirmation and evaluation of the frame and mutations of the cloned gene from Eurofins Genomics India Pvt. Ltd.

2.3.2. Over-expression of the recombinant protein

The recombinant expression vector pET-28c having CLas-ZnuA2 insert, was transformed into the competent *E. coli* host cells BL21 (DE3) for protein expression. The plates are allowed to grow at 37 °C on LB agar plate supplemented with kanamycin (30µg/ml). The random colonies were picked, inoculated in 10 ml LB broth containing kanamycin. The overnight grown culture was further inoculated in the 10 ml of LB-enriched growth medium and protein expression was induced with 0.4 mM isopropyl β-d-1-thiogalactopyranoside (IPTG) after growing the cells at 37°C to an optical density of ~0.6. Induced cells were transferred to 25°C and grown for 6 hrs and then harvested by centrifugation at 6000 rpm at 4°C and stored at -60°C until further use. The expression and solubility of the protein was confirmed by analysis of soluble and insoluble fractions on 12% sodium dodecyl sulfate-polyacrylamide gel electrophoresis (SDS-PAGE).

2.3.3. Purification of recombinant protein and TEV protease cleavage

The CLas-ZnuA2 protein was purified to homogeneity using HIS-Select HF Nickel affinity column (Sigma Aldrich). Briefly, the harvested cells from 250ml culture were re-suspended in 50 mM Tris-HCl buffer pH 8.0 supplemented with 500 mM NaCl (buffer A) and disrupted by sonication giving 5 rounds of sonication pulses (10 sec on and 30 sec off) at 50% amplitude. The obtained cell lysate was clarified by centrifugation at 14000 × g for 40 min at 4°C. The soluble fractions were collected and loaded onto Ni column pre-equilibrated with buffer A. The column was then washed with buffer A to remove any unbound protein and protein was eluted in buffer B (50mM Tris-HCl pH 8.0, 500mM NaCl, and 100mM imidazole). The purified protein was dialyzed against 50mM Tris-HCl pH 8.0 buffer containing 100mM NaCl to remove imidazole. His-tag was removed by TEV protease treatment by adding TEV protease to protein in ratio 1:10 and incubating at 4°C for 12 hrs. The cleaved His-tag and uncleaved tagged protein was removed from cleaved protein by reverse Ni-NTA chromatography by loading the sample again onto Ni-column and the flow-through containing untagged CLas-ZnuA2 was collected. The purity of the protein and cleavage of His-tag was confirmed by analyzing the protein on 12% SDS-PAGE.

2.4. Circular Dichroism Spectroscopy

Circular dichroism (CD) measures the difference in the absorption of left-handed circularly polarized light and right-handed circularly polarised light which arise when a molecule contains one or more chiral chromophores. Proteins have a number of chromophores which can give rise to CD signals. The CD spectrum in the far UV region (240-180nm), which corresponds to peptide bond absorption, can be analyzed to determine regular secondary structural features such as α-helix and β-sheet. In the near UV region (320-260 nm), the CD spectrum reflects the environments of the aromatic amino acid side chains and thus gives information about the tertiary structure of the protein. CD also provides information about protein folding and denaturation, changes in protein conformation upon ligand binding and thermal stability of the proteins in different environments [159, 203].

The CD study was performed using Chirascan CD spectrometer (Applied Photophysics, UK) in sodium cacodylate buffer pH 7.0. Far-UV CD spectra (190-260) were recorded using 0.2 mg/ml of protein in a 1 mm quartz cell at band width 1 nm and time per point 0.25 sec with

three repeats. Sample cuvette has been attached to peltier system, incubated for 5 min and the conformational stability of protein at different temperature (20-90°C) was examined by recording the spectra. Three consecutive scans were accumulated. The average baseline spectrum of buffer blank was subtracted from the average protein sample spectrum. The results of CD measurements were expressed as mean residue ellipticity (MRE) in deg cm^2 $dmol^{-1}$.

2.5. Surface Plamon Resonance

Surface plasmon resonance (SPR) technique is used to determine the kinetics of wide variety of macromolecular interactions for high- and low-affinity small molecule interactions. It is an optical method for measuring the refractive index near a sensor surface. The SPR measurements were performed on a BIAcore T200 instrument operated with the BIAcore T200 control software Version 2.0.

In Biacore, for studying the interaction between two binding partners, one partner (ligand) is attached to the surface and the other (analyte) is passed over the surface in a continuous flow of sample solution. The SPR response is directly proportional to the change in mass concentration close to the surface. Measurement of this change is performed and the result is plotted as response units (RUs) versus time. After a defined association time, a solution without the analyte is injected that dissociates the bound complex between the immobilized protein and the partner. During dissociation, a decrease in SPR signal is observed. From these, kinetic constants can be retrieved [27].

2.5.1. Activation of CM5 chip and immobilization of CLas-ZnuA2 onto CM5

CM-series sensor chips contain a carboxymethylated dextran matrix which is covalently attached to the gold surface (Figure 2.1). The attachment of ligands to the dextran matrix can be achieved using various chemical methods which exploit common functional groups present on the ligand such as amino, thiol, and aldehyde groups. The flexibility of dextran matrix permits relatively free movement of attached ligands inside the surface layer. Sensor Chip CM5 is the most commonly used chip which provides a high surface capacity for immobilizing an extensive range of ligands.

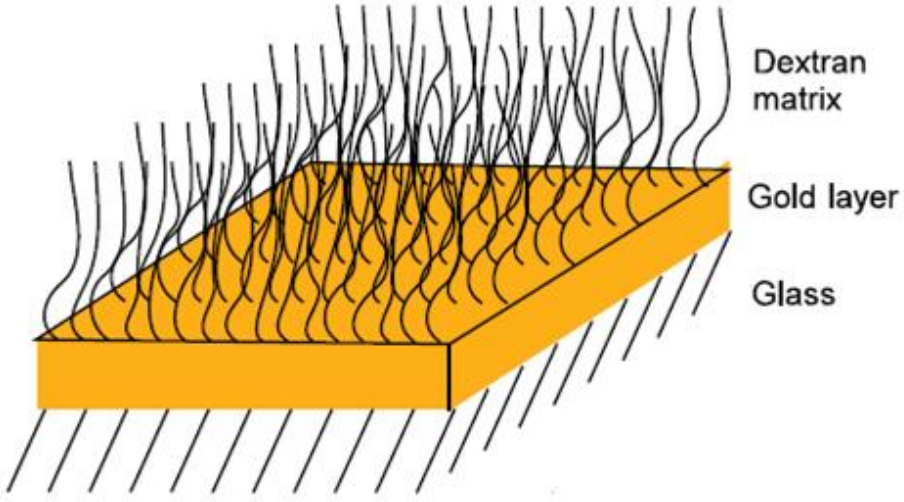

Figure 2.1: A typical sensor chips containing a carboxymethylated dextran matrix which is covalently attached to the gold surface.

The covalent attachment of biomolecules to the CM5 sensor surface is mostly achieved by the amine coupling chemistry. In this method, carboxyl groups on the surface of the sensor chip surface are first activated with a mixture of 1-ethyl-3- (3-dimethylaminopropyl) carbodiimide (EDC) and N-hydroxysuccinimide (NHS) to give reactive succinimide esters. After that, ligand is passed over the surface and the esters spontaneously react with primary amine groups or other nucleophilic groups to make the ligand attach covalently to the dextran matrix (Figure 2.2).

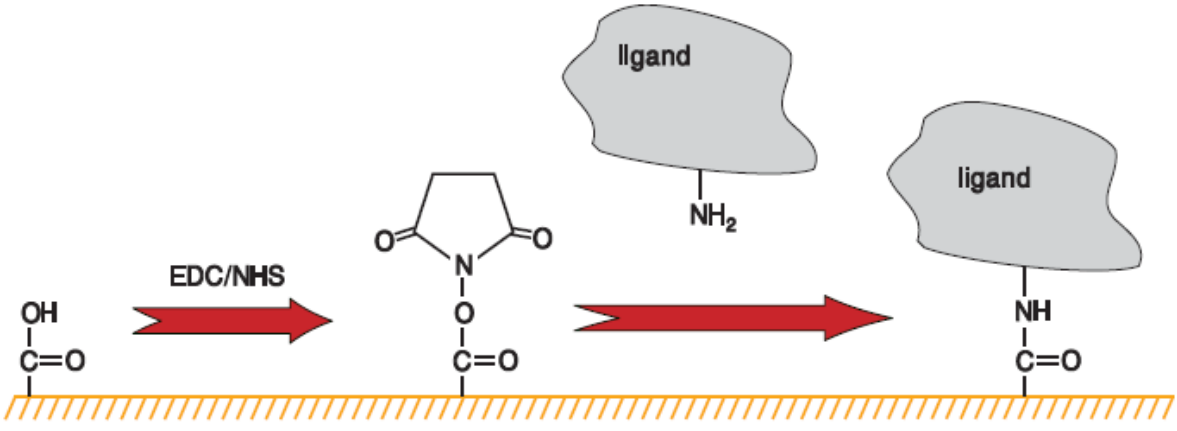

Figure 2.2: Chemistry of attachment of biomolecule to the sensor chip by amine coupling.

In this experiment, the CM5 chip was activated by a freshly made solution containing 0.05M NHS and 0.2M EDC. The solution was injected at a flow rate of 10µl/min. 20µl of 1 mg/ml CLas-ZnuA2 was dissolved in 180 µl immobilization buffer (10mM sodium acetate pH 4.5) to achieve a final concentration of 100 µg/ml. CLas-ZnuA2 solution was passed through the chip at a flow rate of 10µl/min with 0.1M HEPES pH 7.4 running buffer. Finally, 50mM NaOH was injected to remove any remaining ligand molecules. The effectiveness of protein coupling was monitored according to the sensograms obtained after CLas-ZnuA2 injection. The difference in the resonance unit (RU) at the beginning and the end of the coupling reaction represents the quantity of CLas-ZnuA2 bound onto the chip.

2.5.2. Determination of kinetics and affinities

Determination of interaction kinetics is the most characteristic application for Biacore systems. The interactions are monitored by label-free real-time detection and the results are interpreted in relation to a mathematical model of the interaction mechanism to evaluate kinetic parameters (association and dissociation rate constants). Affinity constants, which reflect the strength of binding but not the rate, can be derived either from the rate constants or from analysis of the level of binding at steady state.

2.5.2.1. Kinetic analysis

In BIAcore, kinetics of interaction is analyzed by monitoring the interaction as a function of time over a range of analyte concentrations. The whole data set was then fitted to a mathematical model describing the interaction. The association phase contains information on both association and dissociation processes, while only dissociation happens during the dissociation phase.

2.5.2.2. Affinity analysis

Interaction affinity may be determined by calculation from kinetic constants or measurement of steady-state binding levels.

A. Affinity constants from kinetics

For simple 1:1 binding, the affinity constant is equal to the ratio of the rate constants.

The kinetic evaluation procedure determines association and dissociation constants by fitting the experimental data to a 1:1 interaction model between analyte A and ligand B:

$$A+B \underset{k_d}{\overset{k_a}{\rightleftharpoons}} AB$$

Where k_a (k_{on}) is the association rate constant ($M^{-1}s^{-1}$) and k_d (k_{off}) is the dissociation rate constant (s^{-1}).

The net rate of complex formation during injection is given by

$$d[AB]= k_a [A][B]-k_d [AB]$$

and the rate of dissociation after the end of the injection is

$$\frac{d[AB]}{dt}= -k_d [AB]$$

The concentration of complex formed is measured in response units (RU) by the SPR response: if the total ligand concentration $[B]_0$ is also expressed in RU (as the maximum analyte binding capacity), the rate equations in terms of response values can be written instead of concentrations as

$$\frac{dR}{dt} = k_a CR_{max} - (k_aC+k_d)R$$

In equilibrium, the forward binding transition A+B $\longrightarrow$ AB should be balanced by the backward unbinding transition AB $\longrightarrow$ A+B. That is,

$$k_a [A] [B] = k_d [AB]$$

where [A], [B] and [AB] represent the concentration of unbound free analyte, the concentration of unbound free ligand and the concentration of analyte-ligand complexes respectively. The binding constant or the association constant K_A is defined by

$$K_A = \frac{k_a}{K_d} = \frac{[AB]}{[A]\,[B]}$$

And dissociation constant

$$K_D = \frac{1}{K_A} = \frac{k_d}{K_a} = \frac{[A]\,[B]}{[AB]}$$

B. Steady state affinity

In BIAcore, like many standard techniques, the interaction affinity can also be determined by analyzing the level of steady state or equilibrium binding as a function of interactant.

At steady state, the net rate of complex formation is zero.

$$\frac{dR}{dt} = k_a C R_{max} - (k_a C + k_d) R = 0$$

So

$$k_a C R_{max} = (k_a C + k_d) R$$

Since $R = R_{max}$ (the equilibrium response level)

$$R_{eq}\left(\frac{k_a}{k_d}\right) C + 1 = \frac{k_a}{k_d} C R_{max}$$

As $K_A = \frac{k_a}{k_d}$ $\qquad$ $Req = \frac{K_A C R_{max}}{K_A C + 1}$

The value of K_A is obtained by fitting a plot of R_{eq} against C to this equation and K_D is calculated as the inverse of K_A.

2.5.3. Kinetic assays

After the successful immobilization of CLas-ZnuA2, 10mM sodium cacodylate buffer pH 7.0 was introduced continuously until the reading reached a steady state. Kinetic experiments were also performed in running buffer 10mM sodium cacodylate pH 5.5. Two flow cells monitored the responses for the buffer running through two sensor chips that were coated with and without CLas-ZnuA2 simultaneously, and the difference in RU value detected from the two flow cells was referred to as the baseline value. 1 mM stock solutions of $MnCl_2$

and $ZnCl_2$ were prepared in 10mM sodium cacodylate buffer pH 7.0 and 5.5 and further diluted to 0.05 mM, 0.025 mM, 0.0125 mM and 0.00625 mM for kinetics experiments. The increasing concentrations of metal solutions were subsequently injected at a flow rate of 30 µl/min with contact time 180s and dissociation time of 600s. A duplicate of 0.025 mM was injected at the end. RU values increased with time and reach steady state if binding occurs. The difference in RU values between the two flow cells subtracts that of the baseline value representing the quantity of metal ions bound onto the sensor chip. At the end of each sample injection, cacodylate buffer flowed continuously over the sensor surface to monitor dissociation. After returning to a stable baseline, the sample can then be injected again. Regeneration of the sensor chip was achieved by injecting 200mM EDTA after each sample injection. All the buffers used in this study were filtered (0.22 µm) and degassed. The sensor chips could be sealed in a tube and stored dry at 4 ◦C for more than 5 months.

2.5.4. Affinity assays

For affinity analysis more range of concentrations were used by diluting the 10 mM stock solutions of $MnCl_2$ and $ZnCl_2$ prepared in 10 mM sodium cacodylate buffer pH 7 to 1.6 mM, 0.8 mM, 0.4 mM, 0.2 mM, 0.1 mM, 0.05 mM, 0.025 mM, 0.0125 mM and 0.00625 mM. Experiments were performed in a manner similar to that performed for kinetic assays taking 0.1 mM concentration as duplicate.

2.5.5. Analysis of kinetic parameters

Kinetic parameters were determined using BIAcore T200 evaluation software Version 2.0 using the model 1:1 Binding. Five different concentrations of metal ions were injected, and the sensograms were overlapped. Kinetic parameters (k_{on} and k_{off}) were evaluated by the analytical program accordingly and affinity constants were determined.

2.5.6. Quality assessment for kinetics evaluation

In BIAcore T200 evaluation software, the quality of fitting after kinetics evaluation is assessed in following areas:

1. Magnitude of kinetic constants

If either association or dissociation rate constants are close to or outside the limits that can be determined in the instrument, this is reported by the software.

2. Parameter uniqueness

In some situations, determining a value for a combined function of two or more parameters might be possible without being able to determine unique values for the individual parameters. Such parameters are said to be correlated. Parameter uniqueness is assessed by testing correlation between pairs of the parameters k_a, k_d and R_{max}. If significant correlation is found, this is reported as a warning that parameters cannot be uniquely determined.

3. Bulk refractive index

After reference subtraction and blank subtraction, sensorgrams for kinetic evaluation should not have any bulk refractive index (RI) shifts. If the fitting returns significant values for RI, a warning is reported.

4. Sensogram curvature

The sensorgrams should have sufficient curvature for kinetic determination. Sensorgrams that approximate to "square-wave" pulses (indicating rapid association and dissociation) and those that do not flatten out during the injection usually do not include sufficient kinetic information for reliable evaluation.

5. Residuals

The residuals (the difference between experimental and fitted value for each data point in the sensorgrams) lie within reasonable limits. For a perfect fit, the residuals should scatter around zero (typically ±1-2 RU).

6. Check kinetic data

Kinetic constants obtained from the fitting procedure are only significant if the observed binding is not limited by mass transport of analyte to the surface. For 1:1 binding model, a tool 'check kinetic data' is available which shows the sensitivity of fitting by observing the changes

in shapes of curves on simulating changes in kinetic constant values thereby providing information whether curves contain kinetic information or not.

2.5.7. Quality assessment for affinity evaluation

Steady state affinity evaluations are performed by fitting a plot of R_{eq} against concentration C to a model representing equilibrium 1:1 binding. The plot of R_{eq} against C approaches a limiting value at very high concentrations. As a rule of thumb, the evaluation is acceptable only if the calculated K_D value is less than half the highest analyte concentration used (For a 1:1 interaction, the K_D value is equal to the analyte concentration that gives 50% saturation of the binding sites).

2.6. Structure determination of CLas-ZnuA2 in metal-free, metal-bound and intermediate state

2.6.1. Crystallization of CLas-ZnuA2

The purified untagged protein was dialyzed in Tris-HCl buffer, pH 8.0 (buffer C) and concentrated to 7-10 mg/ml using a 5 kDa cutoff Amicon Ultra-15 concentrator before crystallization. The native protein was crystallized using sitting drop vapour diffusion method in 96 well plates at 20°C and 4°C. Crystal screens from Hampton Research were used for optimization of the crystal-growth conditions. The drops were prepared by mixing 1 µl of protein solution with 1 µl of reservoir solution and equilibrated against 50 µl reservoir solution. 1 mM $MnCl_2$ solution was added to protein before crystallization in order to enhance the crystallization prospects. Crystals were obtained in 0.1 M sodium acetate trihydrate buffer, pH 4.6 containing 2.0 M ammonium sulphate at 4 °C. The intermediate state of metal binding was captured in the crystals obtained in above conditions. Later, the metal-free and metal saturated states of protein were prepared following reported methods [38, 209].

2.6.1.1. Preparation of Metal-free state

The metal-free protein was prepared by dialysing the protein twice in 1 L sodium acetate buffer pH 4.0 containing 20 mM ethylenediamine tetraacetic acid (EDTA). The EDTA was then removed by dialysing protein in buffer C. The metal-free protein was centrifuged at

10,000 rpm for 10 min to remove any insoluble material. It was concentrated and crystallized in presence of 0.5 mM EDTA in similar crystallization conditions.

2.6.1.2. Preparation of Metal-bound states

For metal-bound state, apo-protein was dialysed in buffer C containing 100 μM $MnCl_2$/$ZnCl_2$ and excess $MnCl_2$/$ZnCl_2$ was removed by again dialysing the protein in buffer C. The metal saturated protein was crystallized using above mentioned conditions. However, data collection and structure analysis showed that metal was not present in the metal-binding site. The crystals of metal saturated protein were then soaked in precipitant solution containing 50 mM $MnCl_2$/$ZnCl_2$ for 5 min to obtain metal-bound states.

2.6.2. Data collection

For high-resolution data collection, the composition of the cryo-protectant was optimized by testing various cryo-protection agents. Crystals were cryo-protected by briefly exposing them to well solution containing 20% glycerol and mounted in the cryo-loops prior to the collection of X-ray diffraction data. Data of intermediate state were collected at home source with a MAR 345 image-plate system using Cu Kα radiation generated by a Bruker-Nonius Microstar-H rotating-anode generator. The data of metal-free and bound states were collected at X-ray crystallography facility at Institute of Microbial Technology, Chandigarh, India on a MAR345 image plate detector mounted on Rigaku MicroMax-007HF rotating anode generator. The diffraction data were processed and scaled with iMOSFLM and SCALA program in CCP4i suite [30].

2.6.3. Structure solution and refinement

A molecular replacement solution for intermediate state was obtained with automated molecular replacement pipeline BALBES [139]. The search model used was lipoprotein MtsA structure (PDB id: 3hh8) from *Streptococcus pyogenes* which shares 32% sequence identity with CLas-ZnuA2. The solution obtained was with an initial R_{factor} of 0.36. The initial models were subsequently rebuilt manually using COOT [53, 54] and refined using REFMAC 5.7 [161, 237] and PDB_REDO web server (http://xtal.nki.nl/PDB_REDO/). The quality of the final models was validated by PROCHECK [121] and MOLPROBITY [33]. Structural alignments were done using Superpose [113]. Structure figures were prepared using PyMOL

[40] and Chimera [174]. The metal-free and metal-bound structures were solved by molecular replacement by Molrep [224] using intermediate state as search model.

2.6.4. Accession number

The coordinates have been deposited in the Protein Data Bank with accession codes 4UDN (metal-free state), 4UDO (Mn^{2+}-bound state), 5AFS (Zn^{2+}-bound state) and 4CL2 (intermediate state).

3.1. Cloning, heterologous expression and purification of CLas-ZnuA2

3.1.1. PCR amplification of CLas-ZnuA2

The presence of genomic DNA of CLas in infected citrus plants was confirmed by amplification of 16S rDNA. The fragment of 1160bp size was obtained after PCR using primers specific for 16S rDNA as shown in Figure 3.1A. The CLas-ZnuA2 gene was amplified using gene specific primers with restriction sites. The fragment of 825bp size was obtained which encodes for 275 amino acids lacking coding sequence for signal peptide as shown in Figure 3.1B.

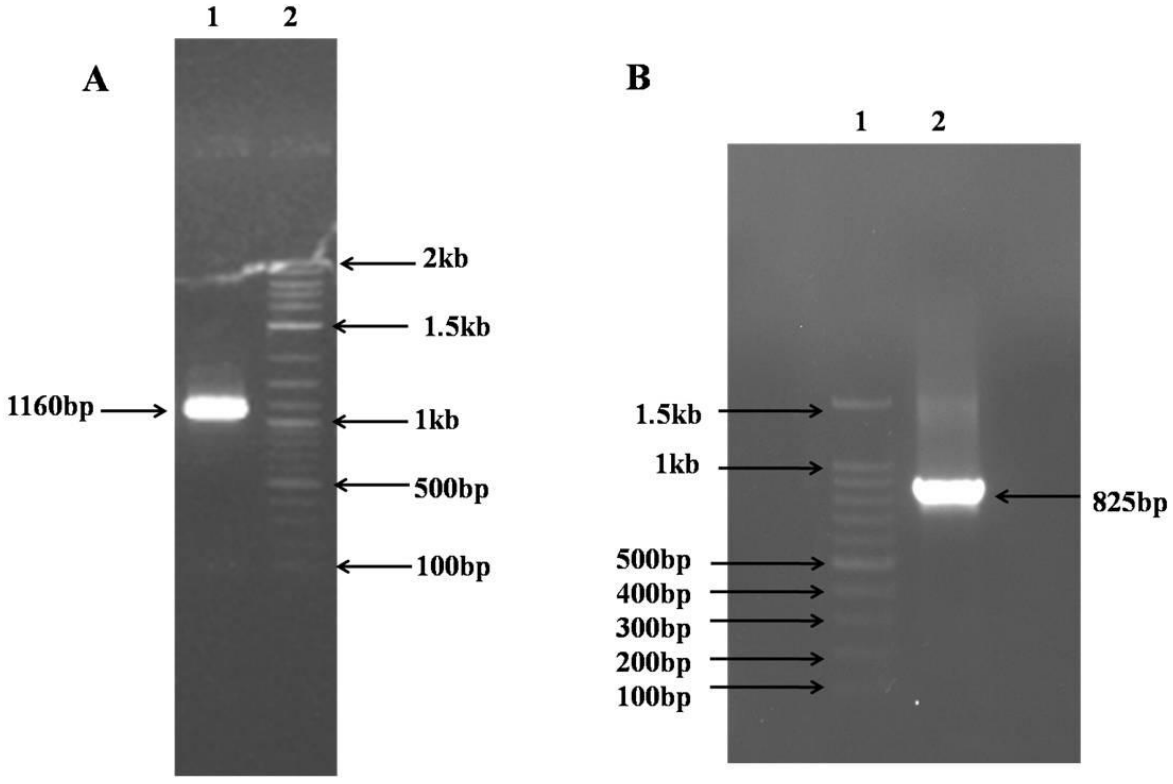

Figure 3.1: Agarose gel electrophoresis showing PCR amplification. Amplification of **A)** 16S rDNA of CLas of 1160bp (lane 1), and **B)** CLas-ZnuA2 gene of 825bp (lane 2).

3.1.2. Cloning of CLas-ZnuA2 gene

Directional cloning of CLas-ZnuA2 gene was done by restriction digestion and ligation into pET-28c expression vector. The colonies obtained through antibiotic selection plates were

screened for presence of positive clones by isolating the plasmids, which were then used as template for PCR amplification using gene specific primers, and restriction digestion of plasmids were also done using Nde I and Xho I restriction enzymes. Correct insert size of 825bp fragment was obtained after PCR amplification and restriction digestion (Figure 3.2). The sequencing result confirmed the correct frame of insert with no mutations.

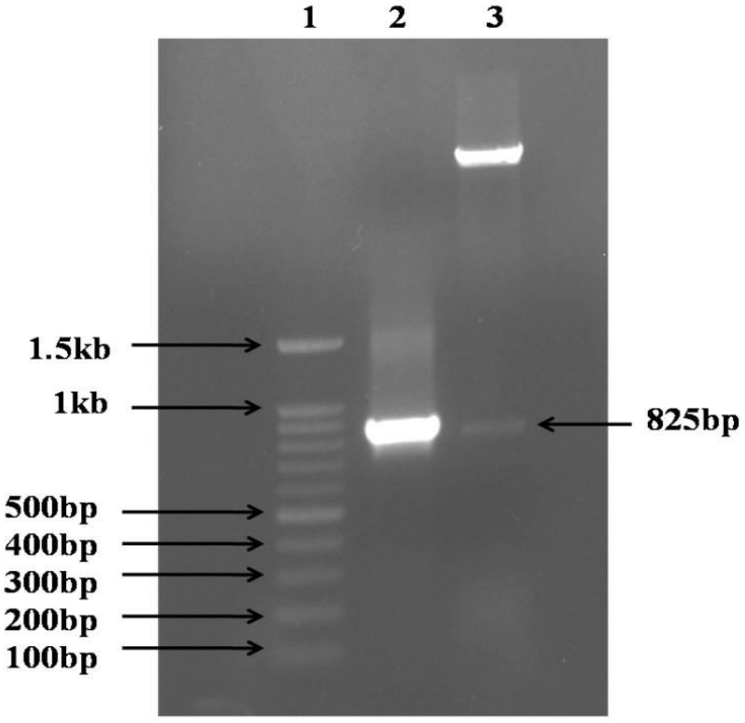

Figure 3.2: Agarose gel electrophoresis confirming the positive clones. Lane 1, DNA ladder; lane 2, PCR amplification from pET-28c plasmid containing CLas-ZnuA2 gene; lane 3, restriction digestion of pET-28c containing CLas-ZnuA2.

3.1.3. Heterologous expression of recombinant CLas-ZnuA2 protein

pET-28c vector containing CLas-ZnuA2 insert was transformed in *E. coli* BL21 cells. A very good amount of protein over-expression was seen in *E. coli* cells in soluble fraction by 0.4 mM IPTG induction at 25° C and 200 rpm. (Figure 3.3)

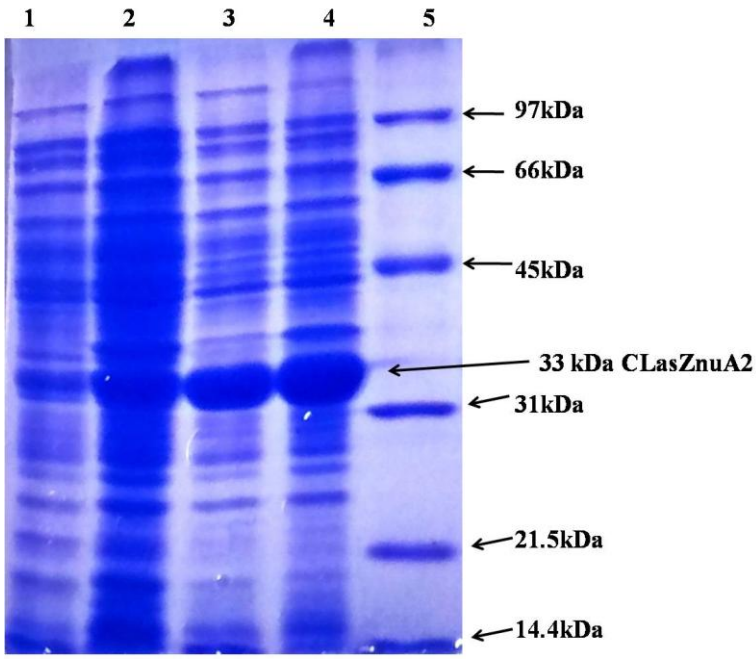

Figure 3.3: SDS-PAGE gel for the over-expression of CLas-ZnuA2. The soluble as well insoluble fractions were examined. The protein expression for the CLas-ZnuA2 and the expressed protein band is visible with high solubility. Lane 1 and 2 shows the uninduced supernatant and pellet respectively. Lane 3 and 4 presents the bands for induced cell supernatant and pellet respectively. Lane 5 shows the protein molecular weight marker.

3.1.4. Purification of recombinant CLas-ZnuA2 protein

The recombinant protein was purified using the IMAC (immobilized metal-affinity chromatography) method. The N-terminal His tag was cleaved by TEV protease and the protein was re-purified using a reverse Ni-NTA column. The flow through of the reverse Ni-NTA column containing CLas-ZnuA2 without His tag was collected and analyzed by SDS-PAGE. The difference in molecular weight was observed in SDS-PAGE before and after TEV-cleavage confirming the His-tag removal (Figure 3.4). Size exclusion chromatography suggested that CLas-ZnuA2 exists in monomeric form (Figure 3.4). Using a standard curve based on molecular-weight markers, the molecular weight of the major elution peak containing CLas-ZnuA2 protein was calculated and was estimated to be approximately 30 kDa which is in agreement with the molecular weight estimated by amino acid sequence. The estimated yield of pure protein was ~ 12 mg per liter of culture. The purified protein was concentrated to ~ 7-10 mg/ml and used for crystallization.

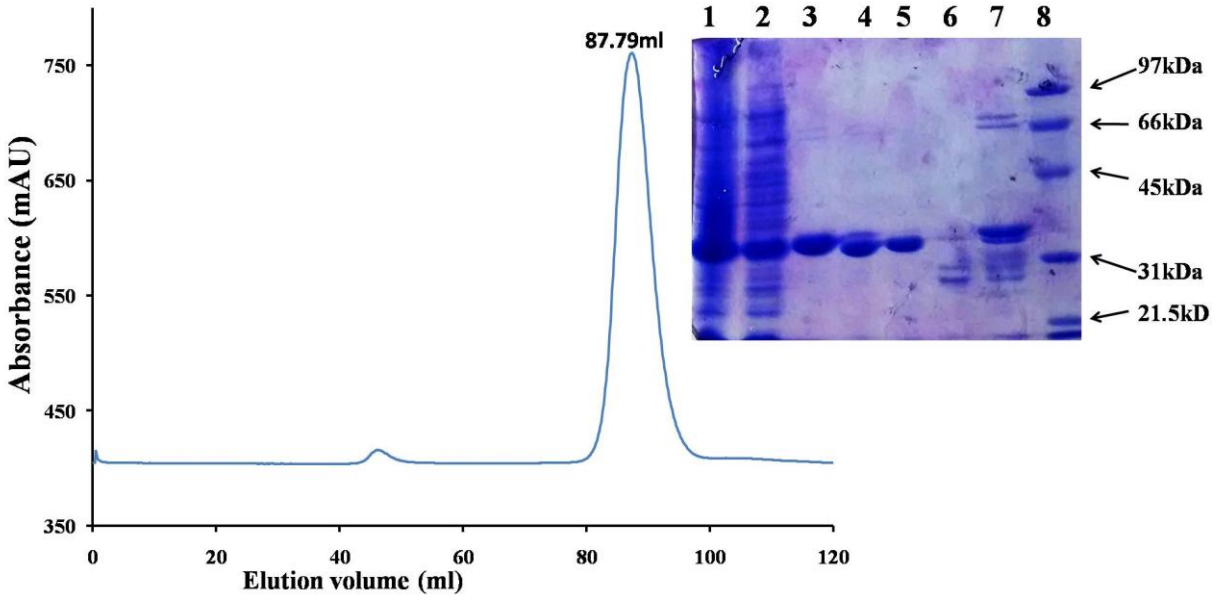

Figure 3.4: Gel-filtration profile and SDS-PAGE analysis of purified CLas-ZnuA2. Lane 1, pellet containing insoluble protein fraction; lane 2, supernatant containing soluble protein fraction; lane 3, purified His-tagged CLas-ZnuA2; lane 4, incubated mixture of purified His-tagged CLas-ZnuA2 and TEV protease; lane 5, purified CLas-ZnuA2 without His tag; Lane 6, TEV protease; lane 7, eluted proteins after reverse Ni-NTA chromatography; lane 8, Protein molecular-weight marker.

3.2. Bioinformatics analysis of CLas-ZnuA2

3.2.1. Prediction of signal peptide

CLas-ZnuA2 protein sequence (295 amino acids) showed presence of 19 residues long signal peptide at the N-terminal end as predicted by SignalP 4.1 server (Figure 3.5). The nucleotide sequence coding this signal peptide has not been included for cloning.

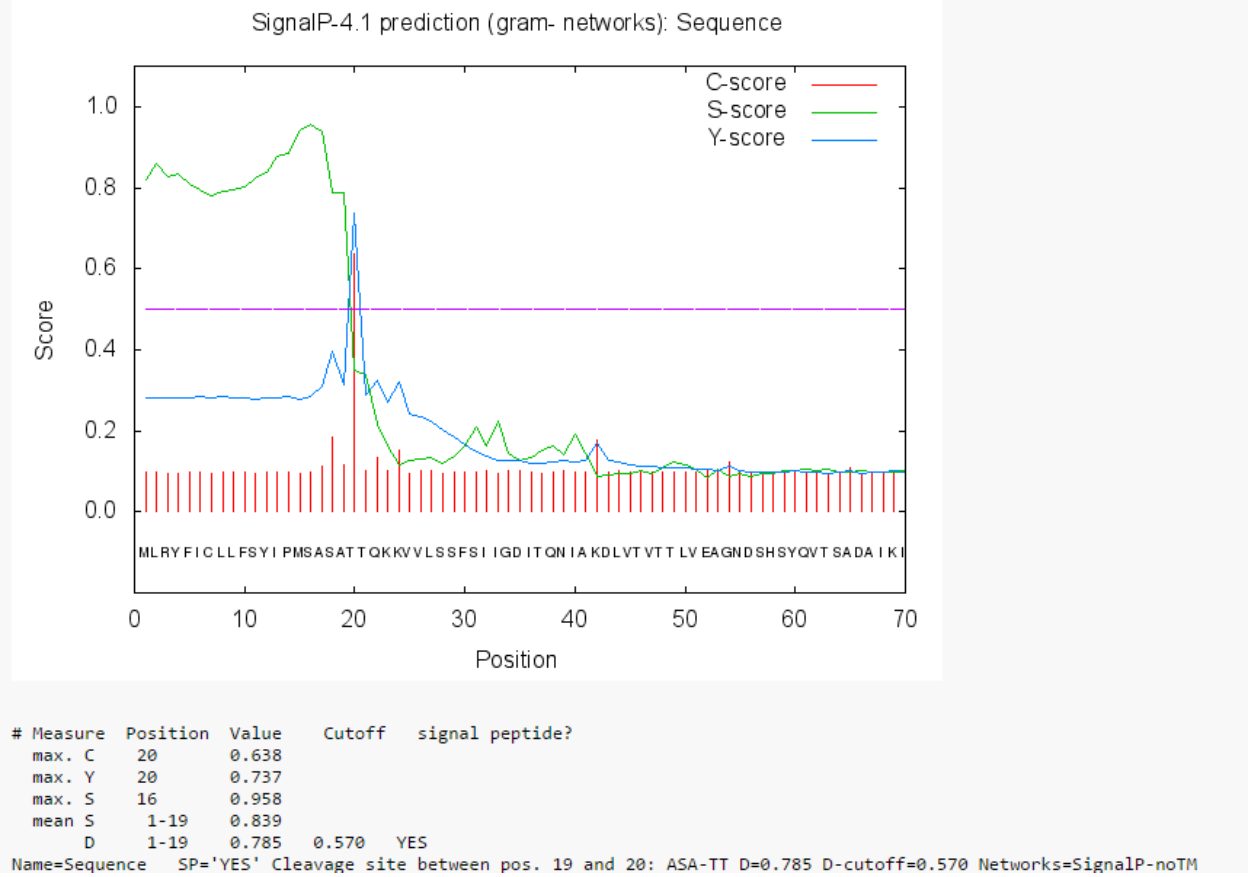

Figure 3.5: Prediction of signal sequence in CLas-ZnuA2. Signal peptide of length 19 residues (residue 1-19) in the CLas-ZnuA2 sequence as predicted by SignalP 4.0 server.

3.2.2. Amino acid sequence similarity search by NCBI-BLAST

A sequence similarity search of CLas-ZnuA2 amino acid sequence using NCBI-BLAST search engine in non-redundant (NR) and Protein Data Bank (PDB) databases showed homology to metal-transporting solute binding proteins (SBPs) of TroA like superfamily as classified by NCBI's Conserved Domain Database (CDD). These proteins belong to Cluster A-I family of substrate binding proteins.

When searched against NR database, CLas-ZnuA2 shared maximum sequence identity with periplasmic chelated iron-binding protein from *Candidatus* Liberibacter solanacearum (65%) and periplasmic solute binding protein from *Candidatus* Liberibacter americanus (60%). Other proteins which shared similarity of 50-45 % belong to families Rhizobiaceae, Pasteurellaceae, Enterobacteriaceae, Xanthobacteraceae and Vibrionaceae. When searched

against PDB database containing known structures, CLas-ZnuA2 shared maximum sequence identity to SBPs of Cluster A-I family including MntC from *Synechocystis* sp. PCC6803 (Syn-MntC) (42%), PsaA from *Streptococcus pneumoniae* (33%), MtsA from *Streptococcus pyogenes* (32%), MntC from *Staphylococcus aureaus* (Sau-MntC) (27%), TroA from *Trepanoma pallidum* (Tp-TroA) (26%), ZnuA from *Synechocystis* sp. PCC6803 (Syn-ZnuA) (24%), Adcaii from *Streptococcus Pneumoniae* (24%), ZnuA from *Salmonella enterica* (Sen-ZnuA) (22%) and ZnuA from *Escherichia coli* (Ec-ZnuA) (22%). All of these proteins are involved in binding of divalent metal ions including Mn^{2+}, Fe^{2+} or Zn^{2+} (Figure 3.6).

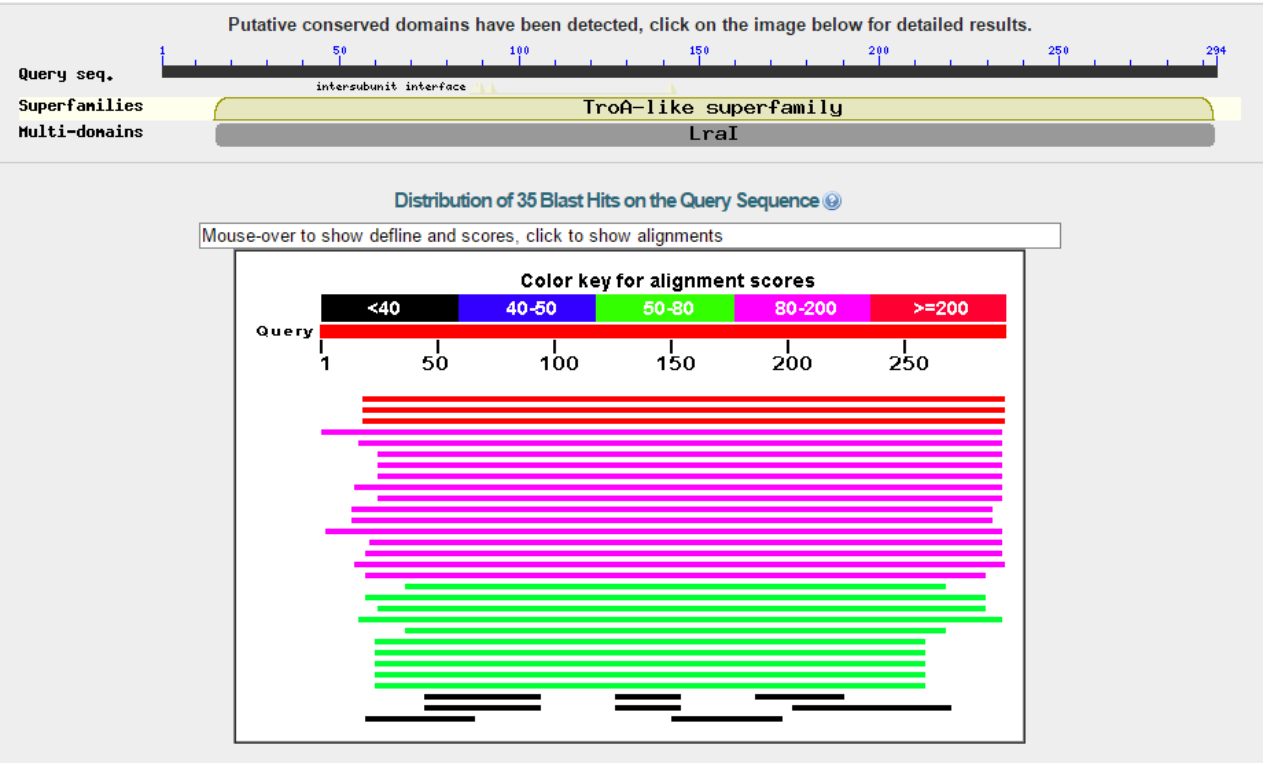

Figure 3.6: Sequence similarity search of CLas-ZnuA2 using NCBI BLAST search tool. Significant similar proteins (maximum 42%) were found in PDB database which belong to Cluster A-I family and involve in divalent metal ion transport.

3.2.3. Multiple sequence alignment

Multiple sequence alignment (MSA) of CLas-ZnuA2 and related proteins present in PDB database revealed the four conserved metal coordinating residues present in CLas-ZnuA2 (Figure 3.7). These are His39, His106, Glu172 and Asp247, which are known to be specific for

either Mn or Fe-binding. Out of the three conserved Trp residues in Mn-SBPs, only two are present in CLas-ZnuA2, while only one Trp is conserved among all Cluster A-I SBPs. There are two cysteines (Cys59 and Cys174) present in CLas-ZnuA2. These cysteines are not involved in disulfide bond formation as observed in Syn-MntC, Ec- ZnuA and Sen-ZnuA [31, 97, 185]. The CLas-ZnuA2 shared only 22% sequence identity with ZnuA of first ZnuABC homologue (CLas-ZnuA1) from CLas. The presence of three conserved His and one Asp as coordinating residues in CLas-ZnuA1 clearly indicated its role in Zn uptake, as evident from the related Zn-binding proteins, which also possess same conserved metal binding residues.

MSA of CLas-ZnuA2 and related proteins present in NR database (Figure 3.8) showed the presence of four conserved residues specific for Mn/Fe binding (2 His, 1 Glu and 1 Asp) in all proteins. Other residues are also conserved among these proteins for example Pro153 and PNPH motif (residues 103-106) is present in all the sequences along with other conserved regions.

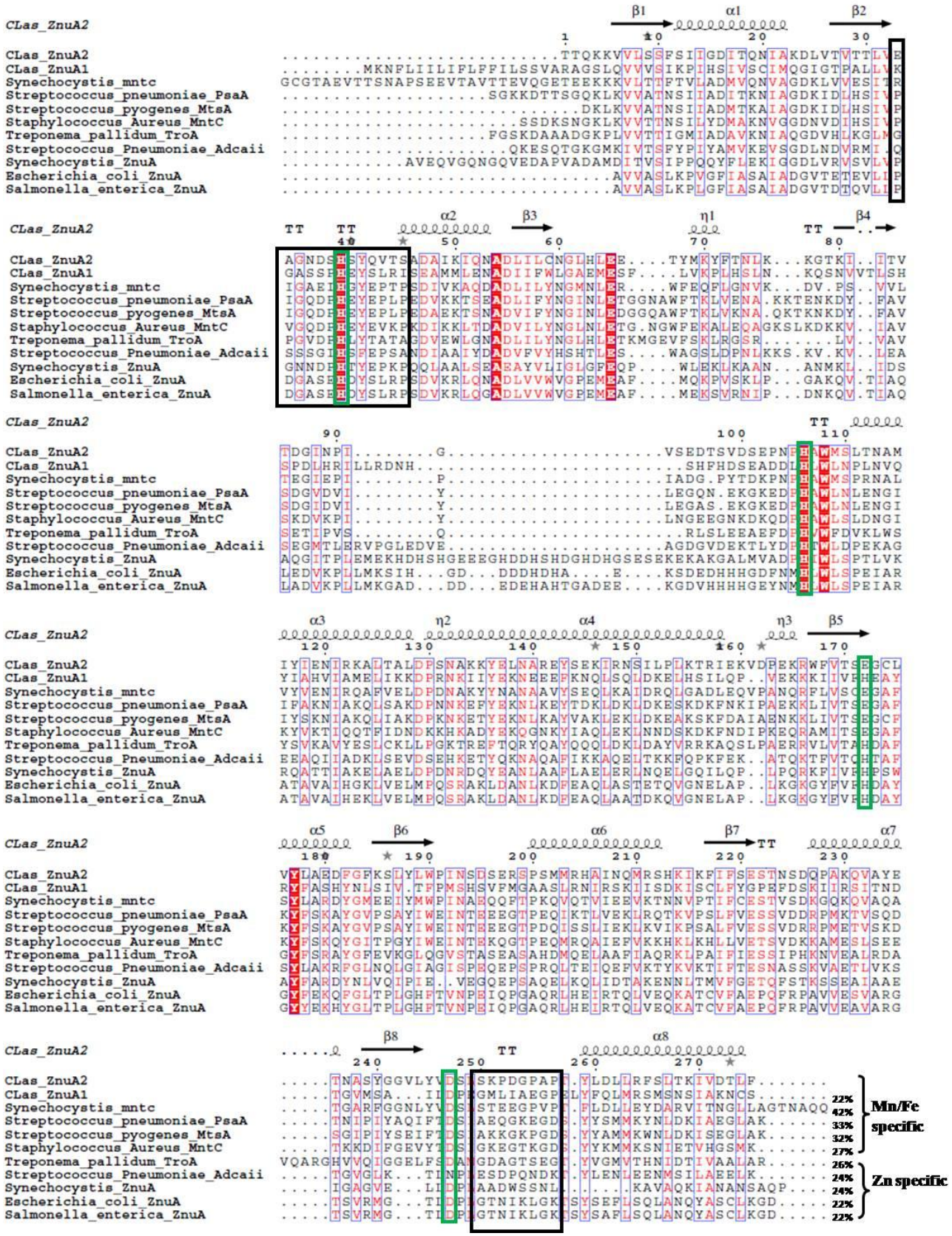
CLas_ZnuA2
CLas_ZnuA1
Synechocystis_mntc
Streptococcus_pneumoniae_PsaA
Streptococcus_pyogenes_MtsA
Staphylococcus_Aureus_MntC
Treponema_pallidum_TroA
Streptococcus_Pneumoniae_Adcaii
Synechocystis_ZnuA
Escherichia_coli_ZnuA
Salmonella_enterica_ZnuA
Mn/Fe specific
Zn specific

Figure 3.7: Multiple sequence alignment of CLas-ZnuA2 with other related Cluster A-I SBPs. The Cluster A-I protein sequences available in PDB database showing maximum identity (involved in Mn^{2+}, Zn^{2+} or Fe^{2+} uptake) along with CLas-ZnuA2 and CLas-ZnuA1 (ZnuA of first homologous ZnuABC system from CLas) were aligned. The residues involved in metal binding are shown in green boxes. Black boxes indicate differences in distribution of Pro between CLas-ZnuA2 and other Cluster A-I SBPs.

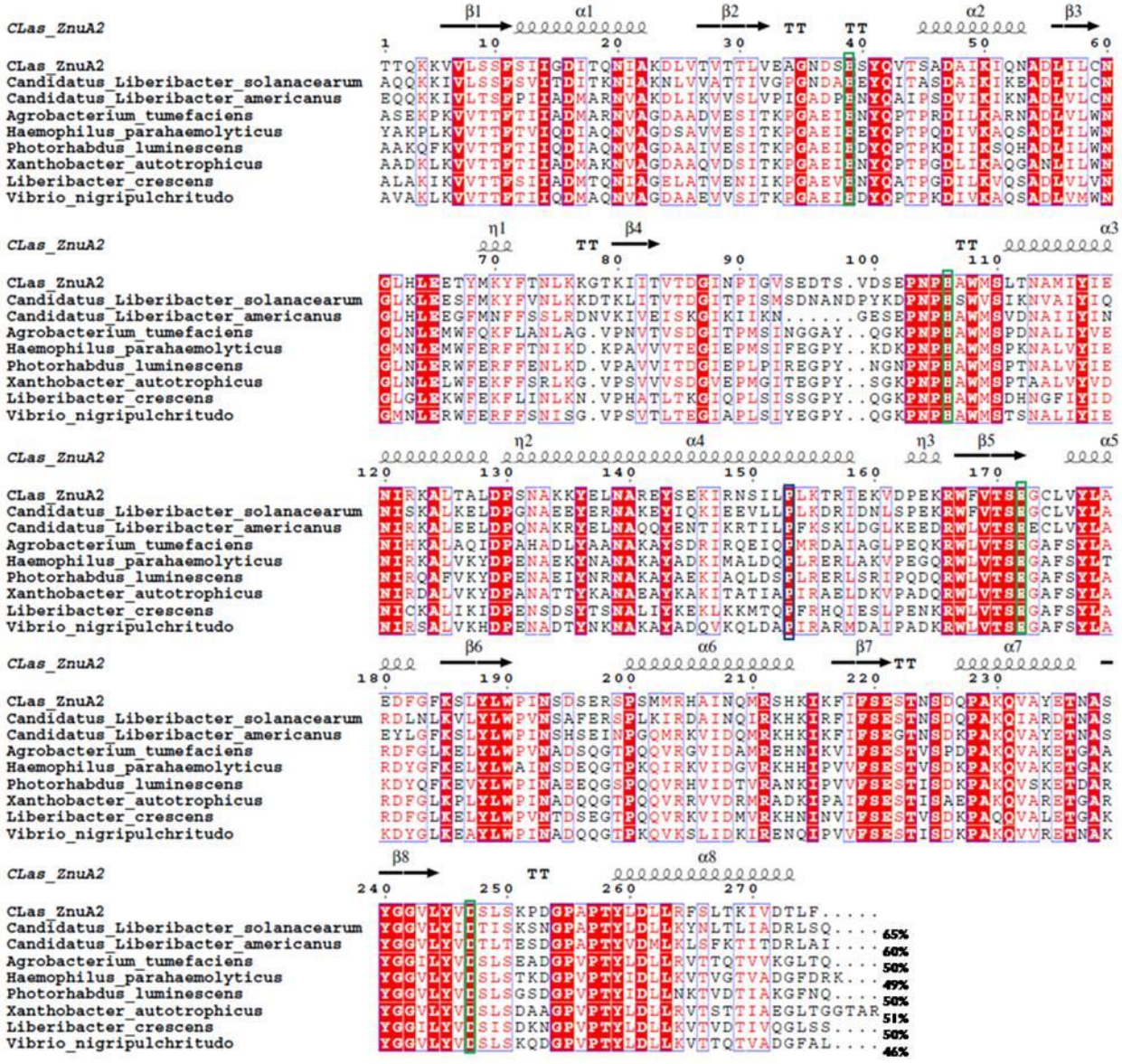

Figure 3.8: Multiple sequence alignment of CLas-ZnuA2 with other related proteins present in NR database. One representative member from each family is included for MSA. *Agrobacterium tumefaciens* from Rhizobiaceae, *Haemophilus parahaemolyticus* from Pasteurellaceae, *Photorhabdus luminescens* from Enterobacteriaceae, *Xanthobacter autotrophicus* Xanthobacteraceae and *Vibrio nigripulchritudo* from Vibrionaceae. Conserved metal binding residues are shown in green boxes and conserved Pro153 is shown in blue box.

3.2.4. Phylogenetic analysis

The phylogenetic analysis of related Cluster A-I proteins present in both NR database and PDB database showed that the tree can be divided into three groups. First group included proteins from NR database. CLas-ZnuA2 is also present in this group along with Syn-MntC which shared maximum identity (42%). The second group contained proteins from PDB database specific for Mn/Fe binding, whereas, third group included proteins from PDB database specific for Zn binding (Figure 3.9).

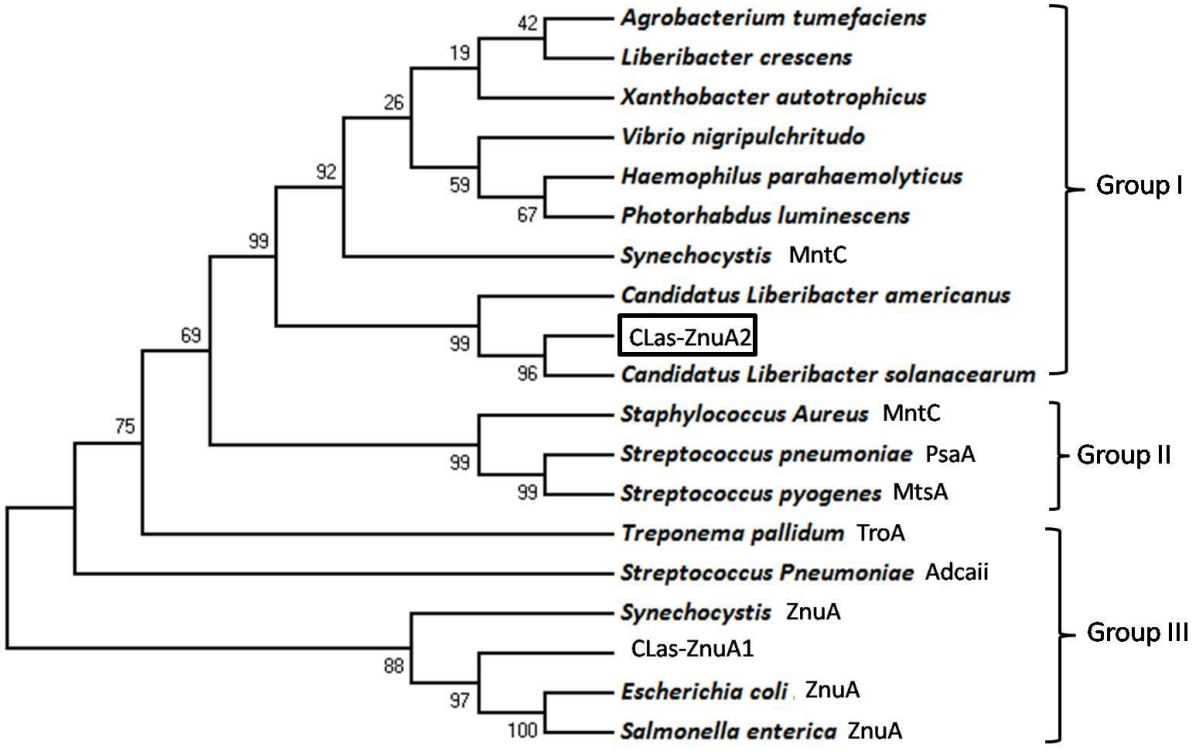

Figure 3.9: Phylogenetic tree of CLas-ZnuA2 and related proteins present in PDB database and NR database constructed by the maximum likelihood method. From NR database, the similar proteins were included in analysis as those taken in MSA. Group I included proteins from NR database while Group II and III includes proteins from PDB database specific for Mn/Fe and Zn binding respectively. The numbers above and below the branch points indicate the confidence levels for the relationship of the paired sequences as determined by bootstrap statistical analysis. The tree is drawn to scale, with branch lengths measured in the number of substitutions per site.

The phylogenetic analysis of related proteins available in PDB database showed that CLas-ZnuA2 clustered with Mn/Fe-specific solute binding proteins (Mn-SBPs) (Figure 3.10).

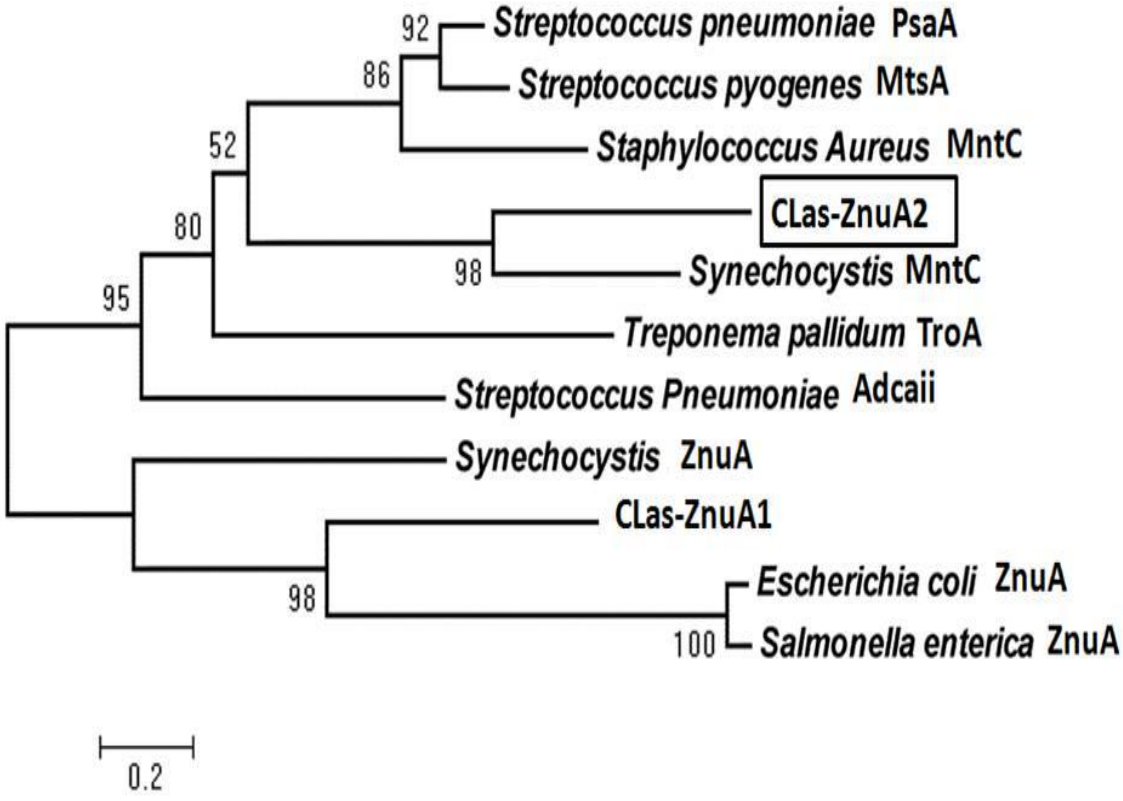

Figure 3.10: Phylogenetic tree of CLas-ZnuA2 and other Cluster A-I proteins present in PDB database along with CLas-ZnuA1 constructed by the maximum likelihood method. The tree shows clustering of CLas-ZnuA2 with Mn-specific SBPs. The numbers above and below the branch points indicate the confidence levels for the relationship of the paired sequences as determined by bootstrap statistical analysis. The tree is drawn to scale, with branch lengths measured in the number of substitutions per site.

3.3. Surface Plasmon Resonance

Surface plasmon resonance (SPR) is a powerful instrument to monitor real time kinetics of binding of two partners. Two types of analyses can be done by SPR to determine the equilibrium constants of an interaction: kinetic analysis and affinity analysis as described in Chapter 2. Here initially, we tried to determine the kinetic parameters of CLas-ZnuA2 upon

binding of Mn^{2+} and Zn^{2+} ions by performing number of experiments (Figure 3.11-3.15). Analysis of the sensograms was done using model for 1:1 binding. The k_a/k_{on} and k_d/k_{off} along with K_D has been shown in Table 3.1 for Mn^{2+} and Zn^{2+} binding at pH 7 and 5.5.

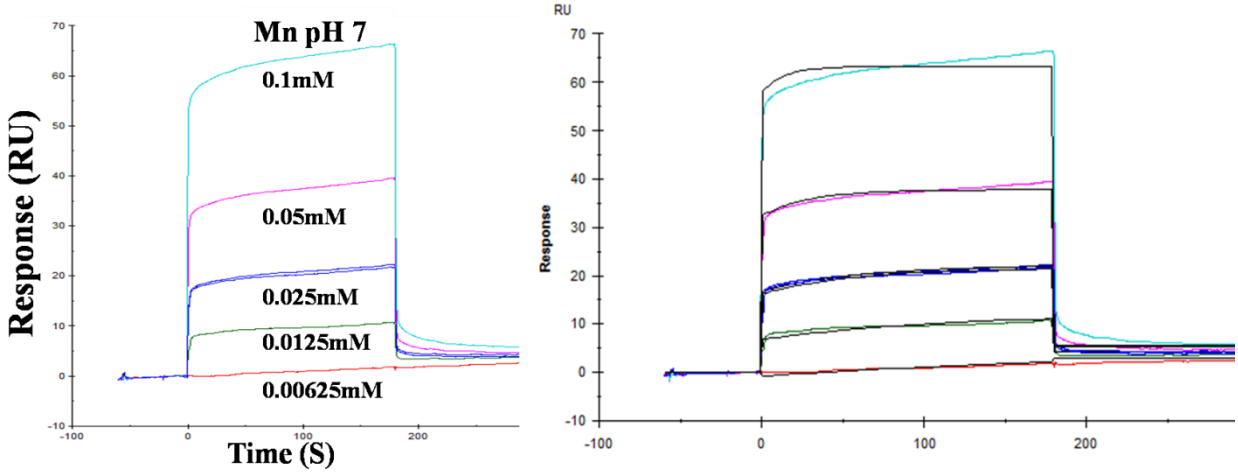

Figure 3.11: SPR sensogram showing CLas-ZnuA2-Mn^{2+} interaction in Experiment 1. The sensogram shows binding kinetics of CLas-ZnuA2 for Mn^{2+} at pH 7 along with the fitting curves obtained from fittings using 1:1 binding model as determined by Experiment 1. The representative fitting curves of sensogram for metal ions binding is shown in black color.

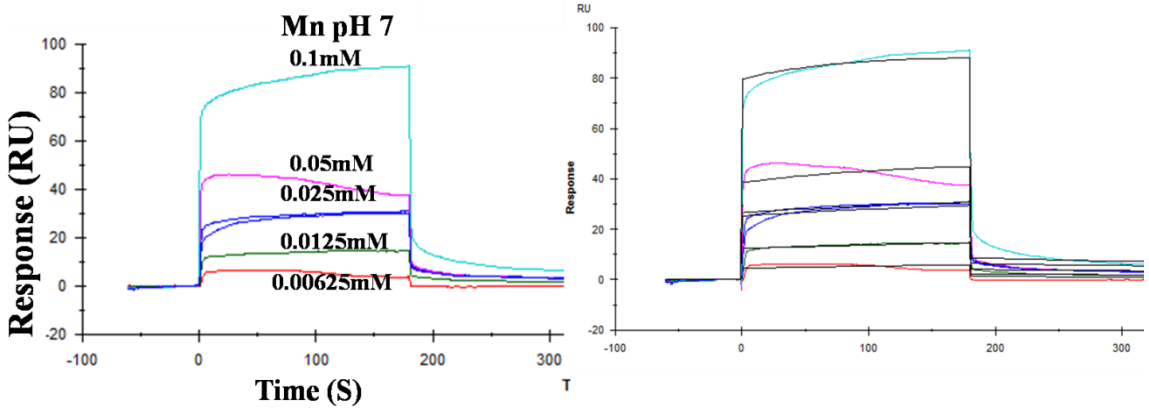

Figure 3.12: SPR sensogram showing CLas-ZnuA2-Mn^{2+} interaction in Experiment 2. The sensogram shows binding kinetics of CLas-ZnuA2 for Mn^{2+} at pH 7 along with the fitting curves obtained from fittings using 1:1 binding model as determined by Experiment 2. The representative fitting curves of sensogram for metal ions binding is shown in black color.

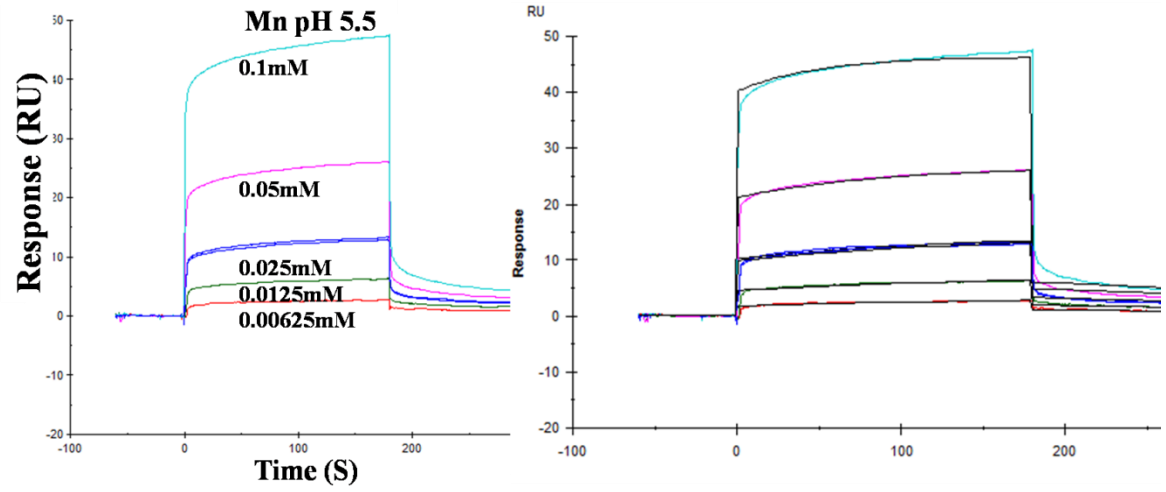

Figure 3.13: SPR sensogram showing CLas-ZnuA2-Mn^{2+} interaction in Experiment 3. The sensogram shows binding kinetics of CLas-ZnuA2 for Mn^{2+} at pH 5.5 along with the fitting curves obtained from fittings using 1:1 binding model as determined by Experiment 3. The representative fitting curves of sensogram for metal ions binding is shown in black color.

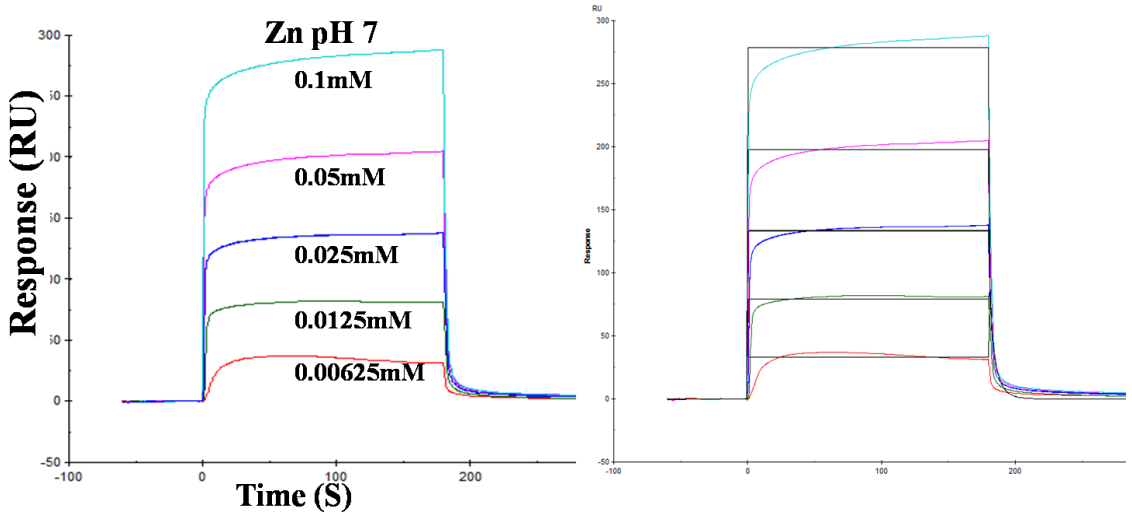

Figure 3.14: SPR sensogram showing CLas-ZnuA2-Zn^{2+} interaction in Experiment 4. The sensogram shows binding kinetics of CLas-ZnuA2 for Zn^{2+} at pH 7 along with the fitting curves obtained from fittings using 1:1 binding model as determined by Experiment 4. The representative fitting curves of sensogram for metal ions binding is shown in black color.

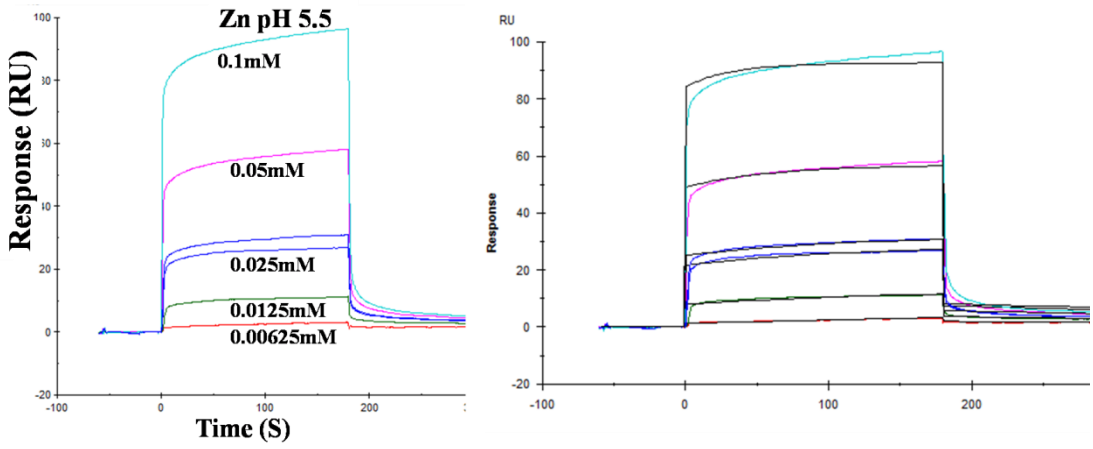

Figure 3.15: SPR sensogram showing CLas-ZnuA2-Zn^{2+} interaction in Experiment 1. The sensogram shows binding kinetics of CLas-ZnuA2 for Zn^{2+} at pH 5.5 along with the fitting curves obtained from fittings using 1:1 binding model as determined by Experiment 5. The representative fitting curves of sensogram for metal ions binding is shown in black color.

However, since for all the kinetic experiments, the quality of the fit was not reliable as reported by the quality control parameters assessed by the software (Table 3.2), therefore trials to determine the affinity constants by steady state affinity analysis experiments were done (Figure 3.16 and 3.17). By this method reliable values of K_D of CLas-ZnuA2 for Mn^{2+} and Zn^{2+} were obtained successfully which were found to be of almost equal order with Mn^{2+} having slightly higher affinity (Table 3.3).

Table 3.1: Kinetic parameters of metal ion-CLas-ZnuA2 interactions determined by SPR using CM5 sensor chip.

Expt.	Metal	pH	k_{on} or k_a (M^{-1} s^{-1})	k_{off} or k_d (s^{-1})	K_D (M)	Chi^2
1	Mn^{2+}	7	702.7	$1.9*10^{-6}$	$2.754*10^{-9}$	0.953
2	Mn^{2+}	7	132.1	0.001332	$1.012*10^{-5}$	3.39
3	Mn^{2+}	5.5	179.5	0.002283	$1.272*10^{-5}$	0.349
4	Zn^{2+}	7	$1.454*10^{8}$	00.5712	$3.928*10^{-9}$	31.3
5	Zn^{2+}	5.5	286	0.001770	$6.188*10^{-6}$	3.17

Table 3.2: Reliablity of fitting of SPR kinetic experiments as indicated by quality control areas reported by the software. The expt. no. mentioned are similar to those given in Table 3.1.

Expt. No.	Magnitude of kinetic constants	Parameter uniquenes s	Bulk refractive index	Sensorgram curvature	Residuals	Kinetic data
1	×	×	×	×	×	×
2	×	✓	×	×	×	✓
3	×	✓	×	×	×	✓
4	×	×	×	×	×	×
5	×	✓	×	×	×	✓

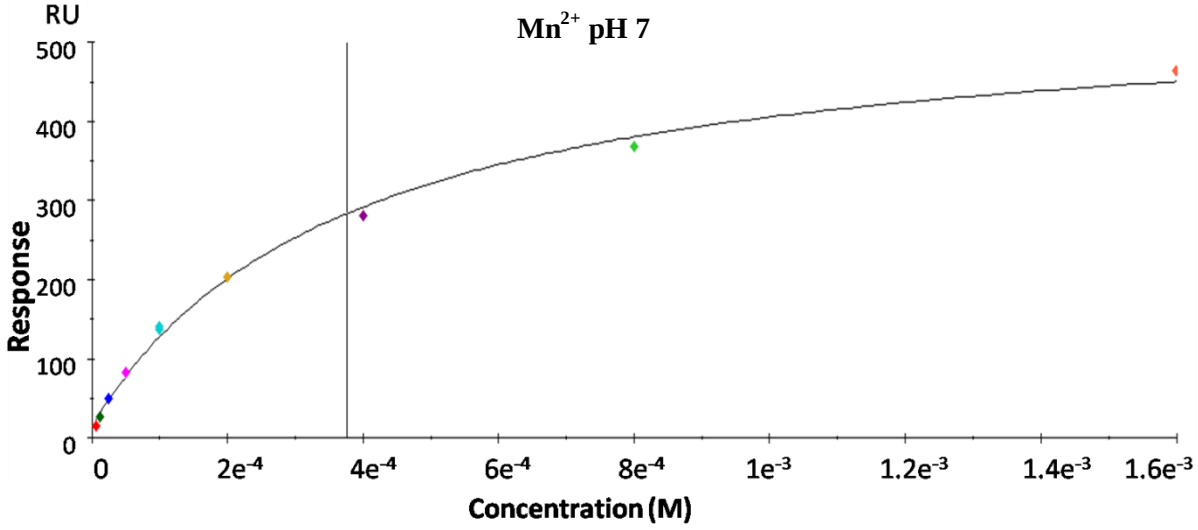

Figure 3.16: Graph showing plot of response R_{eq} against concentration of Mn^{2+} injected. K_D value is represented by vertical line.

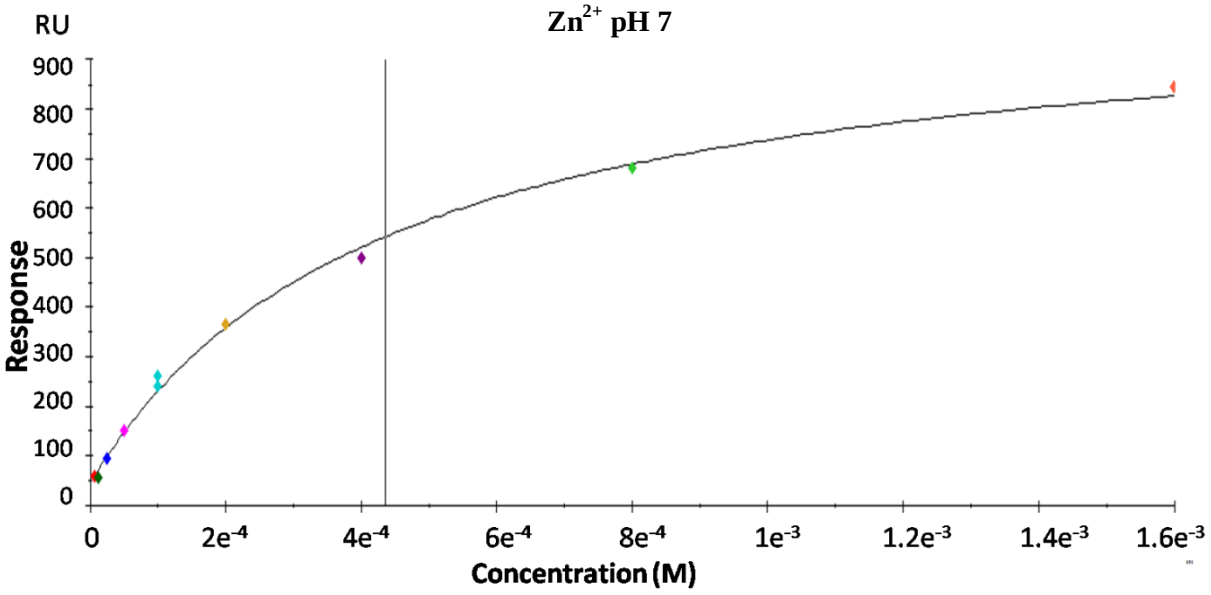

Figure 3.17: Graph showing plot of response R_{eq} against concentration of Zn^{2+} injected. K_D value is represented by vertical line.

Table 3.3: Equilibrium constant **(**K_D) values reported by steady state affinity analysis of CLas-ZnuA2 for Mn^{2+} and Zn^{2+} along with the quality assessment.

Expt.	Metal	pH	K_D(M)	Chi^2	Quality assessment K_D <1/2 highest analyte concentration
1	Mn^{2+}	7	$3.7*10^{-4}$	122	✓
2	Zn^{2+}	7	$4.3*10^{-4}$	309	✓

3.4. Circular dichroism

Circular dichroism technique could be used for studying thermal stability of proteins in different conditions, in this case, in presence of different metal ion concentrations. Far-UV circular dichroism studies (wavelength range of 250-200 nm) were performed in the temperature range of 20-70°C for metal-free CLas-ZnuA2 and in presence of different concentrations of $MnCl_2$ and $ZnCl_2$ (concentrations used were 10 µM, 20 µM, 50 µM, 100 µM, 500 µM, 1 mM and 10 mM). Efforts to record data below 205 nm at increasing temperatures were not successful because of excessive noise. CD spectra of metal-free protein contained negative peaks at around 208 nm and 222 nm, which clearly showed that it contains good

amount of α-helices. Analysis of effect of temperature on metal-free state by increasing the temperature revealed that it begins to unfold at 45°C as shown by the loss of signals in the CD spectra at 45°C (Figure 3.18). On adding $MnCl_2$ to metal-free state, there is no change observed for concentrations 10 µM (1:1), 20 µM (1:2) and 50 µM (1:5) as shown in Figure 3.18, where protein starts to unfold at 45°C, as in the case of metal-free state. Whereas, when the concentration of $MnCl_2$ is increased to 100 µM (1:10), 500 µM (1:50), 1 mM (1:100) and 10mM (1:1000), the temperature of unfolding of CLas-ZnuA2 increased to 55°C, 60°C, 65°C and 70°C respectively (Figure 3.18). Similarly, addition of 10 µM, 20 µM and 50 µM $ZnCl_2$ did not have any effect on CD spectra and proteins started to unfold at 45°C. Addition of 100 µM $ZnCl_2$ stabilized the protein more than $MnCl_2$ and protein was stable up to 60°C, however, further addition of $ZnCl_2$ to 500 µM, 1 mM and 10 mM did not increased the protein stability (Figure 3.19). In fact protein began to destabilize on further $ZnCl_2$ addition, as the CD spectra at 60°C is observed to be shifting upwards suggesting unfolding. This suggested that Mn^{2+} makes the protein more stable at higher concentrations than Zn^{2+} while both the ions stabilize the protein in comparison to its apo-state.

Efforts to perform SPR and CD experiments with Fe^{2+} were not successful which might be due to susceptibility of Fe^{2+} ion to quickly oxidize to Fe^{3+}.

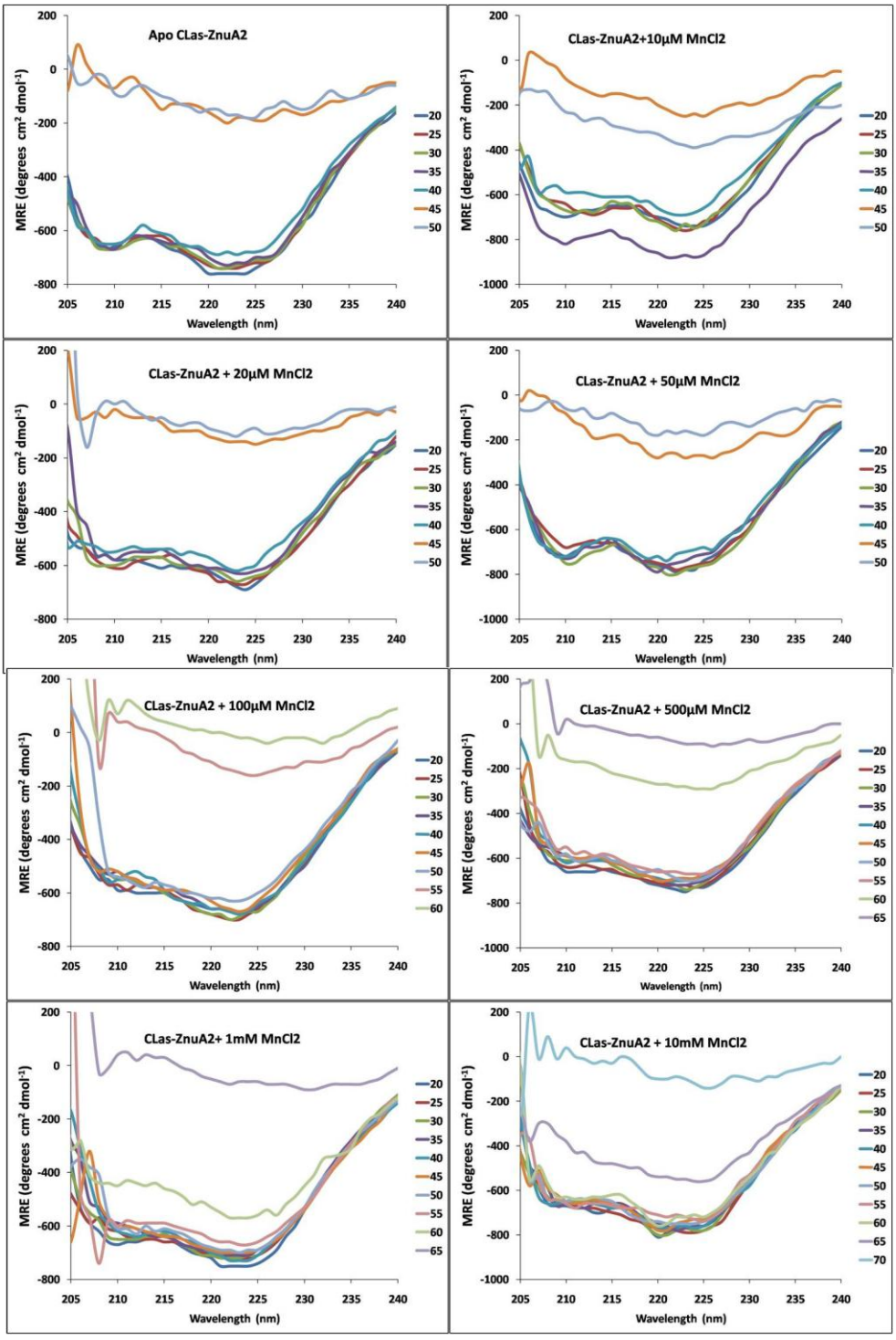

Figure 3.18: **Circular dichroism spectra showing differences in temperature of unfolding of metal-free CLas-ZnuA2 and after adding $MnCl_2$ in different concentrations.** The concentrations of $MnCl_2$ added were 10 µM (1:1), 20 µM (1:2) and 50 µM (1:5) 100 µM (1:10), 500 µM (1:50), 1 mM (1:100) and 10mM (1:1000).

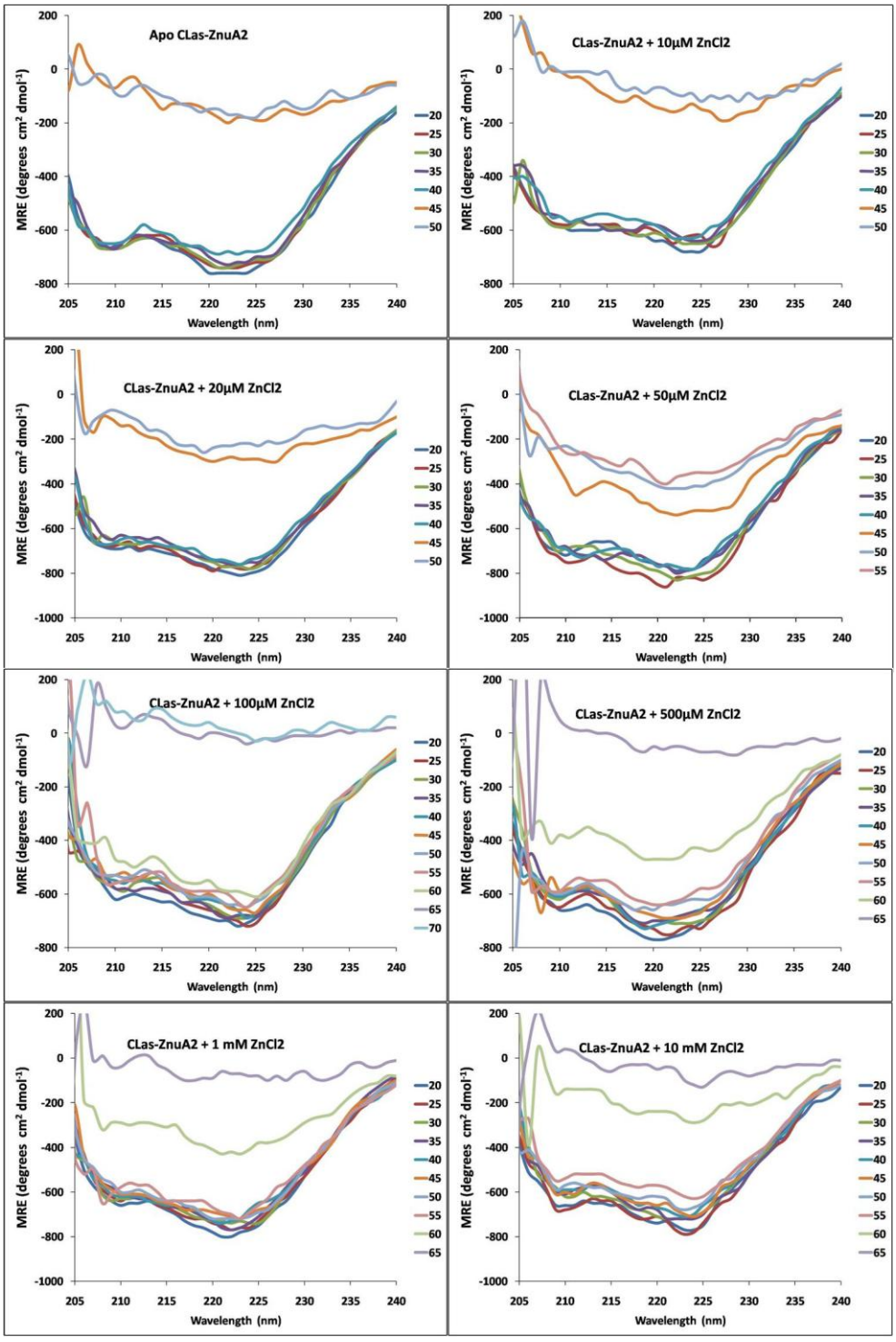

Figure 3.19: **Circular dichroism spectra showing differences in temperature of unfolding of metal-free CLas-ZnuA2 and after adding $ZnCl_2$ in different concentrations.** The concentrations of $ZnCl_2$ added were 10 µM (1:1), 20 µM (1:2) and 50 µM (1:5) 100 µM (1:10), 500 µM (1:50), 1 mM (1:100) and 10mM (1:1000).

3.5. Crystal development and data collection

Crystals of CLas-ZnuA2 were obtained in 15-20 days at 4°C using 0.1 M sodium acetate trihydrate buffer, pH 4.6 containing 2.0 M ammonium sulphate. When 1 mM $MnCl_2$ was added in order to enhance crystallization process, crystals obtained were of CLas-ZnuA2 in intermediate state of metal binding. The crystals of intermediate state were diffracted to 1.55 Å resolution but only data up to 1.65 Å was used for scaling and refinement. The metal-free form of CLas-ZnuA2 was prepared by dialyzing the protein in sodium acetate buffer containing 20mM EDTA. The crystals of metal-free form were diffracted to 2.22 Å resolution (Figure 3.20[198].

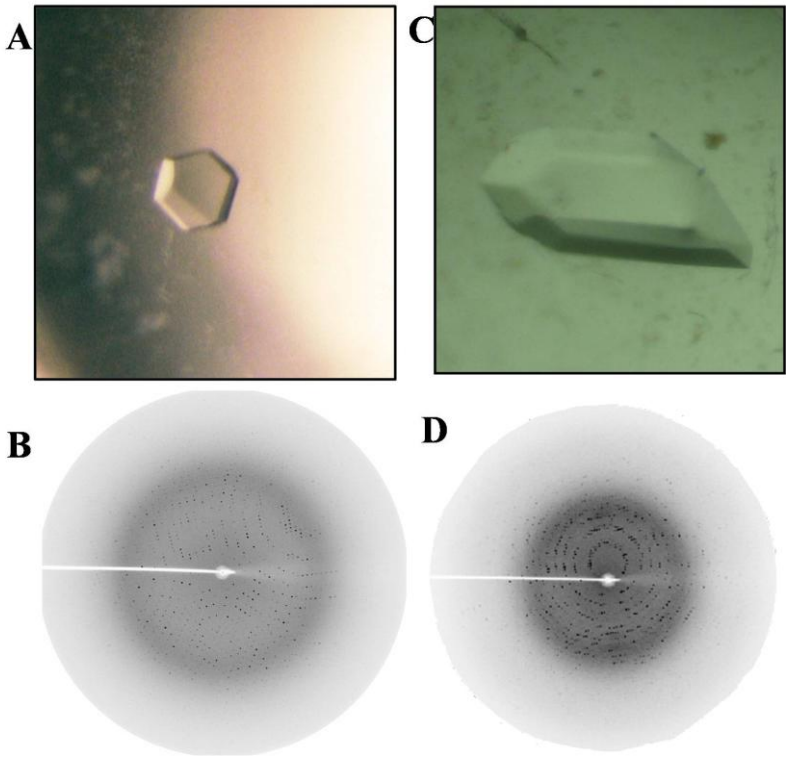

Figure 3.20: Crystals obtained and diffraction pattern of CLas-ZnuA2. A) and **B)** metal free state; **C)** and **D)** intermediate state.

The Mn^{2+} and Zn^{2+}-bound forms were obtained by soaking the crystals in reservoir solution containing 50 mM $MnCl_2$ and $ZnCl_2$ respectively. The data for Mn-bound and Zn-bound form were diffracted to 2.22 Å (Figure 3.21).

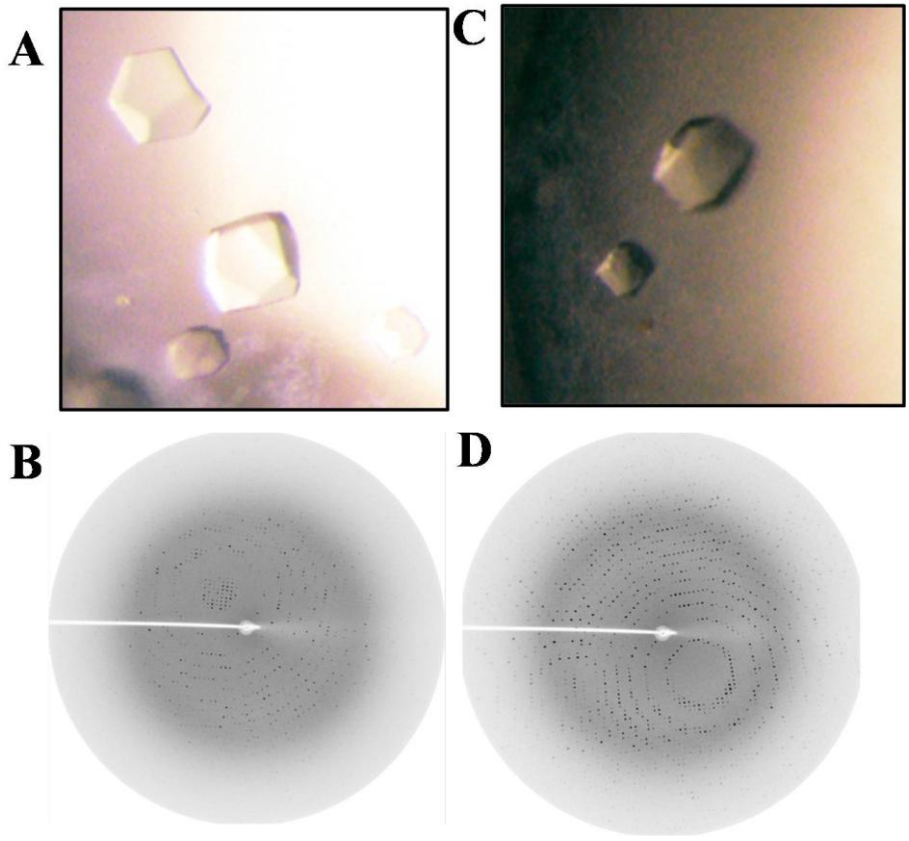

Figure 3.21: Crystals obtained and diffraction pattern of CLas-ZnuA2. A) and **B)** Mn^{2+}-bound state; **C)** and **D)** Zn^{2+}-bound state.

The data-collection statistics for the metal-free, intermediate and metal-bound crystals are summarized in Table 3.4.

Table 3.4: Crystal parameters and data collection parameters for all and structure refinement.

Data collection	**Metal-free CLas-ZnuA2**	**Intermediate CLas-ZnuA2**	**Mn^{2+}-bound CLas-ZnuA2**	**Zn^{2+}-bound CLas-ZnuA2**
Space group	$P3_221$	$P3_221$	$P3_221$	$P3_221$
Unit-cell parameters (Å)				
a	94.53	94.06	94.32	94.37
b	94.53	94.06	94.32	94.37
c	94.36	94.51	94.33	94.43
α, β, γ, (°)	90, 90, 120	90, 90, 120	90, 90, 120	90, 90, 120
Resolution range (Å)	47.18-2.21 (2.33-2.21)	30.85-1.63 (1.72-1.63)	47.18-2.21 (2.33-2.21)	47.22-2.22 (2.33-2.21)
Total reflections	106552	463999	189782	280541
Unique reflections	23857	57802	24410	24473
Completeness (%)	96.3(85.4)	95.4(92.1)	98.9(92.8)	98.9(92.5)
R_{merge} [a]	0.135(0.666)	0.073(0.918)	0.091(0.329)	0.051(0.163)
Multiplicity	4.5(4)	8.0(6.7)	7.8(6.9)	11.5(10.4)
Mean I/σ(I)	10(3.4)	18.5(2.1)	19.3(6.0)	37.2(15.6)

Values in parentheses are for the outermost shell.

a. Rmerge=ΣhklΣi|Ii(hkl)-<I(hkl)>|/ΣhklΣiIi(hkl), where Ii(hkl) is the intensity of an observation and <I(hkl)> is the mean value for its unique reflection; Summations are over all reflections.

The crystals belonged to the trigonal space group $P3_221$ with one molecule per asymmetric unit. The solvent content of all the crystals was much higher ~70 % with Matthews coefficient of 2.0 $Å^3$ Da^{-1}.

3.6. Three-dimensional structure of CLas-ZnuA2

3.6.1. Structure of CLas-ZnuA2 in metal-free state

3.6.1.1. Quality of the model

The crystal structure of CLas-ZnuA2 has been determined in metal-free state to 2.2 Å resolution. The refinement data statistics in Table 3.5 shows that the model is well refined with excellent stereochemistry and crystallographic *R* factor values. The electron density is well defined except for the three N-terminal residues and the two loop regions (involving residues 97-99) with no electron density and residues 194-199 with a weak electron density. The three

N-terminal and some residues in two loops (residues 97-99 and 195-197) were not included in models. The final model of metal-free state consisted of 266 amino acid residues, 171 waters, 5 sulphate ions, 1 acetate ions and 4 glycerol molecules.

Table 3.5: Refinement statistics for metal-free state of CLas-ZnuA2

Data resolution	42.3-2.21
Number of reflections used/free	21314/1209
Biological units per asymmetric unit	1
Wilson B-factor ($Å^2$)	22
Crystallographic R-factor (%)	18.4
Free R-factor (%)	22.3
Average *B*-factors ($Å^2$)	
All atoms	31.4
Protein atoms	31.29
Water atoms	34.21
Ligand atoms	51.18
r.m.s.d. for bond length(Å)/bond angle (°)	0.010/1.273
Ramachandran plot	
Favoured (%)	97.3
Allowed (%)	2.7
Outliers (%)	0

3.6.1.2. Overall structure

The overall structural organization of CLas-ZnuA2 is similar to the related cluster A-I SBPs. It consists of a pair of N and C-terminal $(\alpha/\beta)_4$ sandwich domains linked through a long rigid backbone α-helix running across two domains (Figure 3.22). The partially solvent exposed cleft of N- and C-domain interface constitutes the metal binding site.

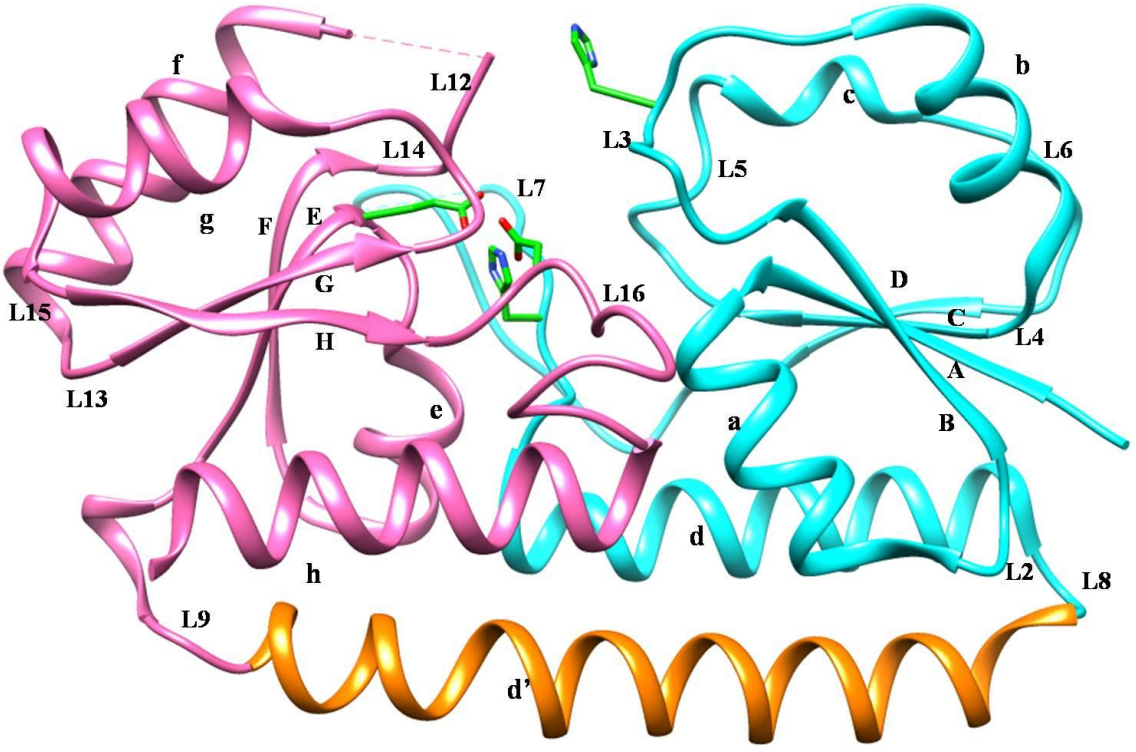

Figure 3.22: Cartoon representation of three-dimensional structure of CLas-ZnuA2 in metal-free state. β-strands are designated as A-H; α-helices as a-h; loops as L2-L16. Four coordinating residues are represented in sticks.

The overall architecture of both domains is almost same despite a low sequence identity of 11%. The superimposition of two domains of metal-free structure gave a root mean square deviation (r.m.s.d.) of 2.9 Å for 89 C_α-atoms. Each domain is made of four-stranded parallel β-sheets (residues 6-11, 27-32, 56-59, 80-83 forms strands A-D in N-domain and residues 167-172, 185-190, 217-221, 239-244 forms strands E-H in C-domain) in the interior with 2-1-3-4 linkage topology and four helices (residues 12-23, 44-54, 68-72, 110-129 forming helices a-d in N-domain and residues 175-183, 199-213, 226-237, 258-275 forming helices e-h in C-domain) on the exterior forming two faces of the domain (PsaA nomenclature). The association of β-strands in two domains showed differences in their architecture and interactions. The β-strands in N-domain are very well arranged by forming backbone H-bonds although strands C and D are shorter. The backbone hydrogen bonding interactions are disrupted between strands E and G in C-domain owing to a large separation at end (~5 Å). There is no water molecule present between the two strands E and G in metal-free state while in intermediate and metal bound

states, three and one water molecules are present. There is a conserved Glu221 from strand G which makes interactions with backbone atoms of E strand (Figure 3.23). Another side chain mediated interaction present in the C-domain but absent in N-domain is an H-bond between Ser220 O^{γ} of strand G and Tyr240 OH of strand H.

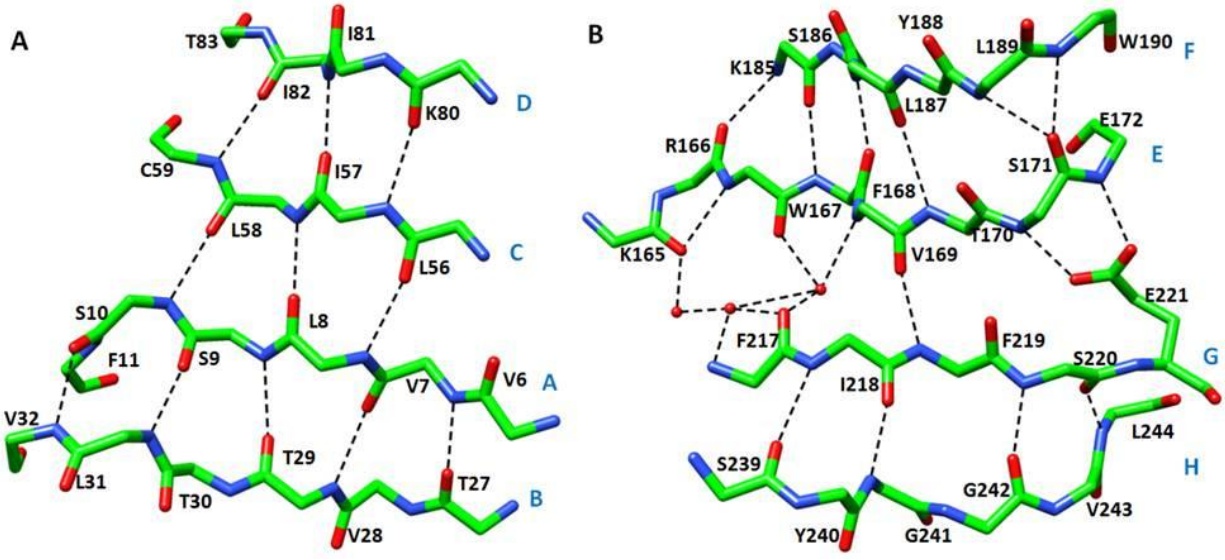

Figure 3.23: β-Strand architecture of two domains in intermediate state. A) N-domain, **B)** C-domain. The backbone hydrogen bonding interactions are disrupted between strands E and G in C-domain while corresponding strands A and C interacting well through backbone H-bonds. Conserved Glu221 from strand G makes interactions with backbone atoms of E strand. Only one water molecule is present between strand G and E in metal bound state and none in metal-free state.

The strands and helices are linked through loops L1-L16 (L1-L7 in N- and L10-L16 in C-domain) of which L1 between strand 'A' and helix 'a' is non-existent unlike other related SBPs. The loops L3, L5 in N-domain and L12, L14 in C-domain are present at the opening of the inter-domain cleft. The loops L2, L7 and helix a (N-domain) and L10, L16 and helix e (C-domain) forms the base/bottom and sides of the cleft. The two domains differ in side-chain and backbone interactions (Figure 3.24). A detailed list of all the interactions and bond distances is given in Table 3.6.

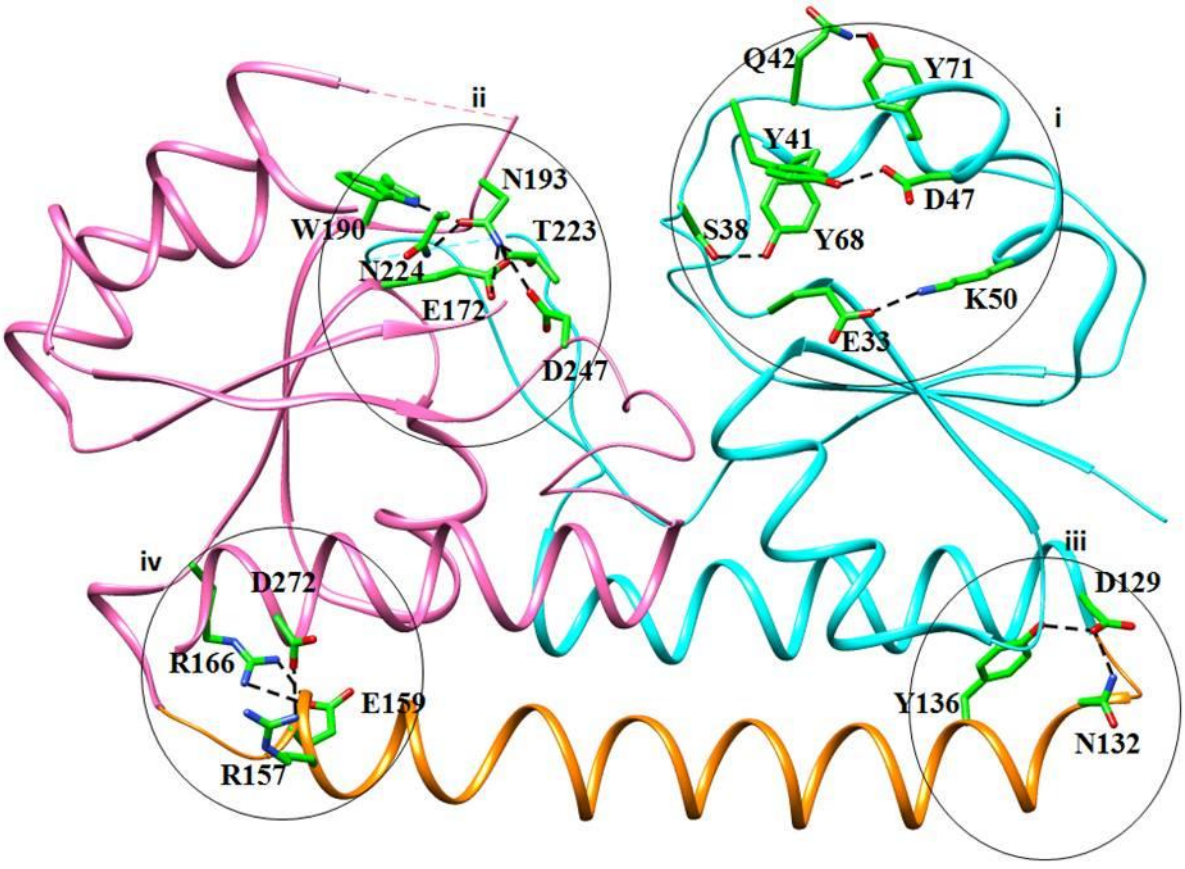

Figure 3.24: The important side-chain interactions of CLas-ZnuA2 structure. The N-domain, C-domain and linker helix is shown in cyan, pink and orange, respectively. Interacting residues are shown in sticks colored by atom type with carbon in green, nitrogen in blue, and oxygen in red. Region **(i)** indicates N-domain interactions involving flexible loop L3. Region **(ii)** indicates interactions in C domain mediated through Asn193. Region **(iii)** and **(iv)** shows interactions in N and C-terminal region of linker helix, respectively. In metal-free state the interaction between Arg157 and Asp272 is absent whereas in Mn-bound state Ser38 main chain O also interacts with Tyr68 OH.

Table 3.6: List of important interactions of CLas-ZnuA2 involving N domain, C domain and linker helix as present in intermediate state.

N domain interactions involving Loop L3, L5 and L7			Distance (Å)
Side chain-side chain	Ser38 OG (L3) Tyr41 OH (L3) Gln42 NE2 (L3) Glu33 OE2 (L3) Asn60 ND2 (L5)	Tyr68 OH (helix c) Asp47 OD2 Tyr71 OH (helix c) Lys50 NZ (helix b) Tyr117 OH (helix d)	2.78 2.59 3.26 2.97 2.67
Side chain-main chain	Asn60 ND2 (L5) His63 ND2 (L5) Val84 O (L7) Asp86 O (L7) Ile91 N (L7) Asn104 O (L7) Trp108 NE1 (L7) Trp108 N Trp108 O	Pro105 O (L7) and Glu102 OE2 (L7) Asn120 ND2 ((helix d) Asn120 ND2 Tyr177 OH (helix e) Tyr177 OH Val246 O (loop 16) Tyr117 OH (helix d) Tyr 259 OH (helix h)	3.04 3.23 2.91 2.88 2.96 2.69 2.70 3.22 2.63
C domain interactions			
	Asn193 OD1 (L12) Asn193 OD2 Asn224 ND2 (strand G)	Trp190 NE1 (strand F) Asn224 ND2 (L14) Thr223 OG1 (loop 14) Glu172 OE1 (strand F) Glu172 OE2 Asp247 (L16) Glu221 OE1 (L14)	2.78 3.09 3.49 3.36 3.33 2.81 2.91
Interactions between N and C domain			
	Ser12 OG (helix a) Asp16 OD2 (helix a) Gly35 N (loop3) Leu111 N (helix d)	Leu249 N (loop 16) Tyr259 N (helix h) Ser248 OG (loop 16) Asp181 OD2 (helix e)	3.12 2.85 2.81 2.82
Interaction involving linker helix			
	Asp129 OD2 (helix d) Glu159 OE1(helix d') Arg157 NH1(helix d') Asn139 ND2 (helix d')	Asn132 (helix d') Tyr136 (helix d') Arg166 (loop 9) NH1 and NH2 Phe182 O (helix e) D272 OD1(helix h) Ile21 O (helix a)	2.80 2.63 3.32 2.90 2.55 3.13 2.90

The 28 residues long backbone helix d′ (residues 132-159) linking two domains runs across the entire length of molecule and packs against fourth helix (d, residues 110-129) of the N-domain and parallel to the fourth helix of the C-domain (h, residues 258-275). The presence

of a rigid helix, which limits the conformational changes between two domains, is a characteristic feature of the Cluster A-I SBPs. In present structure, the backbone helix is curved at the C-terminal end of helix subtending an angle of ~26° which is higher when compared to backbone helices of other SBPs (angle ~ 10°) (Figure 3.25). The two main chain H-bonds within helix (between residues 149 and 153; 150 and 154) are disrupted. This could be due to presence of a proline residue at 22nd position (Pro153) within the helix unlike any other Cluster A-I SBP.

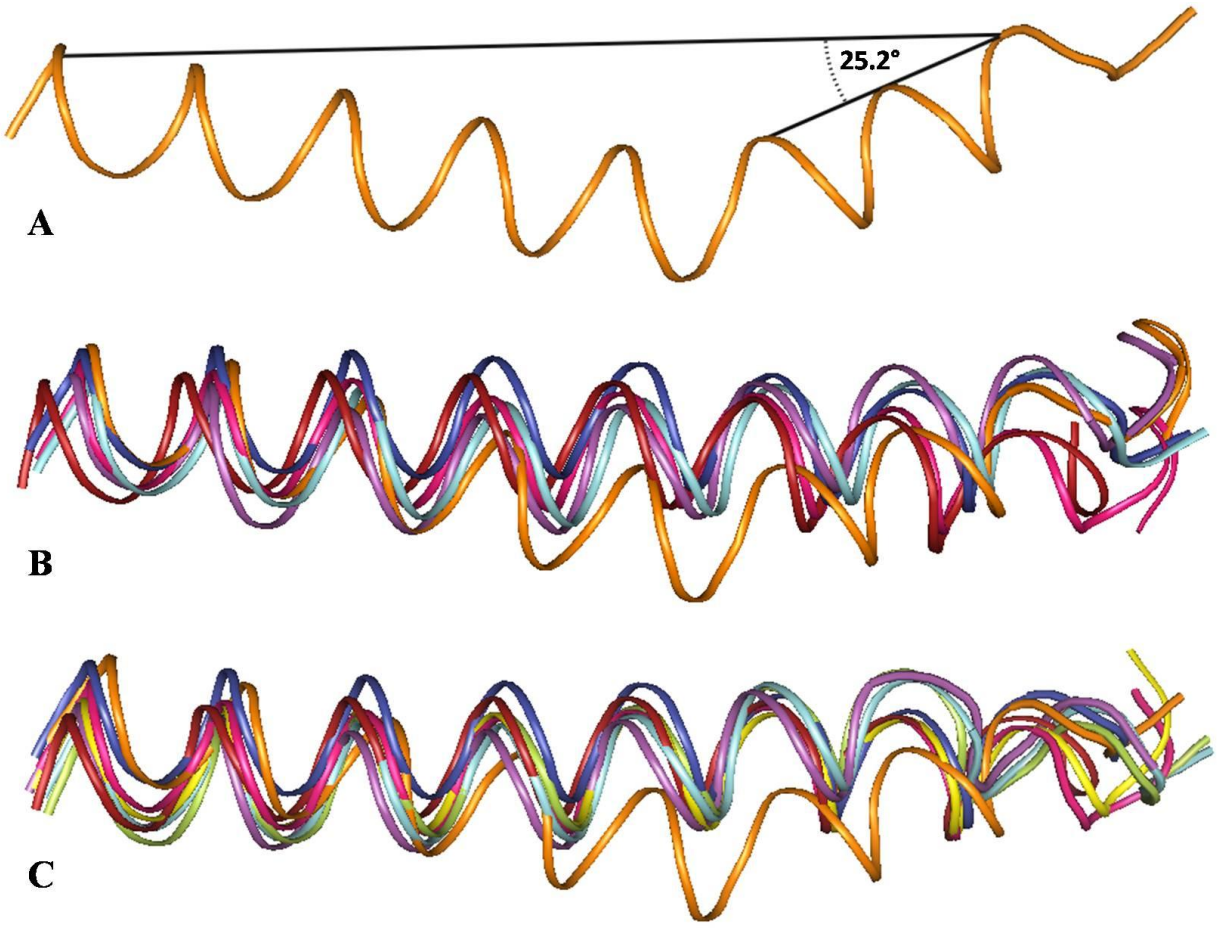

Figure 3.25: Comparison of linker helix of CLas-ZnuA2 with related Cluster A-I SBPs. A) Linker helix of CLas-ZnuA2. **B), C)** Superimposition of linker helices of CLas-ZnuA2 (orange) with other related solute binding proteins in metal free and metal bound states respectively. PsaA-cyan, MtsA-green, Syn-MntC-yellow, *Sau*-MntC-violet, Tp-TroA-magenta, Ec-ZnuA-brick red, Syn-ZnuA-blue.

3.6.1.3. Metal binding site

The metal-free state of CLas-ZnuA2 exhibits an open conformation where one of the metal coordinating residues His39, present on L3 located at the opening of metal binding cleft in N-domain, is displaced away from metal binding cleft with its side chain flipped out exposing the metal-binding site to solvent. A water mediated interaction between coordinating residue His39 and Glu66 (L5) is observed. The other three coordinating residues (His106, Glu172 and Asp247) are present close to each other (~2.5-3.2 Å) comprising a preformed binding site (Figure 3.26A). The imidazole ring of His106 adopts a conformation such that $N^{\delta 1}$ and $N^{\varepsilon 2}$ interact with $O^{\delta 1}$ of Asp247 and $O^{\varepsilon 2}$ of Glu172, respectively. There are seven water molecules present in metal binding site and no electron density was observed for metal ion.

The metal coordinating atoms of four residues make hydrogen bonds with second shell residues in metal binding site and water. In metal-free state, His39 forms H-bonds with Asp37, Tyr41 and three water molecules; His106 interacts with Asn104, Trp108, Met109, and one water molecule; Glu172 with Glu221, Thr170, Cys174, Asn193 and two water molecules; Asp247 with Asn193, Thr223 and seven water molecules (Figure 3.26B). The DPH motif, reported in other bacterial Mn/Fe binding proteins including PsaA, Sau-MntC and MtsA near two coordinating His residues, is absent in CLas-ZnuA2 indicating the sequence divergence. In CLas-ZnuA2, the DPH motif is modified to DSH (at His39) and NPH (at His106). Interestingly, the residue preceding the motif in second case (at His106) is proline (Pro103) which should impart more rigidity towards N-terminal side of coordinating residue (His106). Apart from CLas-ZnuA2, this PNPH motif at second coordinating His residue is present only in the *Syn*-MntC among related proteins. The possible secondary metal binding sites in structure could include HOH2094 bonded with His63, Glu66 and Glu102. Other sites could be HOH2205 and HOH2222 bounded by Glu172 and Asp 247 (metal coordinating residues) together with Thr223, Asn193, Glu221 and Asn224 as reported in MtsA [209].

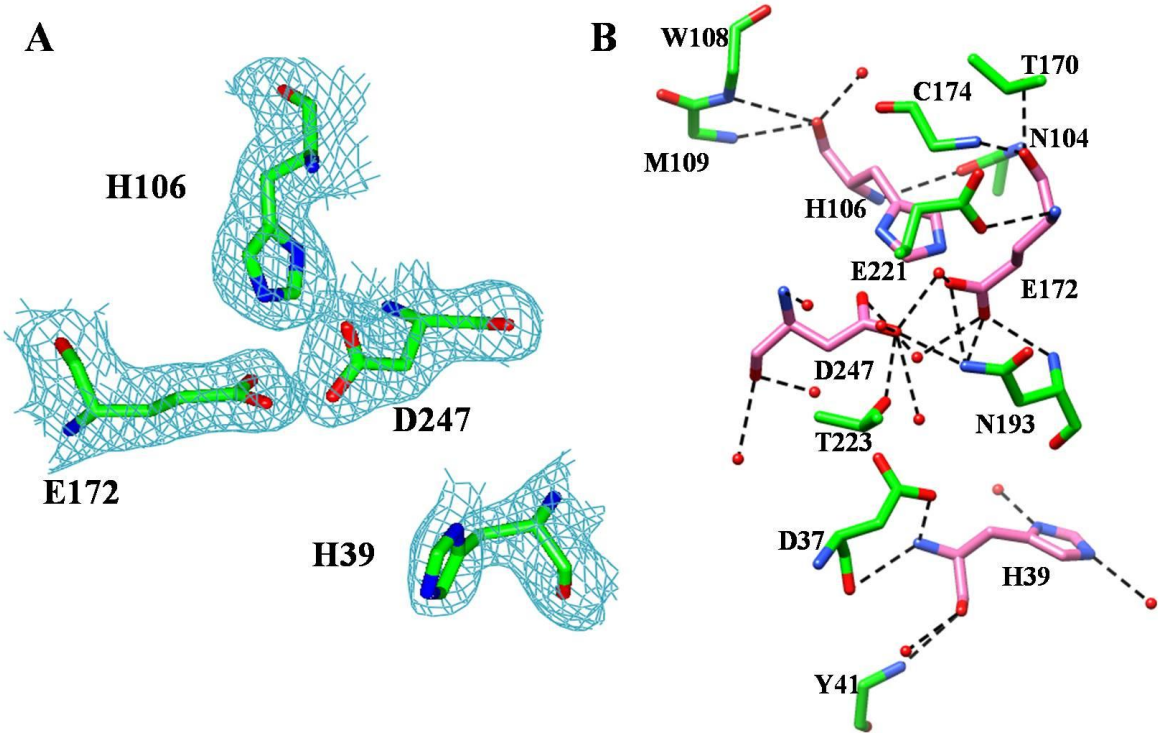

Figure 3.26: Metal-binding site showing electron density and secondary shell interactions in metal-free state. A) 2Fo-Fc electron density map (cyan) contoured at 1σ is shown around metal-binding residue in metal-free state. No electron density was observed for metal ion. **B)** The interactions of metal coordinating residues with water and second shell residues in metal binding site of metal-free state. Metal coordinating residues (pink sticks), and secondary shell residues (green sticks) are shown.

3.6.2. Structure of CLas-ZnuA2 in intermediate state

3.6.2.1. Quality of the model

The crystal structure of CLas-ZnuA2 in intermediate state has been determined to 1.63 Å resolution. The refinement data statistics in Table 3.7 shows that the model is well refined with excellent stereochemistry and crystallographic R factor values. The electron density is well defined except for the three N-terminal residues and the two loop regions (involving residues 96-100) with no electron density and residues 194-199 with a weak electron density. The three N-terminal and some residues in two loops (residues 96-100 and 195-197) were not included in the model.

Table 3.7: Refinement statistics for intermediate state of CLas-ZnuA2

Data resolution	29.29-1.63
Number of reflections used/free	51948/2927
Biological units per asymmetric unit	1
Wilson B-factor ($Å^2$)	21.9
Crystallographic R-factor (%)	16.7
Free R-factor (%)	19.4
Average *B*-factors ($Å^2$)	
All atoms	26.3
Protein atoms	25.47
Water atoms	36.23
Ligand atoms	44.61
r.m.s.d. for bond length(Å)/bond angle (°)	0.018/1.797
Ramachandran plot	
Favoured (%)	97
Allowed (%)	3
Outliers (%)	0

The final model consists of 264 amino acid residues, one metal ion, 262 waters, 6 sulphate ions, 2 acetate ions and 2 glycerol molecules. Of the 264 residues, 8 residues (Ser9, Ser45, Lys146, Ile158, Asp162, Glu180, Ser186, and Thr273) have been refined with alternate conformations and two residues with partial occupancy (His39 and Ser40 with occupancy of 0.8 and 0.5, respectively). The metal ion was modeled as Mn(II) (refined to half occupancy).

3.6.2.2. Overall structure

The overall structure of intermediate state of CLas-ZnuA2 is similar to metal-free state consisting of N and C-domain connected by a linker helix (Figure 3.27). Each domain comprises of four α-helices and four β-strands connected by loops. The association of β-strands is similar to metal-free state with the difference of presence of three water mediated interactions between the two strands E and G, whereas in metal-free state there is no water molecule present.

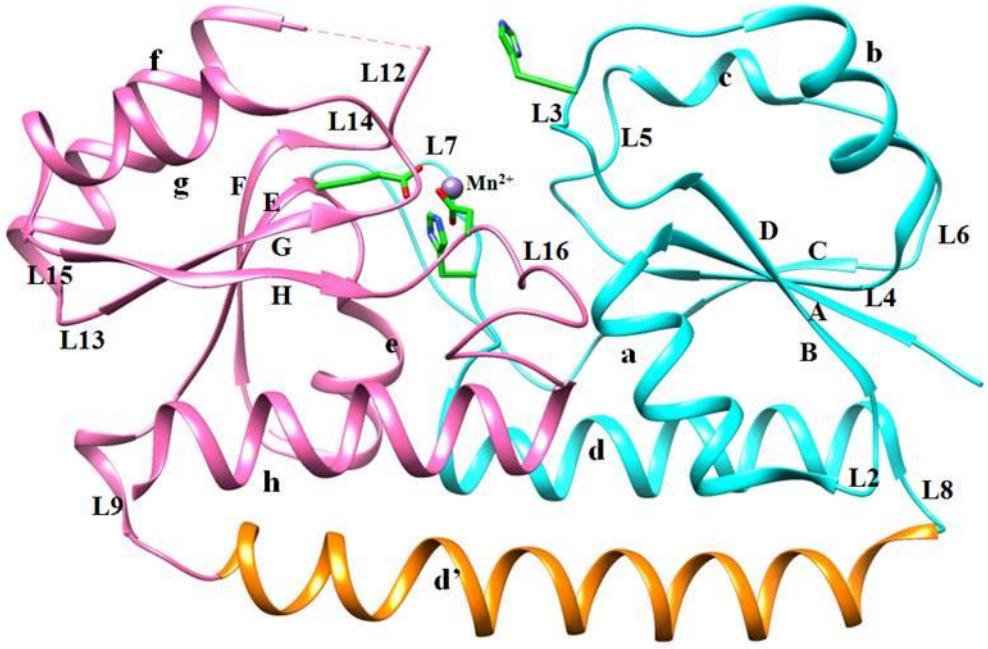

Figure 3.27: Cartoon representation of three-dimensional structure of CLas-ZnuA2 in intermediate state. β-strands are designated as A-H; α-helices as a-h; loops as L2-L16. Four coordinating residues are represented in sticks. Metal ion is shown in sphere.

3.6.2.3. Metal binding site

In intermediate state, a clear electron density in difference Fourier map (up to 8σ) was observed at the metal binding site during the refinement suggesting the presence of a bound metal (Figure 3.28A). The position of the metal in binding site is ~5.4 Å from opening end and 23.4 Å from other end closed by the backbone helix. It is not completely buried but partially solvent accessible (Figure 3.28B). The metal was modeled as Mn(II) and has been refined to an occupancy of 0.5 with distorted coordination geometry. Out of the four coordinating residues only three (His106, Glu172 and Asp247) are involved in the metal coordination.

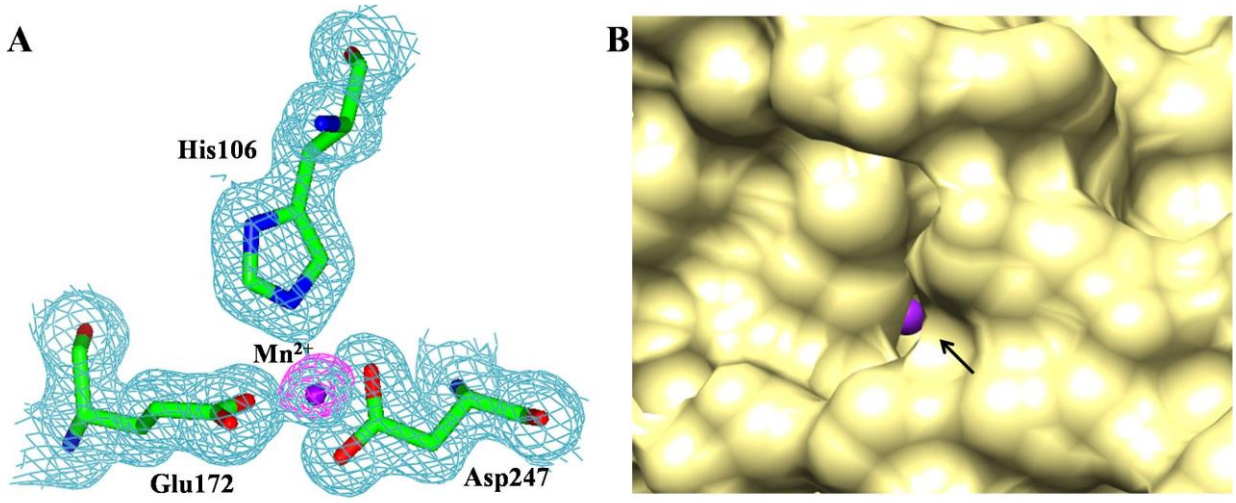

Figure 3.28: Electron density and surface representation around metal-binding site in intermediate state. (A) Difference Fourier (Fo-Fc) electron density map contoured at 3σ (magenta) showing clear electron density around metal during refinement in intermediate state of CLas-ZnuA2. 2Fo-Fc electron density map (cyan) contoured at 1σ is also shown around metal and binding residues. **(B)** Surface representation of metal binding cleft in intermediate state indicating partial solvent accessibility of the metal ion.

The metal-to-protein atomic distances are 2.4 Å for His106 $N^{\varepsilon 2}$, 2.75 Å and 2.28 Å for Glu172 $O^{\varepsilon 1}$ and $O^{\varepsilon 2}$, respectively and 2.5 Å and 2.68 Å for Asp247 $O^{\delta 1}$ and $O^{\delta 2}$, respectively. The coordination distances larger than the ideal values (~2.2 Å) and partial occupancy indicated towards a partial and loose binding of metal. The *B*-factor for metal is 45 $Å^2$ which is higher than the values reported in other structures. The imidazole ring of His106 flips and adopts a conformation where $N^{\delta 1}$ interacts with Asn104 $O^{\delta 1}$ and Gly173 O thereby making $N^{\varepsilon 2}$ available for metal coordination (Figure 3.29A). The side chain of His39, coordinating residue present on the L3 at the opening of the metal-binding cleft, adopts the same conformation as described for metal-free state. However, His39 has been refined to occupancy of 0.8 suggesting an alternate conformation. A protruding electron density seen at the base of the side chain at C_β and a residual electron density towards metal in the binding cleft could be an alternate conformation for His39 side chain (Figure 3.29B). A higher than average *B*-factors (39 and 35 $Å^2$ for side chains of His39 and Ser40, respectively) and a break in electron density between His39 and Ser40 was observed. Also, a weak difference Fourier density is observed which could be an alternate conformation for Ser40 (refined at half occupancy) indicating an inward shift. There are five water molecules present in binding pocket.

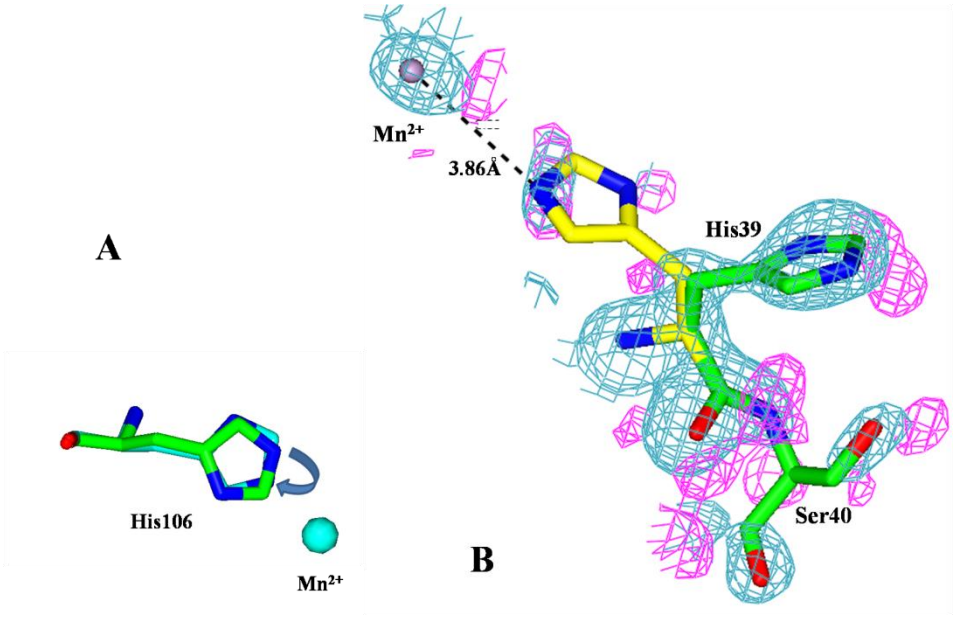

Figure 3.29: L3 loop and His106 side chain showing transitional evidence in intermediate state. A) His106 imidazole ring is flipped in metal-bound state (cyan) in such a manner that $N^{\varepsilon 2}$ can coordinate with metal ion (metal-free state-green). **B)** Conformation of L3 in intermediate state showing a possible alternate conformation for His39 (yellow sticks) with protruding density at C_{β} modeled in residual electron density towards metal. Break in density between His39 and Ser40 and a weak inward difference Fourier density adjacent to Ser40 main chain is shown. 2Fo-Fc map is shown in cyan and Fo-Fc map is shown in magenta.

The metal coordinating atoms of four residues make hydrogen bonds with second shell residues in metal binding site and water (Figure 3.30). In intermediate state, His39 forms H-bonds with Asp37, Tyr41 and three water molecules; His106 interacts with Asn104, Trp108, Met109, Gly173 and one water molecule; Glu172 with Glu221, Thr170, Cys174, Asn193 and two water molecules; Asp247 with Asn193 and five water molecules.

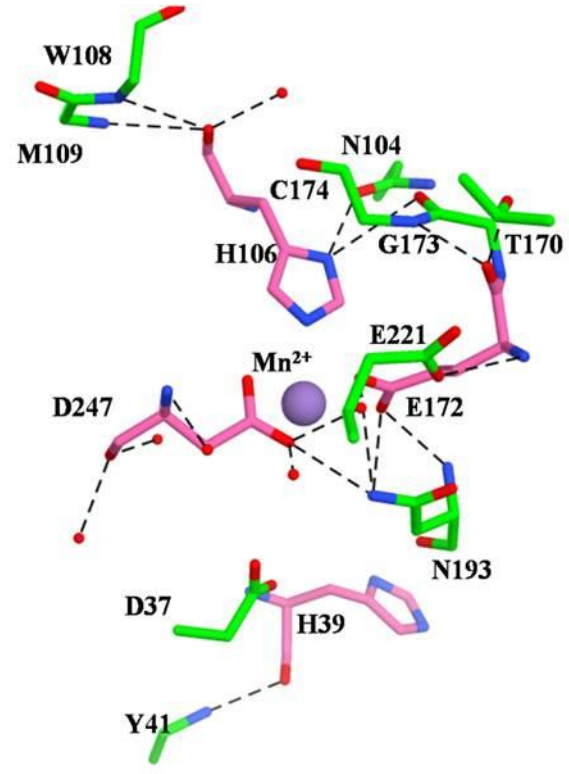

Figure 3.30: The interactions of metal coordinating residues with water and second shell residues in metal binding site of intermediate state. Metal coordinating residues (pink sticks), metal ion (violet sphere) and secondary shell residues (green sticks) are shown.

3.6.3. Structure of CLas-ZnuA2 in Mn^{2+}-bound state

3.6.3.1. Quality of the model

The crystal structure of CLas-ZnuA2 has been determined in Mn^{2+}-bound state to 2.2 Å resolution. The refinement data statistics in Table 3.8 shows that the model is well refined with excellent stereochemistry and crystallographic *R* factor values. The electron density well defined except for the three N-terminal residues and the two loop regions (97-99) with no electron density and residues 194-199 with a weak electron density. The three N-terminal and some residues in two loops (residues 97-99 and195-197) were not included in models. The final model of Mn^{2+}-bound state consists of 266 amino acid residues, one metal ion, 192 waters, 5 sulphate ions, 1 acetate ion and 2 glycerol molecules. Of the 266 residues, 7 residues (Ser9, Ile13, Ser38, Ser45, Arg157, Glu180 and Ser186) have been refined with alternate conformations. The metal ion was modeled as Mn(II).

Table 3.8: Refinement statistics for Mn^{2+}-bound state of CLas-ZnuA2.

Data resolution	47.2-2.22
Number of reflections used/free	21895/1244
Biological units per asymmetric unit	1
Wilson B-factor ($Å^2$)	23.5
Crystallographic R-factor (%)	16.4
Free R-factor (%)	19.6
Average *B*-factors ($Å^2$)	
All atoms	25.8
Protein atoms	25.47
Water atoms	32.861
Ligand atoms	50.57
r.m.s.d. for bond length(Å)/bond angle (°)	0.007/1.113
Ramachandran plot	
Favoured (%)	97.4
Allowed (%)	2.6
Outliers (%)	0

3.6.3.2. Overall structure

The overall structure of Mn^{2+}-bound state of CLas-ZnuA2 is similar to metal-free and intermediate state consisting of N and C-domain connected by a linker helix (Figure 3.31). Each domain comprises of four α-helices and four β-strands connected by loops. However strand E and F shortened by three residues. The association of β-strands is similar to metal-free state with the difference of presence of one water (three in intermediate state) mediated interactions between the two strands E and G, whereas in metal-free state there is no water molecule present.

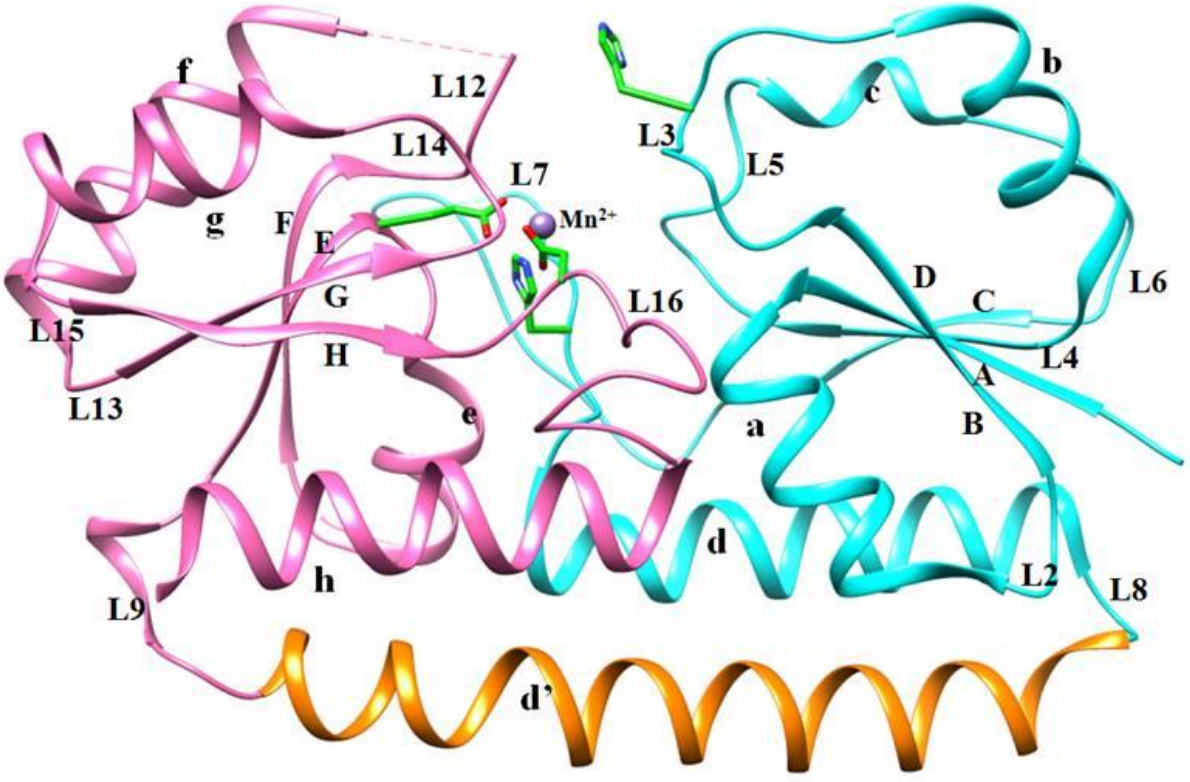

Figure 3.31: Cartoon representation of three-dimensional structure of CLas-ZnuA2 in Mn^{2+}-bound state. Four coordinating residues are represented in sticks and Mn^{2+} ion is shown in sphere.

3.6.3.3. Metal binding site

The structure of CLas-ZnuA2 in intermediate and metal-bound states showed that the cleft of N- and C-domain interface constitutes the metal binding site. The structure in above two states confirmed the metal coordinating residues as demonstrated from multiple sequence alignment. The four conserved metal coordinating residues are two His (His39, His106 from N-domain), one Glu and one Asp (Glu172 and Asp247 from C-domain).

The metal-bound state demonstrated a closed conformation where a large inward displacement of His39 (~2.5 Å C_α displacement) along with a part of L3 was observed. The side chain of His39, flipped out in metal-free state, moved into the metal-binding cleft for coordination. The relative position of other three metal coordinating residues as compared to metal-free state (C_α displacement: His106, 0.1 Å; Glu172, 0.1 Å; Asp247, 0.3 Å,) is almost

same with minor readjustments. The imidazole ring of His106 is flipped and adopts a conformation like intermediate state. The side chains of Glu172 and Asp247 reorient themselves for coordination as compared to metal-free state (Figure 3.32A). A clear electron density was observed for metal ion modeled as Mn(II) ion with temperature factor of 18 $Å^2$ which was completely buried (Figure 3.32B). The metal-to-protein atomic distances are 2.26 Å for His39 $N^{\varepsilon 2}$, 2.23 Å for His106 $N^{\varepsilon 2}$, 2.31 Å and 2.19 Å for Glu172 $O^{\varepsilon 1}$ and $O^{\varepsilon 2}$, respectively and 2.22 Å and 2.18 Å for Asp247 $O^{\delta 1}$ and $O^{\delta 2}$, respectively. Only three water molecules are present in binding pocket.

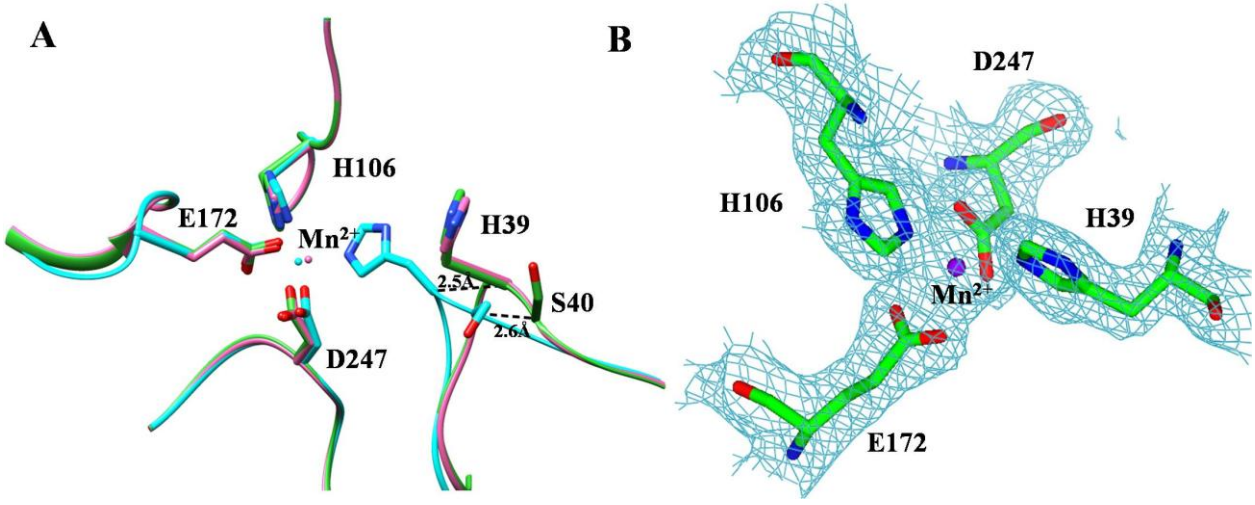

Figure 3.32: Superimposition of metal binding residue and electron density aroung metal binding site in Mn^{2+} bound state. A) Metal binding residues of the three states after superimposition. Metal-free, intermediate and metal-bound states are shown in green, pink and cyan, respectively. His39 and Ser40 are flipped and shifted ~2.5 Å inside towards metal in metal-bound state. Asp247 side chain slightly oriented towards metal in metal-bound form. **B)** 2Fo-Fc electron density map (cyan) contoured at 1σ is shown around metal-binding residues in Mn^{2+}-bound state. Clear electron density was observed for Mn^{2+} ion.

The metal coordinating atoms of four residues make hydrogen bonds with second shell residues in metal binding site and water. In Mn^{2+}-bound state, His39 forms H-bonds with Asp37 and two water molecules; His106 interacts with Asn104, Trp108, Met109, and one water molecule; Glu172 with Glu221, Thr170, Cys174, Asn193 and two water molecules; Asp247 with Asn193, Ser38 and three water molecules (Figure3.33).

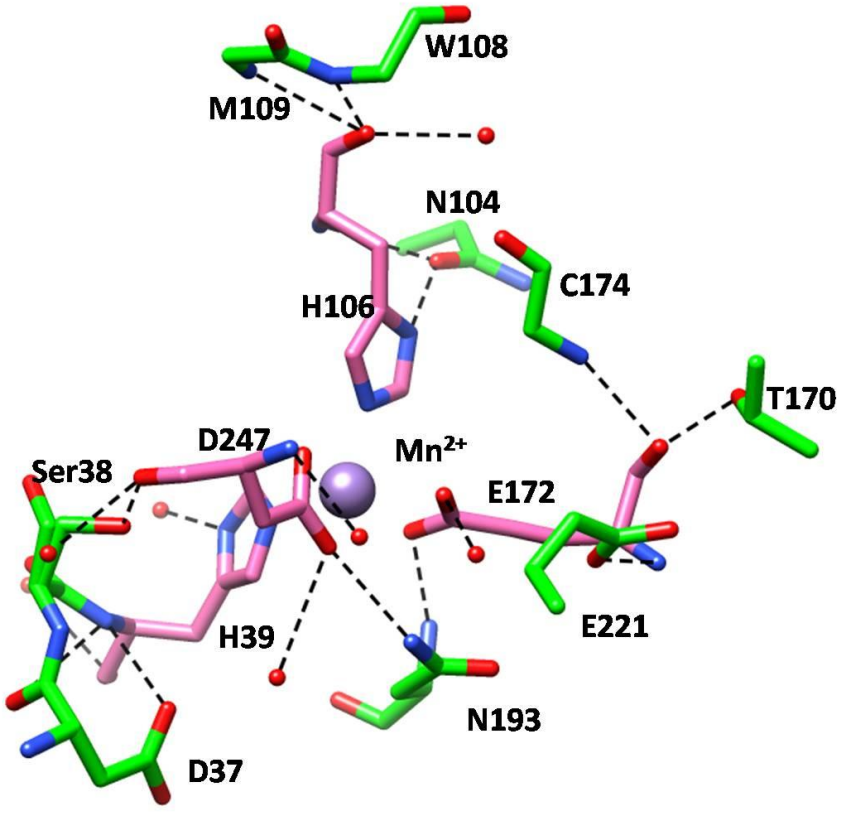

Figure 3.33: The interactions of metal coordinating residues with water and second shell residues in metal binding site of Mn^{2+}-bound state. Metal coordinating residues (pink sticks), metal ion (violet sphere) and secondary shell residues (green sticks) are shown.

3.6.4. Structure of CLas-ZnuA2 in Zn^{2+}-bound state

3.6.4.1. Quality of the model

The crystal structure of CLas-ZnuA2 has been determined in Zn^{2+}-bound state to 2.2 Å resolution. The refinement data statistics in Table 3.9 shows that the model is well refined with excellent stereochemistry and crystallographic R factor values. The electron density well defined except for the three N-terminal residues and the two loop regions (97-99) with no electron density and residues 194-199 with a weak electron density. The three N-terminal and some residues in two loops (residues 97-99 and 195-197) were not included in models.

The final model of Zn^{2+}-bound state consists of 266 amino acid residues, one metal ion, 248 waters, 5 sulphate ions, 1 acetate ion and 3 glycerol molecules. Of the 266 residues, 5

residues (Ser9, Ser38, Ser45, Glu180 and Ser186) have been refined with alternate conformations. The metal ion was modeled as Zn(II).

Table 3.9: Refinement statistics for Zn^{2+}-bound state of CLas-ZnuA2.

Data resolution	42.24-2.22
Number of reflections used/free	23203/1243
Biological units per asymmetric unit	1
Wilson B-factor ($Å^2$)	22.3
Crystallographic R-factor (%)	15.3
Free R-factor (%)	18.1
Average *B*-factors ($Å^2$)	
All atoms	24.17
Protein atoms	22.74
Water atoms	33.23
Ligand atoms	41.19
r.m.s.d. for bond length(Å)/bond angle (°)	0.006/1.083
Ramachandran plot	
Favoured (%)	97.4
Allowed (%)	2.6
Outliers (%)	0

3.6.4.2. Overall structure

The overall structure of Zn^{2+}-bound state of CLas-ZnuA2 is similar to Mn^{2+}-bound state with similar domain organization and secondary structure arrangements (Figure 3.34).

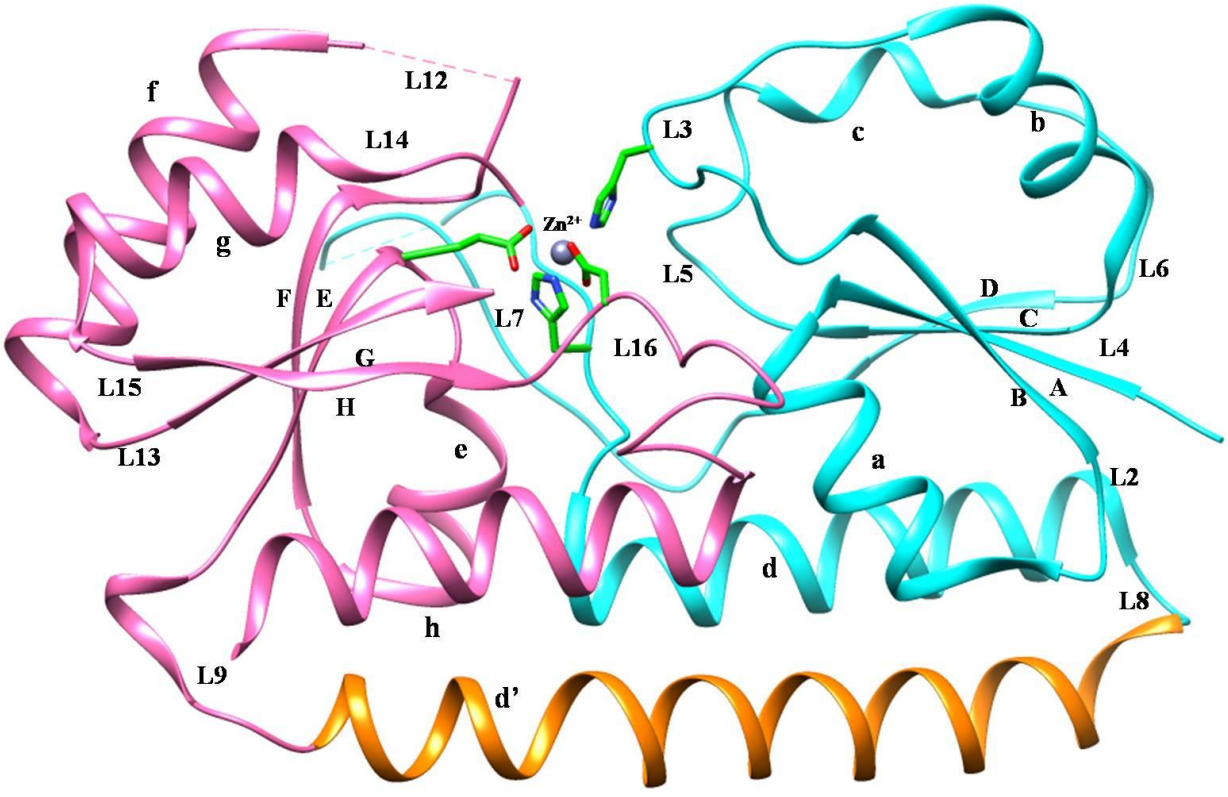

Figure 3.34: Cartoon representation of three-dimensional structure of CLas-ZnuA2 in Zn^{2+}-bound state. Four coordinating residues are represented in sticks and Zn^{2+} ion is shown in sphere.

3.6.4.3. Metal binding site

The metal-binding site for Zn^{2+}-bound state is similar to Mn^{2+}-bound state except the coordination distances are relatively smaller. The metal-to-protein atomic distances are 2.08 Å for His39 $N^{\varepsilon 2}$, 2.07 Å for His106 $N^{\varepsilon 2}$, 2.51 Å and 2.00 Å for Glu172 $O^{\varepsilon 1}$ and $O^{\varepsilon 2}$, respectively and 2.04 Å and 2.03 Å for Asp247 $O^{\delta 1}$ and $O^{\delta 2}$, respectively. The temperature factor of modeled Zn(II) ion is 13.35 $Å^2$ (Figure 3.35). The secondary shell residue interactions are similar to Mn^{2+}-bound state (not shown).

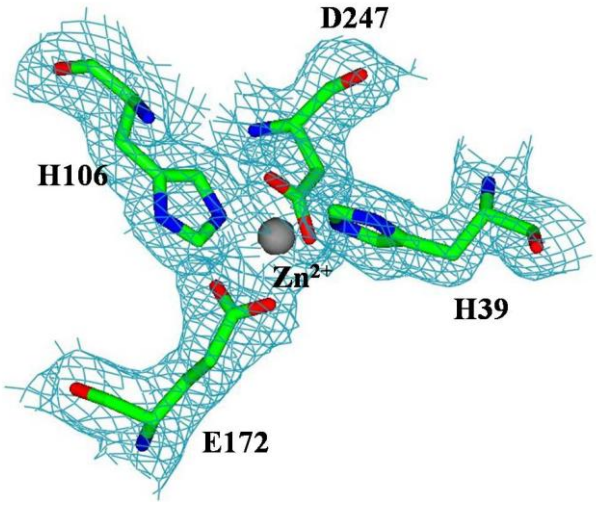

Figure 3.35: 2Fo-Fc electron density map (cyan) contoured at 1σ is shown around metal-binding residues in Zn^{2+}-bound state. Clear electron density was observed for Zn^{2+} ion.

3.6.5. Differences in Mn^{2+}-bound and Zn^{2+}-bound states

The Mn^{2+}-bound and Zn^{2+}-bound states are almost similar giving an r.m.s.d. value of 0.1562 Å on superimposition (Figure 3.36).

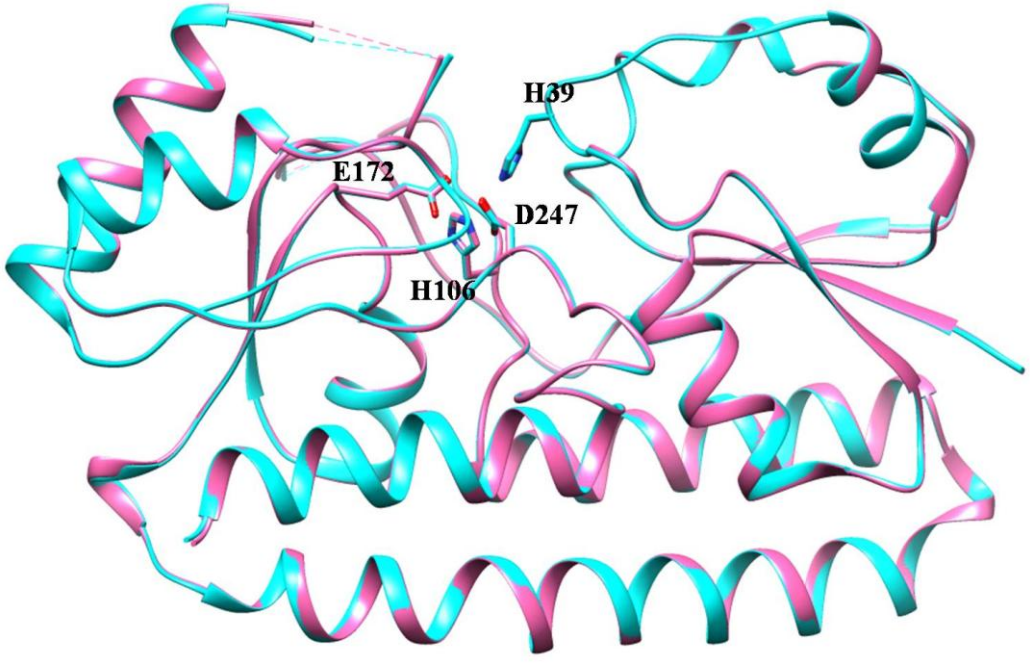

Figure 3.36: Superimposition of Mn^{2+}-bound (cyan) and Zn^{2+}-bound (pink) CLas-ZnuA2. Metal binding residues are shown in sticks and metal ions are shown in spheres.

Some differences were observed in the interactions of the two states shown in Table 3.10 and 3.11. The number of interactions observed in Zn^{2+}-bound state is more than that in Mn^{2+}-bound state which are majorly located on the loops present around metal binding site and in the two termini of the linker helix.

Table 3.10: Interactions which are present in Mn^{2+}-bound state and absent in Zn^{2+}-bound-state.

Residue	Atom	Location in secondary structure	Residue	Atom	Distance (Å)	Location in secondary structure
38 SER	OG	L3	247 ASP	O	3.46	L16
86 ASP	N	L7	120 ASN	ND2	3.48	d
166 ARG	NH2	L9	159 GLU	O	2.9	d'
166 ARG	NH1	L9	182 PHE	O	3.29	e
212 SER	OG	f	209 GLN	O	3.07	f
221 GLU	OE2	G	219 PHE	O	3.5	G
272 ASP	OD1	h	268 THR	O	3.46	h
38 SER	OG	L3	68 TYR	OH	3.45	c
40 SER	OG	L3	37 ASP	OD2	2.65	L3
94 SER	OG	L7	101 SER	OG	3.2	L7
251 LYS	NZ	L16	253 ASP	OD1	3.45	L16

Table 3.11: Interactions which are present in Zn^{2+}-bound state and absent in Mn^{2+}-bound-state.

Residue	Atom	Location in secondary structure	Residue	Atom	Distance (Å)	Location in secondary structure
40 SER	N	L3	37 ASP	OD1	3.47	L3
60 ASN	N	L5	65 GLU	OE1	3.48	L5
86 ASP	OD1	L7	83 THR	O	3.36	C
150 SER	OG	d’	146 LYS	O	3.49	d’
166 ARG	NH1	L9	159 GLU	O	3.48	d'
166 ARG	NH2	L9	182 PHE	O	2.98	e
198 ARG	NH1	L12	192 ILE	O	3.29	L12
202 MET	N	f	199 SER	OG	3.16	f
213 HIS	ND1	f	209 GLN	O	3.14	f
273 THR	OG1	h	270 ILE	O	2.87	h
39 HIS	NE2	L3	106 HIS	NE2	3.34	L7
172 GLU	OE1	E	193 ASN	ND2	3.45	L12
172 GLU	OE1	E	247 ASP	OD2	3.09	L16
172 GLU	OE2	E	247 ASP	OD2	3.09	L16
193 ASN	ND2	L12	172 GLU	OE2	3.27	E
199 SER	OG	f	201 SER	OG	3.39	f

3.6.6. Comparison of metal-free, intermediate and metal-bound states of CLas-ZnuA2

3.6.6.1. Superposition of metal-free, intermediate and metal-bound CLas-ZnuA2

The CLas-ZnuA2 structures in metal-free, intermediate and bound states superpose well with r.m.s.d. values of 0.279 Å (metal-free and intermediate), 0.379 Å (metal-free and Mn^{2+}-bound states) and 0.325 Å (intermediate and Mn^{2+}-bound states) (Figure 3.37).

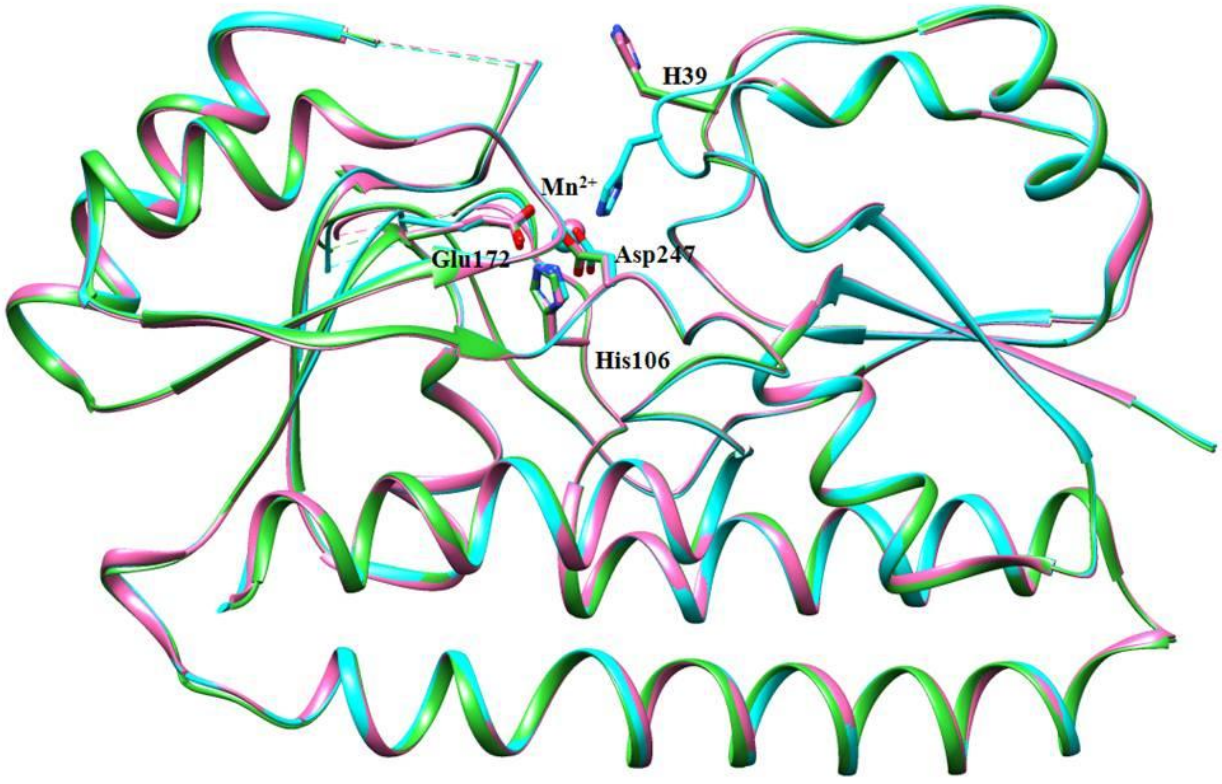

Figure 3.37: Superimposition of metal-free, intermediate and Mn^{2+}-bound states of CLas-ZnuA2. Metal-free, intermediate and Mn^{2+}-bound states are shown in green, pink and cyan, respectively. Metal-binding residues are shown as sticks and Mn^{2+} is shown as sphere. Overall structures are similar and well superimposed for all three states except for loop L3 hosting His39 residue which was shifted inwards in metal-binding state.

3.6.6.2. Analysis of solvent accessible surface area

The analysis of solvent accessible surface area (SASA) calculated by two different programs showed that intermediate state has maximum SASA while Mn^{2+}-bound state has

minimum SASA. The order of SASA is: intermediate state > Zn^{2+}-bound state > metal-free state >Mn^{2+}-bound state. (Table 3.12)

Table 3.12: Overall solvent accessible surface area of all states of CLas-ZnuA2.

Molecule	Solvent accessible surface area	
Metal-free state	11582	11555.64
Intermediate state	11745	11687.72
Mn-bound state	11554	11526.79
Zn-bound state	11614	11581.22
Program used	CCP4	StrucTools

3.7. Comparison of CLas-ZnuA2 with related Cluster A-I structures

The metal-free and metal bound structures of CLas-ZnuA2 were compared with available metal-free open and metal-bound closed forms of structures belonging to the cluster A-I SBPs. The superimposition of metal-free and metal-bound structures gave r.m.s.d. values of 1.62 Å and 1.82 Å with apo and bound Sau-MntC, 1.68 Å and 1.98 Å with apo and bound PsaA, 2.28 Å and 2.06 Å with apo and bound Tp-TroA, 2.53 Å and 2.5 Å with apo and bound Ec-ZnuA and 2.13 Å and 2.09 Å with apo and bound Sy-ZnuA. The superimposition of metal-bound structure gave r.m.s.d. values of 1.75 Å with Syn-MntC and 2.03 Å MtsA (Figure 3.38).

When all Mn/Fe binding proteins are superimposed with three structures of CLas-ZnuA2, the position of His39, Glu172 and Asp247 in all three states was different than those of all other proteins which are almost superimposed, whereas on superimposing Zn-binding proteins, the position of metal binding residues was found not to be conserved among them (Figure 3.39). Also linker helices of all Cluster A-I proteins are superimposed well except for CLas-ZnuA2 due to bending of linker helix (Figure 3.25).

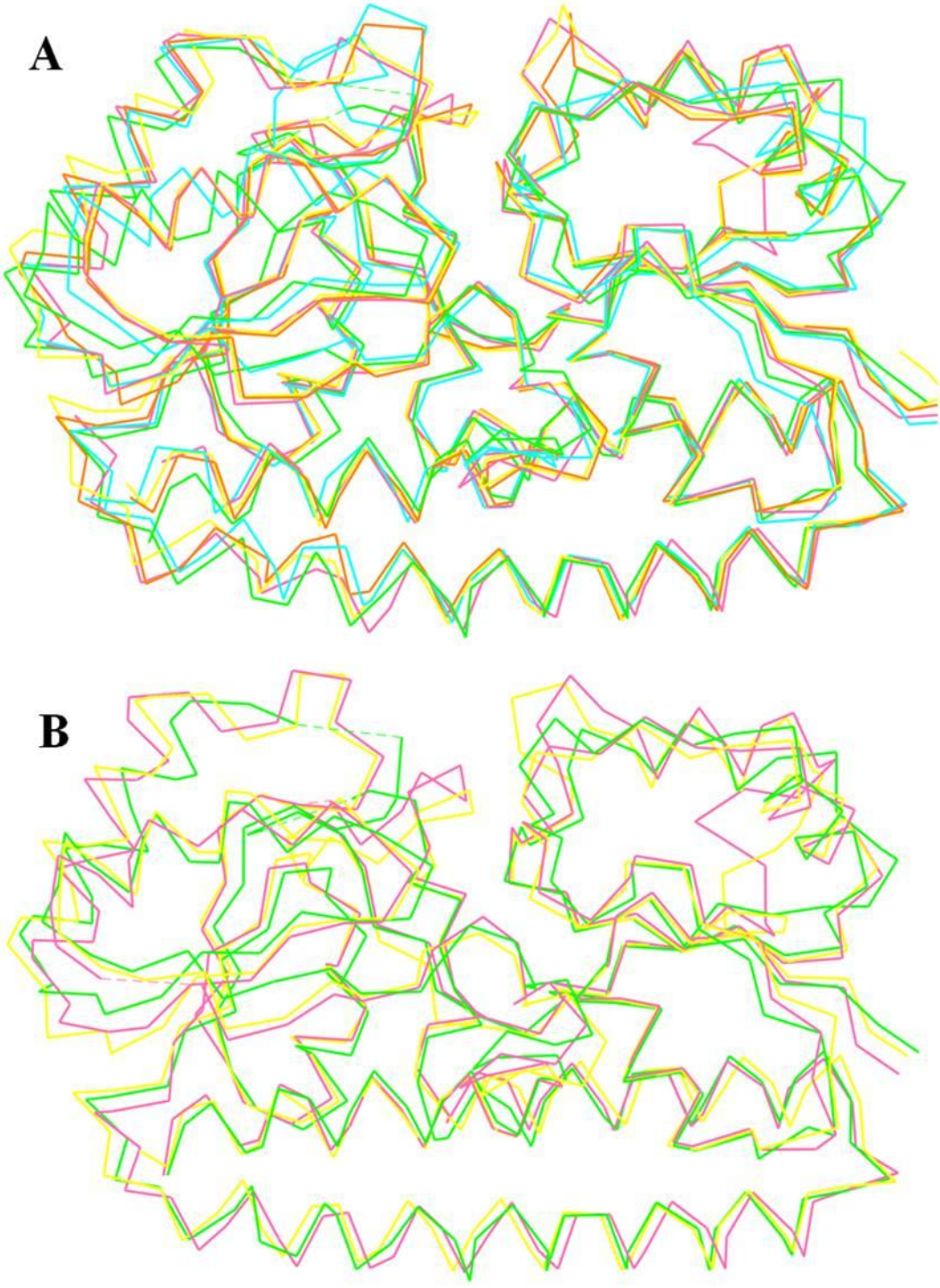

Figure 3.38: Ribbon diagram of superimposition of related Cluster A-I SBPs. Superimposition of **A)** metal-bound and **B)** metal-free forms of CLas-ZnuA2 with related Mn/Fe-specific Cluster A-I family proteins. CLas-ZnuA2, Sau-MntC, Syn-ZnuA, MtsA and PsaA are shown in green, pink, cyan, orange and yellow respectively.

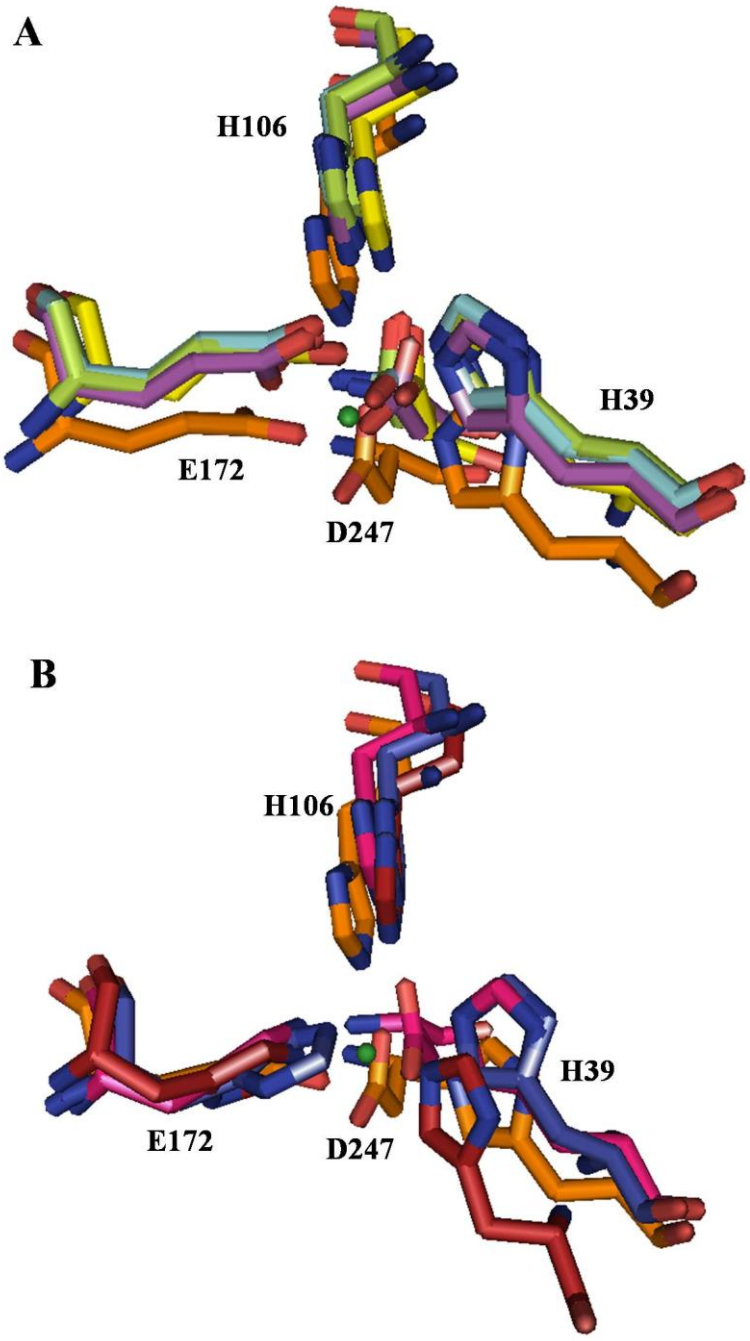

Figure 3.39: Metal binding residues of Cluster A-I proteins. A) Mn^{2+}-bound structures **B)** Zn^{2+}-bound structures. CLas-ZnuA2-orange, PsaA-cyan, MtsA-green, Syn-MntC-yellow, Sau-MntC-violet, Tp-TroA-magenta, Ec-ZnuA-brick red, Syn-ZnuA-blue

3.8. Other conformational differences and some unique features of CLas-ZnuA2

The major conformational differences in the three states were observed only in L3 present at the opening of metal binding cleft in N-domain. Also, subtle differences in conformation and interactions are observed. One of the unique features of CLas-ZnuA2 structure is a highly restrained loop L3. The L3 (residues 33-43) in N-domain hosting one of the metal coordinating residues, His39, is stabilized by four interactions which includes H-bonds between Ser38 O^{γ} and Tyr68 OH (helix c), Tyr41 OH and Asp47 $O^{\delta 2}$ (helix b), Gln42 $N^{\varepsilon 2}$ and Tyr71 OH (helix c) and a salt bridge between Glu33 $O^{\varepsilon 2}$ and Lys50 N^{ζ} (helix b) (Figure 3.24). The H-bond between Tyr41 and Asp47 is conserved among most proteins of cluster A-I family except PsaA where higher bond distance was observed [122]. Also, a conserved Trp residue instead of Tyr68 is present in most cluster A-I family proteins, which makes H-bond interactions with main chain O atom of residues corresponding to amino acids 38 and 39 in the present structure. The absence of any Pro residues in L3, in contrast to other SBPs where one to four Pro residues are present, indicated main-chain flexibility in CLas-ZnuA2. Ser38 (L3) showed two alternate conformations in Mn^{2+}-bound state where in one conformation Ser38 O^{γ} interacts with Tyr68 OH (helix c) with H-bond distance 3.45Å which is much higher as compared to metal-free and intermediate states (~2.8Å) while in second conformation it interacts with Asp247 O (3.46Å). Also Ser38 main chain O interacts with Tyr68 OH and Leu64 O (helix c and L5 respectively). Other key interactions which are present in metal-free state but absent in bound form include Asn36 ND2 and Glu33 O, Ser38 O and Thr67 $O^{\gamma 1}$, Ser40 N and Thr67 $O^{\gamma 1}$, Tyr41 OH and Leu31 O whereas interaction between Asp37 $O^{\delta 2}$ and Ser40 $O^{\gamma 1}$ is present in bound form but absent in apo form. In apo and intermediate structure His39, Glu66 and His63 interacts with each other mediated through water while in bound form interaction between His39 and Glu66 is lost and Glu66 interacts with His63 directly.

4.1. Introduction

Proteins are important functional elements of the cell that carry out diverse biological functions such as transportation, defense, signaling, reaction catalysis, repair and maintenance and structural support. Various proteins are responsible for the transport of different sized substrate inside and outside of the living cell for various functions like fulfilling specific cell requirements or secreting molecules for defense. ATP-binding cassette (ABC) transporters are one of such transporters, which transport various substrates across the membrane and are present in all forms of life. Typical bacterial ABC permease consists of three components; a solute-binding protein (SBP) found in the periplasm in Gram-negative bacteria or linked to the cytoplasmic membrane in Gram-positive bacteria, a trans-membrane permease and a nucleotide-binding protein. SBP are extracellular, high affinity substrate binding proteins that functions as a receptor and bind to the specific substrate. Therefore, SBP are responsible for molecular recognition and specificity for the substrate transported by an ABC transporter. SBP facilitates translocation of various compounds ranging from small sized metal ions to larger molecules such as vitamins and metal chelates. Consequently, SBPs have evolved to have high specificity for their substrates. All SBPs have a conserved fold made up of two α/β domains connected by a linker region. The substrate-binding site is located at the crevice between the two domains. Most SBPs have flexible linker region which allows the opening and closing of substrate binding site by movement of the two domains thereby act in a "Venus flytrap" manner allowing transport of larger sized molecules. The size of the transported molecule depends on the extent of opening of substrate binding site by the domain rotation. In SBP, which transport small size substrates such as metal ions, a rigid linker helix is present which allows no or very slight domain rotation upon metal binding thereby adopting a different mechanism of binding and release.

The SBPs which are involved in uptake of divalent metal ions Mn^{2+}, Zn^{2+} and Fe^{2+} belong to Cluster A-I family [17]. Metal ion specificity in Cluster A-1 SBP is thought to be due to the preference of individual metal-binding sites to the particular coordination chemistry. Structural and biochemical characterization of number of Cluster A-1 proteins implies that the metal binding sites of these proteins are fine-tuned to fulfill the binding requirements for their cognate metals. However, most Cluster A-1 SBP bind to multiple divalent metal ions at least *in*

vitro. In Mn/Fe specific proteins, metal binding site comprises of 2 His, 1 Glu and 1 Asp, whereas, in Zn-specific proteins, 3 His and 1 Asp/Glu/water are known to be involved in metal coordination. Cluster A-I SBPs have evolved in terms of sequence and structure and therefore adopting different mechanisms of metal binding and release in order to cater special metal ion requirements of the bacteria. For example, in cyanobacteria *Synechocystis*, Mn^{2+} uptake is required in higher concentration for proper functioning of photosystem II. Synechocystis MntC (Syn-MntC), the high affinity Mn^{2+} binding proteins, contains disulfide bonds near metal binding site that are absent in all other bacterial Cluster A-I SBP. The reduction in disulfide bonds alters the metal binding affinity and it is proposed that oxidation and reduction state of disulfide bonds determines whether metal ions should be transported into the cytoplasm, or be available for photosystem II biogenesis in the periplasm [185]. Crystal structures of number of Cluster A-I SBP have been reported from various bacteria in metal-free and metal-bound states providing information about mechanism of metal binding and release. In Mn-specific proteins like *Streptococcus pneumonia* PsaA and *Staphylococcus aureus* MntC (Sau-MntC), the binding of metal ion is facilitated by slight movement in C-domain achieved due to backbone disruption in linker helix. These proteins may bind to both Mn^{2+} and Zn^{2+} with tetrahedral geometry; however, the binding is reversible for Mn^{2+} and irreversible for Zn^{2+} [76]. The reversible binding due to imperfect tetrahedral geometry for Mn^{2+} rather than ideal octahedral geometry facilitates the binding and delivery of Mn^{2+} to the cognate membrane permease. While satisfaction of ideal tetrahedral geometry is achieved when Zn^{2+} is bound and it irreversibly locks the protein in closed state. This forms the basis for molecular mechanism of Zn^{2+} toxicity in *Streptococcus pneumonia* which can be harnessed and exploited by host innate immunity system [38].

In Zn-specific proteins, the mechanism of metal binding and release is different from Mn-specific proteins where local rearrangements in secondary structure elements facilitates metal transport without any observed movement in the two domains. Thus irreversible interaction between these proteins with Zn^{2+} may be avoided in spite of the satisfaction of preferred tetrahedral geometry in most Zn-specific proteins. The binding residues are present in loop regions therefore different mechanism without involving domain movement might not lock protein in closed conformation.

Candidatus Liberibacter asiaticus (CLas) causes Huanglongbing in citrus plants, which presents a great challenge to the citrus industry throughout the world since it contributes for major economic loss worldwide by reducing the citrus production. The two gene clusters have been identified as homologues of *znu*ABC transporter in CLas. Vahling-Armstrong et al. have performed complementation assays to see ability of the two *znu*ABC homologues of CLas to restore partially-inactivated Znu systems in *Escherichia coli* and *Sinorhizobium meliloti*. The studies demonstrated that only genes from one of the two *znu*ABC clusters were able to functionally complement the system in these Δ*znu*ABC *E. coli* and Δ*znu*ABC *S. meliloti* [225].The ZnuA gene from second of the two gene clusters encodes for a periplasmic solute binding protein (CLas-ZnuA2), which show high homology to Mn/Fe-specific rather than Zn-specific proteins in Cluster A-I SBPs. It is not known whether the protein is involved in transport of Zn or other metals but possesses metal coordinating residues preferred for Mn/Fe-binding (2His, 1 Asp and 1 Glu).

In the present study, we have unraveled the unique mechanism of metal binding and release in CLas-ZnuA2 that is different from known employed mechanisms of other Mn-specific and Zn-specific proteins. The CLas-ZnuA2 has been diverged and evolved in terms of sequence thereby adopting a unique mechanism that might also be true for other related proteins. The study involves cloning and purification of CLas-ZnuA2 from *E. coli* cells along with bioinformatics analysis and biophysical, biochemical and structural characterization. Though CLas-ZnuA2 shares significant sequence and structural similarity with related proteins, the mechanism of metal binding and release in CLas-ZnuA2 may be completely different from Cluster A-I family metal transport proteins as observed by sequence and structural analysis.

4.2. Comparison of binding affinity of CLas-ZnuA2 with related Cluster A-I proteins

Comparison of binding affinity of CLas-ZnuA2 towards Mn^{2+} and Zn^{2+}, as shown by CD and SPR, with reported binding affinities of related Cluster A-I proteins revealed that CLas-ZnuA2 shows relatively lower binding affinity towards metal ions. The metal-saturation for crystallization also did not produce metal-bound states indicating lower binding affinity in consistent with CD and SPR data.

CD experiments indicated that thermal stability of CLas-ZnuA2 increases on binding of Mn^{2+} and Zn^{2+} at higher concentrations (1:10 or higher), whereas, lower concentration of Mn^{2+} and Zn^{2+} (1:1, 1:2 and 1:5) do not have any effect on thermal stability. Thermal stability assays (TSA) reported for PsaA showed metal ions increase the thermal stability of this protein at even 1:1 concentrations. Therefore CD results also indicated that CLas-ZnuA2 have relatively lower binding affinity than PsaA, as it requires higher concentrations of metal ions for binding.

SPR experiments were performed for determination of equilibrium constants (K_D) for Mn^{2+} and Zn^{2+} interactions. The estimation of kinetic rate constants and thereby equilibrium constants K_D by kinetic analysis did not fulfilled the quality assessment criteria set by manufacturers. Therefore steady state affinity experiments were performed to determine K_D values. The binding affinity was found to be slightly more for Mn^{2+} ($K_D=3.8\times10^{-4}$M) than Zn^{2+} ($K_D=4.4\times10^{-4}$ M). The reported K_D values of PsaA, Sau-MntC and Syn-ZnuA by isothermal titration calorimetry (ITC) are in nanomolar range (10^{-9} M) in all cases (Table 4.1) suggesting that CLas-ZnuA2 have relatively lower binding affinities towards metal ions as compared to related Cluster A-I proteins. The lower binding affinities were also quite evident from crystallization experiments where an intermediate state of metal-binding was captured in the presence of 1 mM $MnCl_2$ (protein : metal molar ratio of 1 : 3) and metal-bound state resulted only after soaking of the crystals in precipitant solution containing 50 mM $MnCl_2$/$ZnCl_2$, whereas, Mn/Zn-saturated protein by excessive dialysis did not retain the metal ion. However, in related Clusrer A-I structures, bound forms were obtained in native forms without any metal-saturation. These observations indicated that CLas-ZnuA2 has tendency towards relatively higher stability of CLas-ZnuA2 structure in metal-free state. The lower affinity might be the reason for the failure of this gene cluster in functional complementation assays as reported by Vahling-Armstrong et al.[225]

Table 4.1: Reported K_D values given by ITC experiments in related Cluster A-I proteins.

Protein	Organism	Metal ion	Reported K_D	Reference
MntC	*Staphylococcus aureus*	Mn^{2+}	4 nM	[76]
ZnuA	*Synechocystis* spp 6803	Zn^{2+}	7.3 nM	[234]
PsaA	*Strepotococcus pneumoniae*	Mn^{2+}	3.3 nM	[150]
		Zn^{2+}	2319 nM	[150]

4.3. Structural comparison revealed rigidity in CLas-ZnuA2 structure

Multiple sequence alignment of CLas-ZnuA2 with related Cluster A-I proteins present in NR and PDB database revealed the presence of conserved metal binding residues in all the sequences. The overall structure is similar to related Cluster A-I structures comprises of a pair of N and C-terminal $(\alpha/\beta)_4$ sandwich domains linked through a long rigid backbone α-helix. Superimposition of CLas-ZnuA2 with related structures showed that the two domains almost superimpose in all structures, however, the linker helix region did not superpose well due to curvature present in CLas-ZnuA2 linker helix (Figure 4.1).

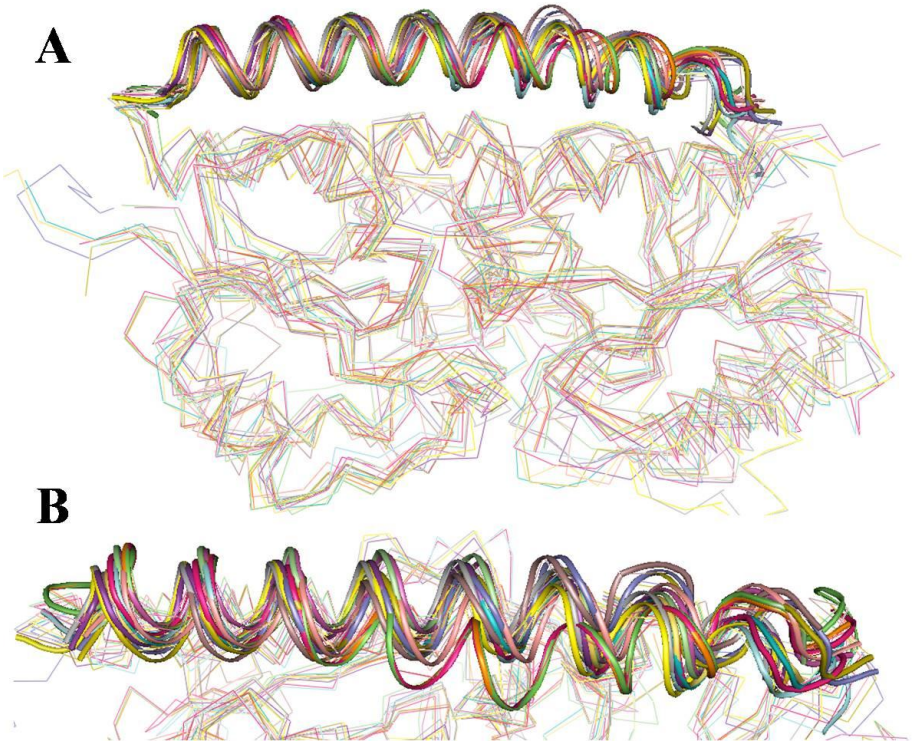

Figure 4.1: Superimposition of CLas-ZnuA2 with the related Cluster A-I structures available in PDB database. A) Overall structural superimposition showing N and C-domain in ribbons and linker helix in cartoon representation. **B)** Linker helix region. Metal-free, intermediate and metal-bound states of CLas-ZnuA2 are shown in orange, magenta and green respectively showing curve in linker helix.

The reason for this curvature in CLas-ZnuA2 is the presence of a proline residue (Pro153) within the linker helix due to which backbone H-bonding is disrupted. When the sequences were searched for the presence of corresponding Pro153 in other proteins, it is found

that none of the proteins available in PDB database (Group P), with known structures, possess this Pro residue in linker helix. However, Pro153 is found to be conserved among all the related proteins present in NR database (Group N) consistent with the fact that these proteins also share overall higher sequence identity than Group P. Although, no structural data is available for Group N proteins, the presence of conserved Pro153 among these proteins indicated towards their structural similarity and similar function, with Pro153 to play an important role in this group of proteins (Figure 4.2).

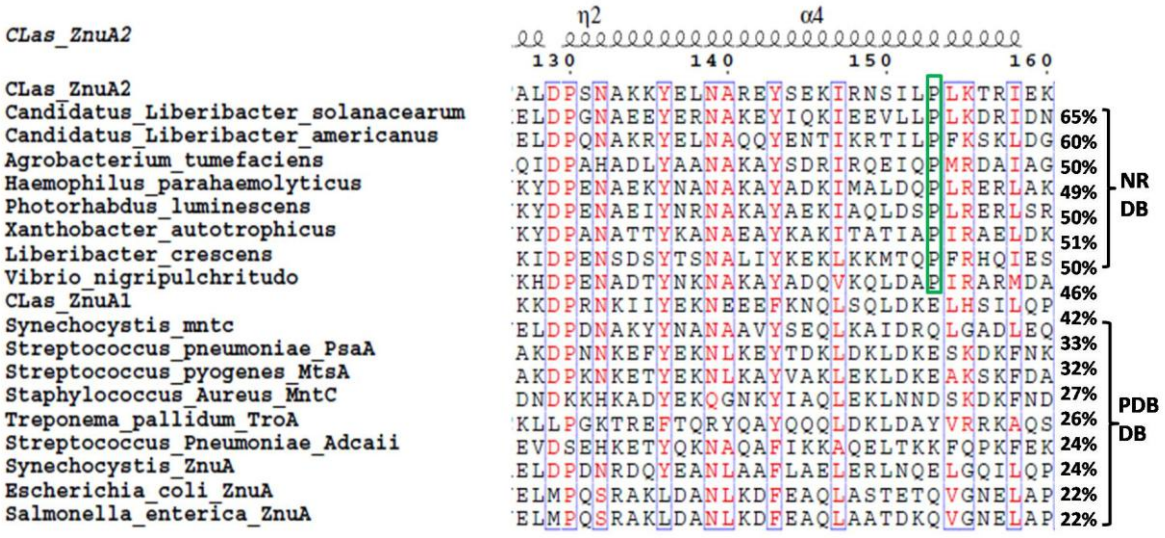

Figure 4.2: Multiple sequence alignment of linker helix region of CLas-ZnuA2 and related proteins present in PDB database and NR database. Green box encloses the conserved Pro153 among NR database proteins. From NR database, only one representative member is taken from each family. *Agrobacterium tumefaciens* from Rhizobiaceae, *Haemophilus parahaemolyticus* from Pasteurellaceae, *Photorhabdus luminescens* from Enterobacteriaceae, *Xanthobacter autotrophicus* from Xanthobacteraceae and *Vibrio nigripulchritudo* from Vibrionaceae.

Comparison of metal-binding and release mechanism of CLas-ZnuA2 (discussed in section 4.4) revealed that no domain movement is observed in CLas-ZnuA2 unlike that in the related Mn-specific proteins (PsaA and Sau-MntC). Thus Pro153 imparts rigidity to CLas-ZnuA2 structure fixing the two domains in the similar position in metal-free and bound states and therefore no movement during metal binding. The movement of domains is also not observed in Zn-specific proteins which involve different sets of metal-binding residues (3 His

and 1Asp/Glu/Water), however, the absence of Pro153 in these proteins do not provide curvature to linker helix.

4.4. Mechanism of metal binding and release

The available three-dimensional structures of cluster A-I SBPs, both in metal-free and metal-bound states, have revealed differences in the mechanism of metal binding and release. The differences in their mechanisms could be attributed to their sequence divergence to cater to subtle differences in their specificities in a particular system.

4.4.1. Mechanism of metal binding and release in CLas-ZnuA2

The present study revealed the unique mechanism of metal binding and release for CLas-ZnuA2 based on the analysis of crystal structure in metal-free, intermediate and metal-bound states. The analysis and comparison with related structures of cluster A-I SBPs revealed the unique features of CLas-ZnuA2 in terms of sequence and structure. The comparison of metal-free and bound states of CLas-ZnuA2 structure showed major conformational changes at the opening of metal binding cleft in N-domain on metal binding. The rest of the structure, including linker helix and C-domain, are unaltered except for minor conformational changes.

The metal-free state of CLas-ZnuA2 exhibited an open conformation where His39, one of the metal coordinating residues, present on L3 located at the opening of metal binding cleft in N-domain is displaced away from metal binding cleft with its side chain flipped out exposing the metal-binding site to solvent. To coordinate metal, not only side chain of His39 needs to flip inward towards metal but also a large inward shift of part of loop (around His39) is required to bring it within coordinating distance.

The metal binding resulted in closed conformation where a large inward displacement of His39 (~2.5 Å Cα displacement) is observed along with a part of L3 and its side chain flipping inside for metal coordination. The relative positions of three other metal coordinating residues almost remained the same with minor changes in side chain orientations.

The CLas-ZnuA2 structure in intermediate state of metal binding facilitated a glimpse into the transition from metal-free open to metal-bound closed conformation where loop L3 with unique features plays an important role. The L3 is a highly restrained, unlike other related

SBPs, due to a series of H-bond and salt bridge interactions. The L3 is stabilized by four interactions, which include H-bonds between Ser38 O^{γ} and Tyr68 OH (helix c), Tyr41 OH and Asp47 $O^{\delta 2}$ (helix b), Gln42 $N^{\varepsilon 2}$ and Tyr71 OH (helix c) and a salt bridge between Glu33 $O^{\varepsilon 2}$ and Lys50 N^{ζ} (helix b) (Figure 3.24). The H-bond between Tyr41 and Asp47 is conserved among most proteins of Cluster A-I family except PsaA where higher bond distance was observed [122]. Also, a conserved Trp residue instead of Tyr68 is present in most Cluster A-I family proteins, which makes H-bond interactions with main chain O atom of residues corresponding to amino acids 38 and 39 in the present structure. However, the absence of Pro residues, in contrast to other SBPs where one to four Pro residues are present in corresponding loop, imparts main-chain flexibility to L3 in CLas-ZnuA2 (Figure 4.3).

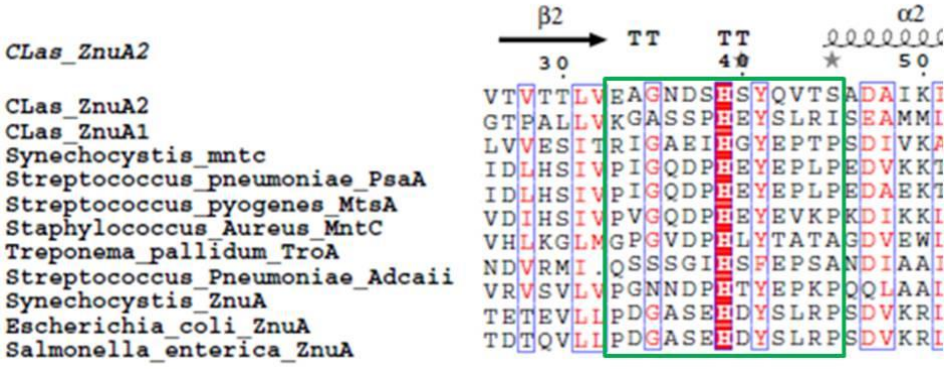

Figure 4.3: Distribution of Pro in related Cluster A-I proteins in L3 loop. CLas-ZnuA2 does not contain any Pro in L3 loop whereas other proteins have one-four Pro in L3.

An inward shift of Ser40 and flipping of His39 towards the metal binding site initiated the metal binding. The transition of L3 is quite evident from higher than average *B*-factors for side chains of His39 and Ser40, a break in electron density between His39 and Ser40 with indications for an inward flip of Ser40 (refined at half occupancy) into a weak difference Fourier electron density and partial occupancy for His39 (Figure 3.29). The inward shift of L3 results into sliding of Ser38 in reference to Tyr68 where a change in interaction between Ser38 and Tyr68 is observed. Ser38 shows two alternate conformations in metal-bound state where in one conformation Ser38 O^{γ} interacts with Tyr68 OH (helix c) with H-bond distance 3.45 Å that is much higher as compared to metal-free and intermediate states (~2.8 Å) while in second

conformation it interacts with Asp247 O (3.46 Å) (Figure 4.4). Also Ser38 main chain O interacts with Tyr68 OH and Leu64 O (helix c and L5, respectively).

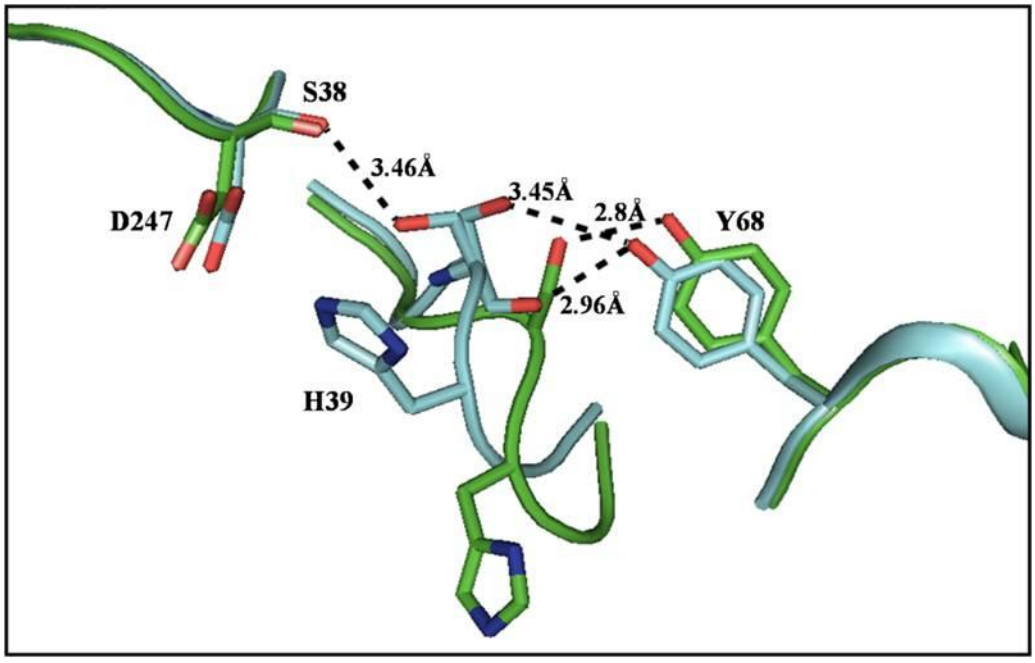

Figure 4.4: **Difference in position of His39 and Ser38 in metal-free (green) and Mn^{2+}-bound (cyan) states.** Ser38 side chain makes interaction with Tyr68 in metal-free state whereas it shows alternate conformation in metal-bound state. In one conformation it interacts with Tyr68 while in other conformation it interacts with Asp247. Additionally its main chain also interacts with Tyr68.

The transition from metal-free open to metal-bound closed state leads to the changes in interactions between:

(i) L7 and L5 (Glu102 and His63) where a high mobility of Glu102 is evident from broken and poorly defined electron density for side chain in only intermediate state. In PsaA, similar transition was observed where in metal-free PsaA, interaction is present between corresponding Glu136 and Asn91 but absent in metal bound PsaA.

(ii) L7 and helix e (Asn89 and Glu180) where water mediated interaction occurs in metal-free and with one of the alternate conformations of Glu180 in

intermediate and metal-bound state. Similar transition was observed in PsaA upon metal binding where in metal free form, Lys corresponding to Glu180 of helix e directly interacts with corresponding main chain of L7 and the interaction is lost in metal-bound state.

(iii) L5 and L3 (a water mediated interaction between coordinating residue His39 and Glu66) which is absent in the metal-bound closed state and,

(iv) The interaction between His63and Glu66 within L5 in only metal-bound state (Figure 4.5).

These interactions indicate towards subtle internal communications on transition. Almost similar results for corresponding interactions were reported for metal-free open and metal-bound closed forms of PsaA [38, 122].

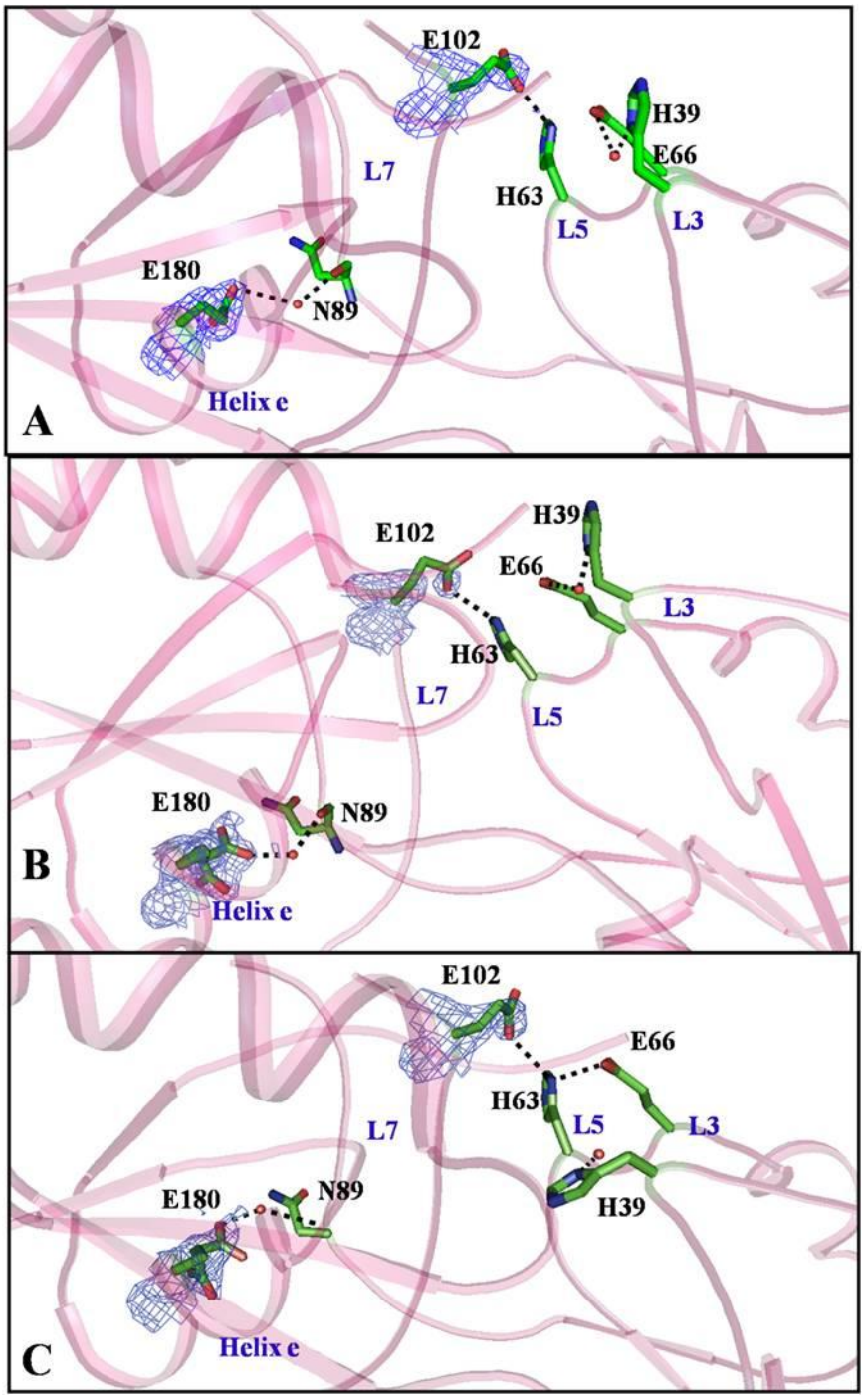

Figure 4.5: Interactions between L3, L5, L7 and helix e. A) metal-free state **B)** intermediate state and **C)** metal-bound state. Electron density around Glu102 and Glu180 is shown. Glu180 shows two alternate conformations in metal-bound and intermediate states and interacts with Asn89 mediated through water in all three states.

An important and interesting aspect, which certainly needs to be further investigated, is low binding affinity of CLas-ZnuA2 for metal and a possible role of restrained L3. The available crystal structures of Cluster A-I SBP crystallized in native forms are found to be in metal-bound states in all SBP unless the metal ion was removed by some chelating agent. This suggests that lower concentration of metal ions is sufficient to shift the equilibrium towards metal-bound states in these proteins. In contrast, in CLas-ZnuA2, metal bound states could be obtained only after soaking the crystals in presence of higher concentration of metal ions indicating metal-free state as the preferred state. The assumption of metal-free state being more stable is supported by the presence of high number of amino acid residues, particularly in L3, in alternate conformations in intermediate and metal-bound states as compared to metal-free state. One of the alternate conformations, which need a mention, is that of Glu180 present in intermediate and metal-bound states but not in metal-free state (Figure 4.5). This crucial water mediated interaction between Glu180 (helix e) and Asn89 (L7) in metal-free state is not completely disrupted as interaction is partly maintained through one of the alternate conformations in other two states. Also, Ser38 adopts two alternate conformations in Mn^{2+}-bound state (Figure 4.4). The above observations point towards a relative tendency of CLas-ZnuA2 structure to attain metal-free state.

4.4.2. Mechanism of metal binding and release in related Cluster A-I proteins

The mechanism of metal binding and release in CLas-ZnuA2 seems to be quite different from both Zn- and Mn-specific SBPs where metal-free and bound forms have been reported. Although flipping of side chain of His (corresponding to His39) inwards for metal binding has been observed for Sau-MntC and PsaA (Mn-specific SBPs), the relative position of coordinating His (C_α position) remains unchanged. Further, a rigid body movement of C-domain and partial unfolding of linker helix at its C-terminal is observed in PsaA and Sau-MntC, which is not observed in CLas-ZnuA2 on metal binding. The position of Glu172 (corresponding to metal binding residue Glu205 in PsaA) in CLas-ZnuA2 alters marginally (0.1 Å C_α displacement) on metal binding as opposed to a large displacement of corresponding residue (~2.4 Å) due to rigid body movement of PsaA C-domain (Figure 4.6). The soaking of metal did not disrupt the crystals in contrast to PsaA also suggest absence of large domain movement [38].

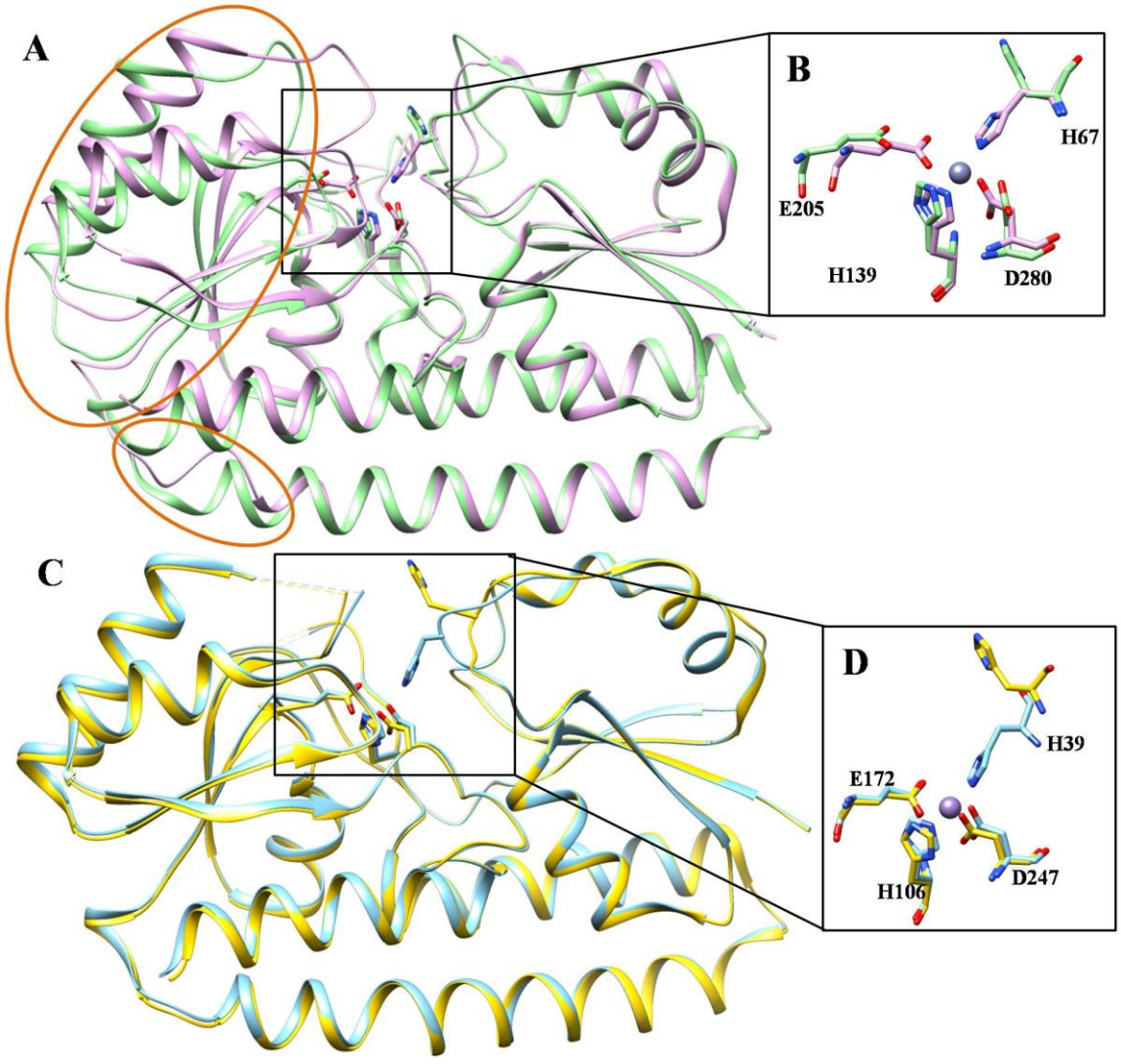

Figure 4.6: Comparison of metal-free and metal-bound states of PsaA and CLas-ZnuA2. A) Superimposition of N-domain of metal-free (green) and metal-bound (purple) states of PsaA showing rigid body movement of C-domain and unfolding of C-terminal linker helix (shown inside orange circles). **B)** Enlarged view of PsaA metal binding residues showing shift in position of Glu205 and side chain flipping of His67 and His139. **C)** Superimposition of N-domain of metal-free (yellow) and metal-bound (cyan) states of CLas-ZnuA2 with no observed rigid body domain movement and C-terminal linker helix unfolding as observed in PsaA. **D)** Enlarged view of metal CLas-ZnuA2 metal binding residues showing no shift in Glu172 position. Only His39 is flipped and moved away.

The metal binding and release in Zn-specific SBPs is largely accomplished through local conformational changes and like CLas-ZnuA2, does not involve any significant change in relative domain movements and the linker helix. However, a large displacement along with

inward flipping of His39 on L3 in N-domain on metal binding like in CLas-ZnuA2 is not observed in all the Zn-specific SBPs. In Syn-ZnuA [234], only flipping out of corresponding His is observed whereas in Ec-ZnuA the loop displacement is observed [240] (Figure 4.7). Therefore, overall mechanistic resemblance of CLas-ZnuA2 seems to be closer to the Zn-specific rather than Mn/Fe-specific SBPs of Cluster A-I family.

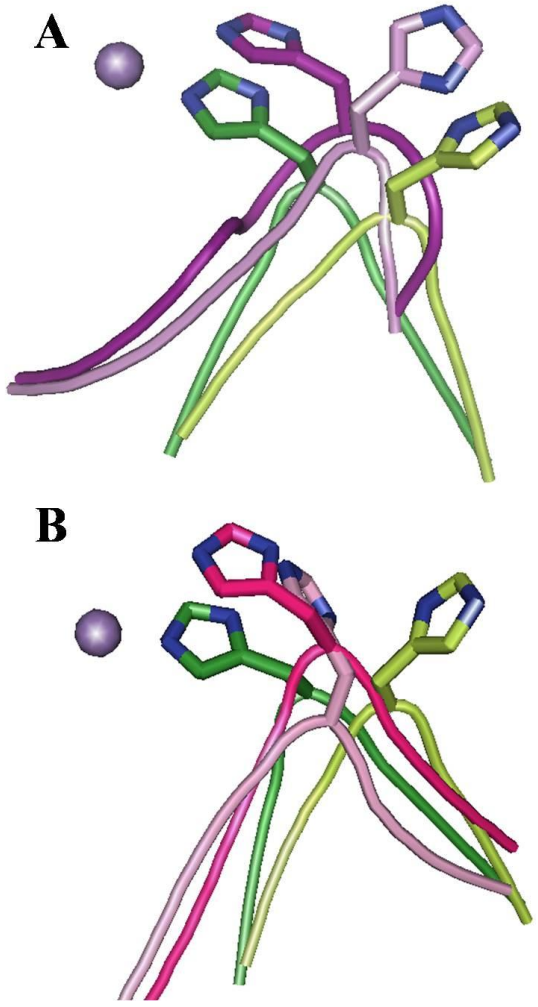

Figure 4.7 Comparison of position and side chain of His39 in Zn-specific proteins. A) Flipping out of His39 in metal-free state of CLas-ZnuA2 (light green) and Syn-ZnuA (light purple) was observed upon metal release from bound state (CLas-ZnuA2 dark green, Syn-ZnuA dark purple). **B)** Loop movement was observed in L3 hosting His39 towards metal upon metal binding in CLas-ZnuA2 (metal-free-light green, metal-bound-dark green) and Ec-ZnuA (metal-free-light pink, metal-bound-dark pink). Metal ion was shown in sphere bound to CLas-ZnuA2.

It should be noted that among Mn/Fe-specific SBPs, structures has been reported for PsaA and Sau-MntC in both metal-free and bound forms. The crystal structure of other Mn/Fe-specific SBPs in metal-free form, therefore, may reveal additional mechanistic differences. The absence of partial unfolding of linker helix at its C-terminal along with rigid body movement of C-domain in CLas-ZnuA2 could be attributed to the presence of Pro153 within the linker helix, which results in higher bending of linker helix towards C-terminal subtending an angle of ~26° as opposed to ~10° in most SBPs. Therefore, positioning of the C-domain of CLas-ZnuA2, in both metal-free and bound states, is similar to metal bound state of related SBPs. None of the related Cluster A-I SBPs with known structures possesses an internal Pro in linker helix. In addition, the curved linker helix in CLas-ZnuA2 is held together by making interactions at its two termini only with both domains. This is a unique example of sequence divergence to attain structure-function divergence in Cluster-AI SBPs.

The absence of partial unfolding has also been observed in case of Syn-MntC Mn-bound structure where one disulfide bond is present near metal binding site providing rigidity to the site. The disruption of disulfide bond decreases the affinity of the protein towards Mn^{2+}. However, the metal-free states have not been crystallized for Syn-MntC therefore the exact mechanism of metal binding and release is not known. It has been proposed that Syn-MntC is under tighter and varied control compared to other Cluster A-I SBP proteins with respect to metal binding and release owing to the absolute requirement of Mn^{2+} import for photosystem II activity together with the need to avoid alternative ion binding when Mn^{2+} concentrations are extremely low. In phylogenetic tree, this protein clusters with group consists of proteins containing Pro residue in linker helix region showing evolution of this group of proteins as rigid molecules which might imply a different mechanism of metal-binding and release than PsaA and Sau-MntC.

Multiple sequence alignment of CLas-ZnuA2 with the related sequences present in NR database revealed presence of conserved Pro in linker helix in all the sequences, and therefore, indicated its crucial role. It might be possible that this group of proteins having conserved Pro have been diverged both in sequence and in structure adopting a different mechanism of metal binding and release where domain movement is not required as in the case of other related Mn-binding proteins. However minor secondary structural changes are enough for facilitating metal uptake and release, as in the case of Zn-binding proteins.

4.5. Metal preference of CLas-ZnuA2 and other Cluster A-I proteins

Mn^{2+} ion normally exists in high spin state in biological systems, which is the ground state, energetically more stable with five unpaired electrons in d-orbital. The ionic radius of Mn^{2+} in high spin state (0.97 Å) is more than that in low spin state (0.81 Å; induced when more strong ligand is present). Zn^{2+} has no spin states with all paired d-orbital electrons with ionic radius of 0.88 Å. Thus ionic radius of Zn^{2+} is less than Mn^{2+} ion in high spin state. The metal-ligand distances also play a central role in metal discrimination in proteins. It is stated that native metal ions fulfill the best "fit" conditions in metalloproteins, and when substituted with an alien ion, their structures adopt different arrangements [117].

CLas-ZnuA2 metal binding cavity is compact (stabilized by primary and secondary shell interactions) and designed to fit Mn^{2+} ion with 1Asp, 1Glu, and 2His residues. However, Zn^{2+} with smaller ionic radius has better chance getting into the active site pocket. Zn^{2+} ion usually prefer tetrahedral geometry but octahedral geometry is also observed in some cases [51]. Mn^{2+} ion is most stabilized when coordinated by six ligands with octahedral geometry. However, in CLas-ZnuA2, both Mn^{2+} and Zn^{2+} ions are coordinated pentavalently with square pyramidal geometry therefore the preferred geometry is not achieved. Pentavalently coordinated Zn^{2+} is observed in some proteins but they are not stable because it creates strain in structure [51]. This strain is evident from more overall solvent accessibility surface area (SASA) for Zn^{2+} bound structure compared to metal-free and Mn^{2+} bound states (Zn^{2+}-bound > Apo >Mn^{2+}-bound; Table 3.12) indicating Zn^{2+}-bound state to be more opened than metal-free and Mn^{2+}-bound states. Zn^{2+}-bound structure also has more waters compared to metal-free and Mn^{2+}-bound structures. So less SASA in Mn^{2+}-bound structure indicated it is more compact compared to metal-free and Zn^{2+}-bound structure.

Analysis of coordination distances (Table 4.2) of other Mn-specific proteins shows that Mn^{2+} binding is achieved by imperfect tetrahedral coordination via two N and two O atoms (provided by 2 His, 1 Glu and 1 Asp) rather than stable octahedral coordination preferred by Mn^{2+}, thereby reversible binding, which facilitates the transport of Mn^{2+} ion. However, the similar coordinating atoms bind with Zn^{2+} perfectly with preferred tetrahedral geometry (in PsaA and Sau-MntC), thereby making stable interaction. For binding to Zn^{2+}, C- domain bends

more towards inside with greater distortion disrupting H-bonding of the linking helix, and locks up irreversibly with Zn^{2+} ion with preferred tetrahedral geometry.

Table 4.2: Metal coordination distances in Mn-specific available structures of Cluster A-I proteins. The values indicated by * represents the higher than ideal coordination distance.

Protein	Metal ion	Metal coordinating residues						Observed geometry
		His39	His106	Glu172		Asp247		
		NE2	NE2	OE1	OE2	OD1	OD2	
CLas-ZnuA2	Mn^{2+}	2.26	2.23	2.31*	2.19	2.22	2.18	Square pyramidal
	Zn^{2+}	2.08	2.07	2.51*	2.00	2.04	2.03	Square pyramidal
PsaA	Mn^{2+}	2.11	2.15	2.08	2.39*	2.43*	2.14	Tetrahedral
	Zn^{2+}	2.00	2.01	2.05	2.60*	2.03	2.84*	Tetrahedral
Sau-MntC	Mn^{2+}	2.05	2.07	2.28	2.77*	2.32*	2.22	Tetrahedral
	Zn^{2+}	2.05	2.10	2.56*	2.07	2.05	2.54*	Tetrahedral
MtsA	Fe	2.09	2.02	2.12	2.44*	2.79*	1.99	Tetrahedral
Syn-MntC	Mn^{2+}	2.17	1.87	2.28	2.42*	2.86*	1.93	Tetrahedral

In case of CLas-ZnuA2, both $Mn^{2+}$and Zn^{2+} are bound by pentavalent coordination, and thus square pyramidal geometry, which is different from preferred octahedral and tetrahedral geometry for Mn^{2+} and Zn^{2+} respectively. Therefore inability to bind both metal ions in preferred geometry might cause reversible binding for both the metal ions and thus it might be able to transport both metal ions. This might be a possible mechanism by which zinc toxicity could be avoided in CLas-ZnuA2 in higher mineral concentration environment of host plants. Therefore, although having coordinating residues for Mn^{2+} binding, the protein might have evolved to bind reversibly to Zn^{2+}, thereby, making the bacteria tolerable to zinc toxicity. Therefore reversible binding of Zn^{2+} to CLas-ZnuA2 does not block Mn^{2+} transport causing the bacteria to survive, in contrast to irreversible binding of Zn^{2+} to PsaA in *Streptococcus pneumoniae,* where direct inhibition of PsaA mediated Mn^{2+} transport by Zn^{2+} ions has been implicated as part of the host innate immune response against bacterial colonization. The assumption of binding and transport of Zn^{2+} is also in accordance with the mechanistic resemblence of CLas-ZnuA2 to Zn-specific proteins.

4.6. Push-pull hypothesis for metal binding specificity towards Mn^{2+} and Zn^{2+}

The comparison of metal binding site between Mn^{2+} and Zn^{2+}-bound structures as well with the metal-free structure revealed slight changes in the orientation of metal binding residues. Superimposition of all three states and observation around metal binding residues in the three states showed that Asp247 is slightly pulled towards metal in Zn^{2+}-bound state and pushed away in Mn^{2+}-bound state when compared to metal-free state. Similarly, other metal-binding residues (His106, Glu172 and Asp247) are closer to metal in Zn^{2+}-bound state compared to Mn^{2+}-bound state (Figure 4.8). In this structure, Glu172 is rigid and located in similar position in all states due to lack of C-domain movement, in contrast to other Mn-specific proteins, where it moves up to 2.4 Å towards metal upon metal binding. The movement of domains is inhibited due to the presence of Pro in linker helix. Rigidity in metal binding site is also maintained in Syn-MntC by a disulfide linkage near metal binding site, where partial unfolding of linker helix in Mn^{2+}-bound structure is not observed and Pro is absent within linker helix.

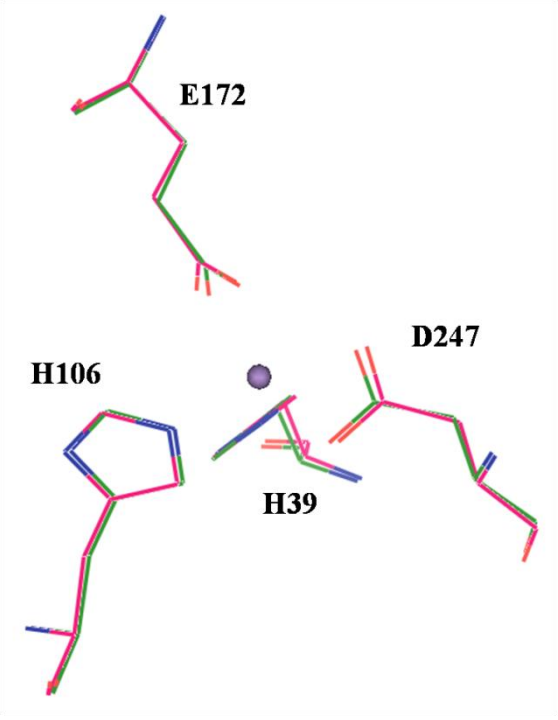

Figure 4.8: Comparison of position and orientation of metal-binding residues in Mn^{2+} and Zn^{2+}- bound states of CLas-ZnuA2. Metal-binding residues His106, Glu172 and Asp247 are closer to metal in Zn^{2+}-bound structure (green) compared to Mn^{2+}-bound structure (pink).

In CLas-ZnuA2, metal cavity is compact and the size is maintained by network of interactions between metal binding residues and secondary shell residues in all states. This cavity size could be slightly small for Mn^{2+} ions and slightly large for Zn^{2+} ions. Binding of Mn^{2+} ion in metal cavity changed the orientation of Asp247 by pushing it to small extent making space for proper accommodation. This also leads to interaction of Asp247 with Ser38 (in alternate conformation) as distance between them reduced <3.5Å favoring H-bonding. This stabilizes protein-Mn^{2+} coordination complex interaction. This reaction could be reversible when this interaction (Asp247and Ser38) is broken upon binding of CLas-ZnuA2 to permease for transport. When Zn^{2+} binds, due to its small size, the residues needs to stretch out to make coordination with the metal, as coordination distances are less than 2.1Å. So Zn^{2+} pulls Asp247 and His106 towards it, due to which interaction between Asp247 and Ser38 could not be established (distance >3.5 Å). This might be the reason for less stable binding of Zn^{2+}, as observed by slight lower binding affinity for Zn^{2+} than Mn^{2+} in SPR. Therefore Mn^{2+} might push the away and Zn^{2+} pulls the residues inside employing slightly different mechanisms for metal binding and stability.

In conclusion, CLas-ZnuA2 showed overall mechanistic resemblance to Zn-specific SBP, although metal coordinating residues are specific for Mn^{2+} binding. It binds to both Mn^{2+} and Zn^{2+} ions with lower binding affinity, and therefore, physiologically it might transport both Mn^{2+} and Zn^{2+} ions. So it might have been specifically evolved to avoid zinc-toxicity, unlike in PsaA mediated Zn^{2+} toxicity in *Streptococcus pneumonia*. The toxicity of zinc is avoided by modification of single residue in linker helix to Pro in sequence, thus making the two domains rigid, unlike other Mn-specifc SBPs where movement was observed upon metal binding. The lack of domain movement facilitates reversible binding achieved by imperfect geometry for both metal ions in CLas-ZnuA2 structure and therefore transport of both metal ions might be facilitated.

Chapter 4: Discussion

The present study aims on biophysical and structural characterization of a periplasmic solute binding protein component of second homologous ZnuABC transporter from *Candidatus* Liberibacter asiaticus (CLas-ZnuA2) which cause destructive citrus Huanlongbing disease in citrus plants, and thereby, providing directions for developing new control strategies. The symptoms of the disease mimic with those of zinc deficiency. The conclusions of the study are as follows:

- The bioinformatics analysis using similarity search showed significant similarity to Cluster A- I solute binding proteins (SBP) which are involved in uptake of divalent metal ions (Mn^{2+}, Fe^{2+} or Zn^{2+}). Multiple sequence alignment showed presence of four conserved residues His39, Hi106, Glu172 and Asp247 which are specific for Mn^{2+}/Fe^{2+} binding. Phylogenetic analysis also revealed that protein clusters with the Mn^{2+}/Fe^{2+} binding proteins. All these studies indicated towards the possible role of CLas-ZnuA2 in Mn^{2+}/Fe^{2+} uptake.

- Circular dichroism studies revealed that metal-bound states of CLas-ZnuA2 are thermally more stable than metal-free states. Also, binding of Mn^{2+} increased the thermal stability on increasing concentrations, whereas, Zn^{2+} binding stabilize the protein at relatively lower concentration, and increase in concentration has destabilizing effect on protein conformation.

- The steady state affinity analysis by SPR showed that CLas-ZnuA2 have almost equal order of affinity for Mn^{2+} and Zn^{2+} ions with slightly higher affinity for Mn^{2+}. However, affinity comparisons with related Cluster A-I SBP revealed that CLas-ZnuA2 has relatively lower binding affinity towards metal ions (Mn^{2+} and Zn^{2+}) than all the known Cluster A-I SBPs, for which binding affinity has been determined.

- Crystal structure analysis of CLas-ZnuA2 in metal-free, intermediate and metal bound states revealed that overall structure is similar to related Cluster A-I SBP comprising of a pair of N and C-terminal $(\alpha/\beta)_4$ sandwich domains linked

througha long rigid backbone α-helix running across two domains. Structural analysis also demonstrated a unique mechanism of metal binding quite different from both Zn-and Mn-specific SBPs. However, mechanistic resemblance of CLas-ZnuA2 seems to be closer to the Zn-specific rather than Mn/Fe-specific SBPs of cluster A-I family.

- The sequence and structure analysis revealed the unique features in terms of sequence divergence and structure like presence of curved linker helix in structure unlike related Cluster A-I SBP. The presence of Pro in linker helix caused disruption of backbone H-bonds resulting in curved helix.

- CLas-ZnuA2 structure has relative tendency to attain metal-free state as demonstrated by failure of obtaining metal-bound state after metal saturation, unlike other Cluster A-I SBP, which are reported to be in bound forms in native state.

- Analysis of metal coordination chemistry revealed that both Mn^{2+} and Zn^{2+} binds with similar square pyramidal geometry which is different from related Cluster A-I SBP where protein-metal coordination complex shows tetrahedral geometry in almost all cases. The deviation from ideal geometry of Mn^{2+} and Zn^{2+} binding with CLas-ZnuA2 and therefore suboptimal coordination might facilitate transport of both ions across membrane.

- Comparison of sequence and structural analysis with related Cluster A-I SBP indicated that CLas-ZnuA2 and some other significant similar proteins might have evolved in terms of sequence and structure in order to adopt unique mechanism of metal binding and might be able to facilitate transport of both Mn^{2+} and Zn^{2+}. This evolution through change in sequence and structure might be the basis for avoiding zinc susceptibility in the bacteria containing this group of proteins.

- In future, mutational studies might be performed in order to confirm the role of Pro153 (present in linker helix) on metal binding affinities of CLas-ZnuA2.

Structure based drug design might be performed by screening small molecules which can block metal binding site or some antibody fragments might also be screened for blocking the interaction of CLas-ZnuA2 with the cognate membrane permease and therefore inhibiting this ZnuABC mediated metal ion transport.

Conclusions

1. Abate, F., Malito, E., Cozzi, R., Surdo, P. L., Maione, D. and Bottomley, M. J. Apo, Zn^{2+}-bound and Mn^{2+}-bound structures reveal ligand-binding properties of SitA from the pathogen *Staphylococcus pseudintermedius*. *Biosci Rep* 34(6):743-758 (2014).

2. Adir, N., Rukhman, V., Brumshtein, B. and Anati, R. Preliminary X-ray crystallographic analysis of a soluble form of MntC, a periplasmic manganese-binding component of an ABC-type Mn transporter from *Synechocystis* sp. PCC 6803. *Acta Crystallogr D Biol Crystallogr* 58(9):1476-1478 (2002).

3. Ahuja, S., Rougé, L., Swem, D. L., Sudhamsu, J., Wu, P., Russell, S. J., Alexander, M. K., Tam, C., Nishiyama, M. and Starovasnik, M. A. Structural analysis of bacterial ABC transporter inhibition by an antibody fragment. *Structure* 23(4):713-723 (2015).

4. Albrecht, U. and Bowman, K. D. Gene expression in *Citrus sinensis* (L.) Osbeck following infection with the bacterial pathogen *Candidatus* Liberibacter asiaticus causing Huanglongbing in Florida. *Plant Sci* 175(3):291-306 (2008).

5. Ammendola, S., Pasquali, P., Pistoia, C., Petrucci, P., Petrarca, P., Rotilio, G. and Battistoni, A. High-affinity Zn^{2+} uptake system ZnuABC is required for bacterial zinc homeostasis in intracellular environments and contributes to the virulence of *Salmonella enterica*. *Infect Immun* 75(12):5867-5876 (2007).

6. Andreini, C., Bertini, I., Cavallaro, G., Holliday, G. L. and Thornton, J. M. Metal ions in biological catalysis: from enzyme databases to general principles. *J Biol Inorg Chem* 13(8):1205-1218 (2008).

7. Asana, R. The citrus dieback problem in relation to cultivation of citrus fruits in India. *Indian J Hort* 15:283-286 (1958).

8. Aubert, B. Citrus greening disease, a serious limiting factor for citriculture in Asia and Africa. *Proc Int Soc Citricul* 817-820 (1992).

9. Aubert, B. and Bové, J. Effect of penicillin or tetracycline injections of citrus trees affected by greening disease under field conditions in Reunion Island. *Proc 8th Conf IOCV* 103-108 (1980).

10. Aubert, B. and Quilici, S. Monitoring adult psyllas on yellow traps in Reunion Island. *Proc 10th Conf IOCV* 249-254 (1986).

11. Bajaj, M., Mamidyala, S. K., Zuegg, J., Begg, S. L., Ween, M. P., Luo, Z., Huang, J. X., McEwan, A. G., Kobe, B. and Paton, J. C. Discovery of novel Pneumococcal surface antigen A

(PsaA) inhibitors using a fragment-based drug design approach. *ACS Chem Biol* DOI: :10.1021/cb501032x (2015).

12. Banerjee, S., Wei, B., Bhattacharyya-Pakrasi, M., Pakrasi, H. B. and Smith, T. J. Structural determinants of metal specificity in the zinc transport protein ZnuA from *Synechocystis 6803*. *J Mol Biol* 333(5):1061-1069 (2003).

13. Basu, B. and Apte, S. K. A novel serralysin metalloprotease from *Deinococcus radiodurans*. *BBA-Proteins Proteom* 1784(9):1256-1264 (2008).

14. Bayle, L., Chimalapati, S., Schoehn, G., Brown, J., Vernet, T. and Durmort, C. Zinc uptake by *Streptococcus pneumoniae* depends on both AdcA and AdcAII and is essential for normal bacterial morphology and virulence. *Mol Microbiol* 82(4):904-916 (2011).

15. Begg, S. L., Eijkelkamp, B. A., Luo, Z., Couñago, R. M., Morey, J. R., Maher, M. J., Cheryl-lynn, Y. O., McEwan, A. G., Kobe, B. and O'Mara, M. L. Dysregulation of transition metal ion homeostasis is the molecular basis for cadmium toxicity in *Streptococcus pneumoniae*. *Nat Commun* 6:6418 (2015).

16. Belas, R., Manos, J. and Suvanasuthi, R. Proteus mirabilis ZapA metalloprotease degrades a broad spectrum of substrates, including antimicrobial peptides. *Infect Immun* 72(9):5159-5167 (2004).

17. Berntsson, R. P. A., Smits, S. H. J., Schmitt, L., Slotboom, D. J. and Poolman, B. A structural classification of substrate-binding proteins. *FEBS Lett* 584(12):2606-2617 (2010).

18. Bhagabati, K. Survey of greening disease of mandarin orange in the northeastern states of India. *Proc 12th Conf IOCV* 441-442 (1993).

19. Bhattacharyya, A., Stilwagen, S., Reznik, G., Feil, H., Feil, W. S., Anderson, I., Bernal, A., D'Souza, M., Ivanova, N. and Kapatral, V. Draft sequencing and comparative genomics of *Xylella fastidiosa* strains reveal novel biological insights. *Genome Res* 12(10):1556-1563 (2002).

20. Bonavia, E. The cultivated oranges and lemons of India and Ceylon. *WH Allen & Co, London* (1888).

21. Bora, H., Garg, S., Sen, P., Kumar, D., Kaur, P., Khan, R. H. and Sharma, Y. D. *Plasmodium vivax* tryptophan-rich antigen PvTRAg33. 5 contains alpha helical structure and multidomain architecture. *PLoS One* 6(1):e16294 (2011).

22. Bourret, T. J., Porwollik, S., McClelland, M., Zhao, R., Greco, T., Ischiropoulos, H. and Vázquez-Torres, A. Nitric oxide antagonizes the acid tolerance response that protects *Salmonella* against innate gastric defenses. *PLoS One* 3(3):e1833 (2008).

23. Bové, J., Bonnet, P., Garnier, M. and Aubert, B. Penicillin and tetracycline treatments of greening disease-affected citrus plants in the glasshouse, and the bacterial nature of the procaryote associated with greening. *Proc of 8th Conf IOCV* 91-102 (1980).

24. Bové, J. and Saglio, P. Stubborn and Greening: a review, 1969-1972. *Proc of 6th Conf IOCV* 1-11 (1974).

25. Bové, J. M. Huanglongbing: a destructive, newly-emerging, century-old disease of citrus. *J Plant Pathol* 88:7-37 (2006).

26. Campoy, S., Jara, M., Busquets, N., de Rozas, A. M. P., Badiola, I. and Barbé, J. Role of the high-affinity zinc uptake *znu*ABC system in *Salmonella enterica* serovar typhimurium virulence. *Infect Immun* 70(8):4721-4725 (2002).

27. Cannon, M. J., Papalia, G. A., Navratilova, I., Fisher, R. J., Roberts, L. R., Worthy, K. M., Stephen, A. G., Marchesini, G. R., Collins, E. J. and Casper, D. Comparative analyses of a small molecule/enzyme interaction by multiple users of Biacore technology. *Anal Biochem* 330(1):98-113 (2004).

28. Capoor, S. Decline of citrus trees in India. *Bull Nat Inst Sci India* 24:48-64 (1963).

29. Capoor, S., Rao, D. and Viswanath, S. *Diaphorina citri* Kuway., a vector of the greening disease of citrus in India. *Indian J Agric Sci* 37:572-576 (1967).

30. CCP4. The CCP4 suite: programs for protein crystallography. *Acta Crystallogr D Biol Crystallogr* 50(Pt 5):760-763 (1994).

31. Chandra, B. R., Yogavel, M. and Sharma, A. Structural analysis of ABC-family periplasmic zinc binding protein provides new insights into mechanism of ligand uptake and release. *J Mol Biol* 367(4):970-982 (2007).

32. Chen, M., Miyakawa, T. and Matsui, C. Citrus Likubin pathogens in salivary glands of *Diaphorina citri*. *Phytopathology* 63:194-195 (1973).

33. Chen, V. B., Arendall, W. B., Headd, J. J., Keedy, D. A., Immormino, R. M., Kapral, G. J., Murray, L. W., Richardson, J. S. and Richardson, D. C. MolProbity: all-atom structure validation for macromolecular crystallography. *Acta Crystallogr D Biol Crystallogr* 66(1):12-21 (2010).

34. Chin, E. L., Mishchuk, D. O., Breksa, A. P. and Slupsky, C. M. Metabolite signature of *Candidatus* Liberibacter asiaticus infection in two citrus varieties. *J Agric Food Chem* 62(28):6585-6591 (2014).

35. Claverys, J. P. A new family of high-affinity ABC manganese and zinc permeases. *Res Microbiol* 152(3):231-243 (2001).

36. Coleman, J. E. Zinc enzymes. *Curr Opin Chem Biol* 2(2):222-234 (1998).

37. Cotter, P., Chepuri, V., Gennis, R. and Gunsalus, R. Cytochrome o (cyoABCDE) and d (cydAB) oxidase gene expression in *Escherichia coli* is regulated by oxygen, pH, and the fnr gene product. *J bacteriol* 172(11):6333-6338 (1990).

38. Couñago, R. M., Ween, M. P., Begg, S. L., Bajaj, M., Zuegg, J., O'Mara, M. L., Cooper, M. A., McEwan, A. G., Paton, J. C. and Kobe, B. Imperfect coordination chemistry facilitates metal ion release in the Psa permease. *Nat Chem Biol* 10(1):35-41 (2014).

39. Davidson, A. L., Dassa, E., Orelle, C. and Chen, J. Structure, function, and evolution of bacterial ATP-binding cassette systems. *Microbiol Mol Biol Rev* 72(2):317-364 (2008).

40. DeLano, W. L. The PyMOL molecular graphics system San Carlos, CA: DeLano Scientific. (2002).

41. Deng, X., Lou, Z., Feng, Z., Li, H., Chen, J. and Civerolo, E. First Report of *'Candidatus* Liberibacter asiaticus' from *Atalantia buxifolia* in Guangdong, China. *Plant Dis* 92(2):314-314 (2008).

42. Deng, X., Zhou, G., Li, H., Chen, J. and Civerolo, E. L. Detection of *Candidatus* Liberibacter asiaticus from Wampee (*Clausena lansium* Skeels) by nested PCR. *Plant Health Prog* doi::10.1094/PHP-2007-0419-1001-BR (2007).

43. Desrosiers, D. C., Sun, Y. C., Zaidi, A. A., Eggers, C. H., Cox, D. L. and Radolf, J. D. The general transition metal (Tro) and Zn^{2+} (Znu) transporters in *Treponema pallidum*: analysis of metal specificities and expression profiles. *Mol Microbiol* 65(1):137-152 (2007).

44. DeVeaux, L. C. and Kadner, R. J. Transport of vitamin B12 in *Escherichia coli:* cloning of the btuCD region. *J bacteriol* 162(3):888-896 (1985).

45. Dhaked, R. K., Singh, M. K., Singh, P. and Gupta, P. Botulinum toxin Bioweapon & magic drug. *Indian J Med Res* 132(5):489 (2010).

46. Ding, F., Wang, G., Yi, G., Zhong, Y., Zeng, J. and Zhou, B. Infection of wampee and lemon by the citrus huanglongbing pathogen (*Candidatus* Liberibacter asiaticus) in China. *J Plant Pathol* 87:207-212 (2005).

47. Doeven, M. K., Abele, R., Tampé, R. and Poolman, B. The binding specificity of OppA determines the selectivity of the oligopeptide ATP-binding cassette transporter. *J Biol Chem* 279(31):32301-32307 (2004).

48. Doi, Y., Teranaka, M., Yora, K. and Asuyama, H. Mycoplasma-or PLT group-like microorganisms found in the phloem elements of plants infected with mulberry dwarf, potato witches' broom, aster yellows, or paulownia witches' broom. *Ann Phytopathol Soc Jpn* 33(4):259-266 (1967).

49. Duan, Y. P., Gottwald, T., Zhou, L. J. and Gabriel, D. W. First report of dodder transmission of '*Candidatus* Liberibacter asiaticus' to tomato *(Lycopersicon esculentum*). *Plant Dis* 92(5):831-831 (2008).

50. Duan, Y. P., Zhou, L., Hall, D. G., Li, W., Doddapaneni, H., Lin, H., Liu, L., Vahling, C. M., Gabriel, D. W. and Williams, K. P. Complete genome sequence of citrus huanglongbing bacterium '*Candidatus* Liberibacter asiaticus' obtained through metagenomics. *Mol Plant Microbe Interact* 22(8):1011-1020 (2009).

51. Dudev, T. and Lim, C. Tetrahedral vs octahedral zinc complexes with ligands of biological interest: A DFT/CDM study. *J Am Chem Soc* 122(45):11146-11153 (2000).

52. Dutta, D., Dutta, A., Bhattacharjee, A., Basak, A. and Das, A. K. Cloning, expression, crystallization and preliminary X-ray diffraction studies of staphylococcal superantigen-like protein 1 (SSL1). *Acta Crystallogr F Struct Biol Commun* 70(5):600-603 (2014).

53. Emsley, P. and Cowtan, K. Coot: model-building tools for molecular graphics. *Acta Crystallogr D Biol Crystallogr* 60(12):2126-2132 (2004).

54. Emsley, P., Lohkamp, B., Scott, W. G. and Cowtan, K. Features and development of Coot. *Acta Crystallogr D Biol Crystallogr* 66(4):486-501 (2010).

55. Fan, G. C., Cai, Z. J., Weng, Q. Y., Ke, C., Liu, B., Zhou, L. J. and Duan, Y. P. First report of a new host (*Pithecellobium lucidum* Benth) of the citrus huanglongbing bacterium, *Candidatus* Liberibacter asiaticus. *2nd Internatl Res Conf. Huanglonbing* (2011).

56. Fan, J., Chen, C., Brlansky, R. H., Gmitter Jr, F. and Li, Z. G. Changes in carbohydrate metabolism in *Citrus sinensis* infected with '*Candidatus* Liberibacter asiaticus'. *Plant Pathol* 59(6):1037-1043 (2010).

57. Fan, J., Chen, C., Yu, Q., Brlansky, R. H., Li, Z. G. and Gmitter, F. G. Comparative iTRAQ proteome and transcriptome analyses of sweet orange infected by "*Candidatus* Liberibacter asiaticus". *Physiol Plantarum* 143(3):235-245 (2011).

58. Fan, J., Chen, C., Yu, Q., Khalaf, A., Achor, D. S., Brlansky, R. H., Moore, G. A., Li, Z. G. and Gmitter Jr, F. G. Comparative transcriptional and anatomical analyses of tolerant rough lemon and susceptible sweet orange in response to '*Candidatus* Liberibacter asiaticus' infection. *Mol Plant Microbe Interact* 25(11):1396-1407 (2012).

59. Folimonova, S. Y., Robertson, C. J., Garnsey, S. M., Gowda, S. and Dawson, W. O. Examination of the responses of different genotypes of citrus to Huanglongbing (citrus greening) under different conditions. *Phytopathology* 99(12):1346-1354 (2009).

60. Fraser, L. and Singh, D. Citrus dieback in India-the contribution of greening virus. *Proc 4th Conf IOCV* 141-144 (1968).

61. Fraser, L., Singh, D., Capoor, S. and Nariani, T. Greening virus, the likely cause of citrus dieback in India. *FAO Plant Protect B Bull* 14(6):127-130 (1966).

62. Frolet, C., Beniazza, M., Roux, L., Gallet, B., Noirclerc-Savoye, M., Vernet, T. and Di Guilmi, A. M. New adhesin functions of surface-exposed pneumococcal proteins. *BMC Microbiol* 10(1):190 (2010).

63. Fujikawa, T. and Iwanami, T. Sensitive and robust detection of citrus greening (huanglongbing) bacterium "*Candidatus* Liberibacter asiaticus" by DNA amplification with new 16S rDNA-specific primers. *Mol Cell Probes* 26(5):194-197 (2012).

64. Gabbianelli, R., Scotti, R., Ammendola, S., Petrarca, P., Nicolini, L. and Battistoni, A. Role of ZnuABC and ZinT in *Escherichia coli* O157: H7 zinc acquisition and interaction with epithelial cells. *BMC Microbiol* 11(1):36 (2011).

65. Gahloth, D., Selvakumar, P., Shee, C., Kumar, P. and Sharma, A. K. Cloning, sequence analysis and crystal structure determination of a miraculin-like protein from *Murraya koenigii*. *Arch Biochem Biophys* 494(1):15-22 (2010).

66. Gangwar, S. P., Meena, S. R. and Saxena, A. K. Cloning, purification, crystallization and preliminary X-ray analysis of ESX-1-secreted protein regulator (EspR) from *Mycobacterium tuberculosis*. *Acta Crystallogr Sect F Struct Biol Cryst Commun* 67(1):83-86 (2010).

67. Garnier, M. and Bové, J. M. Transmission of the organism associated with citrus greening disease from sweet orange to periwinkle by dodder. *Phytopathology* 73(10):1358-1363 (1983).

68. Garnier, M., Danel, N. and Bové, J. Aetiology of citrus greening disease. *Ann Inst Pasteur Microbiol* 169-179 (1984).

69. Garnier, M., Danel, N. and Bové, J. The greening organism is a gram negative bacterium. *Proc 9th Conf IOCV* 115-124 (1984).

70. Garnier, M., Jagoueix-Eveillard, S., Cronje, P. R., Le Roux, H. F. and Bové, J. M. Genomic characterization of a liberibacter present in an ornamental rutaceous tree, *Calodendrum capense*, in the Western Cape Province of South Africa. Proposal of '*Candidatus* Liberibacter africanus subsp. capensis'. *Int J Syst Evol Microbiol* 50(6):2119-2125 (2000).

71. Garnier, M., Latrille, J. and Bové, J. *Spiroplasma citri* and the organism associated with likubin: comparison of their envelope systems. *Proc 7th Conf IOCV* 13-17 (1976).

72. Garnier, M., Martin-Gros, G. and Bové, J. M. Monoclonal antibodies against the bacterial-like organism associated with citrus greening disease. *Ann Inst Pasteur Microbiol* 639-650 (1987).

73. Gómez-Cadenas, A., Mehouachi, J., Tadeo, F. R., Primo-Millo, E. and Talon, M. Hormonal regulation of fruitlet abscission induced by carbohydrate shortage in citrus. *Planta* 210(4):636-643 (2000).

74. Gottwald, T. R. Current epidemiological understanding of citrus Huanglongbing. *Annu Rev Phytopathol* 48:119-139 (2010).

75. Gouaux, E. α-Hemolysin from *Staphylococcus aureus*: an archetype of β-barrel, channel-forming toxins. *J Struct Biol* 121(2):110-122 (1998).

76. Gribenko, A., Mosyak, L., Ghosh, S., Parris, K., Svenson, K., Moran, J., Chu, L., Li, S., Liu, T. and Woods, V. L. Three-dimensional structure and biophysical characterization of *Staphylococcus aureus* cell surface antigen-manganese transporter MntC. *J Mol Biol* 425(18):3429-3445 (2013).

77. Griffiths, E. and Williams, P. The Iron-Uptake Systems of Pathogenic Bacteria, Fungi, and Protozoa: John Wiley & Sons Chichester, UK (1999).

78. Guan, K. and Dixon, J. E. Protein tyrosine phosphatase activity of an essential virulence determinant in *Yersinia*. *Science* 249(4968):553-556 (1990).

79. Guarnieri, M. T., Blagg, B. S. and Zhao, R. A high-throughput TNP-ATP displacement assay for screening inhibitors of ATP-binding in bacterial histidine kinases. *Assay Drug Dev Technol* 9(2):174-183 (2011).

80. Guarnieri, M. T., Zhang, L., Shen, J. and Zhao, R. The Hsp90 inhibitor radicicol interacts with the ATP-binding pocket of bacterial sensor kinase PhoQ. *J Mol Biol* 379(1):82-93 (2008).

81. Gunasekera, T. S., Herre, A. H. and Crowder, M. W. Absence of ZnuABC-mediated zinc uptake affects virulence-associated phenotypes of uropathogenic *Escherichia coli* CFT073 under Zn (II)-depleted conditions. *FEMS Microbiol Lett* 300(1):36-41 (2009).

82. Gupta, P., Singh, M. K., Singh, P., Tiwari, M. and Dhaked, R. K. Antibodies against recombinant Shiga toxin subunit B neutralize Shiga toxin toxicity in HeLa cells. *Protein Pept Lett* 17(6):774-781 (2010).

83. Halbert, S. E. and Manjunath, K. L. Asian citrus psyllids (Sternorrhyncha: Psyllidae) and greening disease of citrus: a literature review and assessment of risk in Florida. *Fla Entomol* 87(3):330-353 (2004).

84. Handali, M., Neupane, D. P., Roychowdhury, H. and Yukl, E. T. Transcriptional regulation, metal binding properties and structure of Pden1597, an unusual Zn transport protein from *Paracoccus denitrificans*. *J Biol Chem* pii: jbc.M115.645853 (2015).

85. Harding, M. M. Small revisions to predicted distances around metal sites in proteins. *Acta Crystallogr D Biol Crystallogr* 62(6):678-682 (2006).

86. Hariprasad, G., Kaur, P., Srinivasan, A., Singh, T. P. and Kumar, M. Structural analysis of secretory phospholipase A2 from *Clonorchis sinensis*: therapeutic implications for hepatic fibrosis. *J Mol Model* 18(7):3139-3145 (2012).

87. Hartung, J. S., Paul, C., Achor, D. and Brlansky, R. Colonization of Dodder, *Cuscuta indecora*, by '*Candidatus* Liberibacter asiaticus' and '*Ca*. L. americanus'. *Phytopathology* 100(8):756-762 (2010).

88. Hartung, J. S., Shao, J. and Kuykendall, L. D. Comparison of the '*Ca*. Liberibacter asiaticus' genome adapted for an intracellular lifestyle with other members of the Rhizobiales. *PLoS One* 6(8):e23289 (2011).

89. Hazlett, K. R., Rusnak, F., Kehres, D. G., Bearden, S. W., La Vake, C. J., La Vake, M. E., Maguire, M. E., Perry, R. D. and Radolf, J. D. The *Treponema pallidum* tro operon encodes a multiple metal transporter, a zinc-dependent transcriptional repressor, and a semi-autonomously expressed phosphoglycerate mutase. *J Biol Chem* 278(23):20687-20694 (2003).

90. Higgins, C. F. ABC transporters: from microorganisms to man. *Annu Rev Cell Biol* 8(1):67-113 (1992).

91. Hocquellet, A., Bové, J.-M. and Garnier, M. Production and evaluation of non-radioactive probes for the detection of the two '*Candidatus* Liberobacter' species associated with citrus huanglongbing (greening). *Mol Cell Probes* 11(6):433-438 (1997).

92. Hollenstein, K., Frei, D. C. and Locher, K. P. Structure of an ABC transporter in complex with its binding protein. *Nature* 446(7132):213-216 (2007).

93. Horsburgh, M. J., Wharton, S. J., Cox, A. G., Ingham, E., Peacock, S. and Foster, S. J. MntR modulates expression of the PerR regulon and superoxide resistance in *Staphylococcus aureus* through control of manganese uptake. *Mol Microbiol* 44(5):1269-1286 (2002).

94. Hsiang, L. K. Yellow shoot of citrus. Symptomatology. Investigations in the cause of huanglongbing. Natural transmission and spread. General conclusions. *Acta Phytopatho Sinic* 2:1-42 (1956).

95. Hung, T. H., Wu, M. L. and Su, H. J. Identification of alternative hosts of the fastidious bacterium causing citrus greening disease. *J Phytopathol* 148(6):321-326 (2000).

96. Hung, T. H., Wu, M. L. and Su, H. J. Identification of the Chinese box orange (*Severinia buxifolia*) as an alternative host of the bacterium causing citrus huanglongbing. *Eur J Plant Pathol* 107(2):183-189 (2001).

97. Ilari, A., Alaleona, F., Petrarca, P., Battistoni, A. and Chiancone, E. The X-ray structure of the zinc transporter ZnuA from *Salmonella enterica* discloses a unique triad of zinc-coordinating histidines. *J Mol Biol* 409(4):630-641 (2011).

98. Islam, Z., Kumar, A., Singh, S., Salmon, L. and Karthikeyan, S. Structural basis for competitive inhibition of 3, 4-dihydroxy-2-butanone-4-phosphate synthase from *Vibrio cholerae*. *J Biol Chem* pii:jbc.M114.611830 (2015).

99. Jagoueix, S., Bove, J. m. and Garnier, M. The phloem-limited bacterium of greening disease of citrus is a member of the α subdivision of the Proteobacteria. *Int J Syst Bacteriol* 44(3):379-386 (1994).

100. Jagoueix, S., Bové, J. M. and Garnier, M. PCR detection of the two '*Candidatus*' liberobacter species associated with greening disease of citrus. *Mol Cell Probes* 10(1):43-50 (1996).

101. Janulczyk, R., Ricci, S. and Björck, L. MtsABC is important for manganese and iron transport, oxidative stress resistance, and virulence of *Streptococcus pyogenes*. *Infect Immun* 71(5):2656-2664 (2003).

102. Jones, P. and George, A. The ABC transporter structure and mechanism: perspectives on recent research. *Cell Mol Life Sci* 61(6):682-699 (2004).

103. Kaniga, K., Uralil, J., Bliska, J. B. and Galán, J. E. A secreted protein tyrosine phosphatase with modular effector domains in the bacterial pathogen *Salmonella typhimurlum*. *Mol Microbiol* 21(3):633-641 (1996).

104. Kanteev, M. and Adir, N. Arginine 116 stabilizes the entrance to the metal ion-binding site of the MntC protein. *Acta Crystallogr Sect F Struct Biol Cryst Commun* 69(3):237-242 (2013).

105. Karpowich, N., Martsinkevich, O., Millen, L., Yuan, Y.-R., Dai, P. L., MacVey, K., Thomas, P. J. and Hunt, J. F. Crystal structures of the MJ1267 ATP binding cassette reveal an induced-fit effect at the ATPase active site of an ABC transporter. *Structure* 9(7):571-586 (2001).

106. Kim, J. S., Sagaram, U. S., Burns, J. K., Li, J. L. and Wang, N. Response of sweet orange *(Citrus sinensis*) to '*Candidatus* Liberibacter asiaticus' infection: microscopy and microarray analyses. *Phytopathology* 99(1):50-57 (2009).

107. Kim, J. s. and Wang, N. Characterization of copy numbers of 16S rDNA and 16S rRNA of *Candidatus* Liberibacter asiaticus and the implication in detection in planta using quantitative PCR. *BMC Res Notes* 2(1):37 (2009).

108. Koh, E. J., Zhou, L., Williams, D. S., Park, J., Ding, N., Duan, Y. P. and Kang, B. H. Callose deposition in the phloem plasmodesmata and inhibition of phloem transport in citrus leaves infected with "*Candidatus* Liberibacter asiaticus". *Protoplasma* 249(3):687-697 (2012).

109. Koizumi, M., Prommintara, M., Linwattana, G. and Kaisuwan, T. Field evaluation of citrus cultivars for greening disease resistance in Thailand. *Proc 12th Conf IOCV* 274-279 (1993).

110. Konstantinidis, K. T., Ramette, A. and Tiedje, J. M. The bacterial species definition in the genomic era. *Philos Trans R Soc Lond B Biol Sci* 361(1475):1929-1940 (2006).

111. Korsten, L., Jagoueix, S., Bové, J. and Garnier, M. Huanglongbing (greening) detection in South Africa. *Proc 13th Conf IOCV* 395-398 (1996).

112. Koul, A., Choidas, A., Treder, M., Tyagi, A. K., Drlica, K., Singh, Y. and Ullrich, A. Cloning and characterization of secretory tyrosine phosphatases of *Mycobacterium tuberculosis*. *J bacteriol* 182(19):5425-5432 (2000).

113. Krissinel, E. and Henrick, K. Secondary-structure matching (SSM), a new tool for fast protein structure alignment in three dimensions. *Acta Crystallogr D Biol Crystallogr* 60(12):2256-2268 (2004).

114. Kube, M., Schneider, B., Kuhl, H., Dandekar, T., Heitmann, K., Migdoll, A. M., Reinhardt, R. and Seemüller, E. The linear chromosome of the plant-pathogenic mycoplasma '*Candidatus* Phytoplasma mali'. *BMC genomics* 9(1):306 (2008).

115. Kumar, P., Singh, M., Gautam, R. and Karthikeyan, S. Potential anti-bacterial drug target: Structural characterization of 3, 4-dihydroxy-2-butanone-4-phosphate synthase from *Salmonella typhimurium* LT2. *Proteins* 78(16):3292-3303 (2010).

116. Kumar, P., Singh, M. and Karthikeyan, S. Crystal structure analysis of icosahedral lumazine synthase from *Salmonella typhimurium*, an antibacterial drug target. *Acta Crystallogr D Biol Crystallogr* 67(2):131-139 (2011).

117. Kuppuraj, G., Dudev, M. and Lim, C. Factors Governing Metal-Ligand Distances and Coordination Geometries of Metal Complexes. *J Phys Chem B* 113(9):2952-2960 (2009).

118. Kuykendall, L. D., Shao, J. Y. and Hartung, J. S. '*Ca*. Liberibacter asiaticus' proteins orthologous with pSymA-encoded proteins of *Sinorhizobium meliloti*: hypothetical roles in plant host interaction. *PLoS One* 7(6):e38725 (2012).

119. Lafleche, D. and Bové, J. Mycoplasmes dans les agrumes atteints de "greening", de "stubborn" ou de maladies similaires. *Fruits* 25(6):455-465 (1970).

120. Lafleche, D. and Bové, J. Structures de type mycoplasme dans les feuilles d'orangers atteints de la maladie du greening. *CR Acad Sci Ser D* 270:455-465 (1970).

121. Laskowski, R. A., MacArthur, M. W., Moss, D. S. and Thornton, J. M. PROCHECK: a program to check the stereochemical quality of protein structures. *J Appl Crystallogr* 26(2):283-291 (1993).

122. Lawrence, M. C., Pilling, P. A., Epa, V. C., Berry, A. M., Ogunniyi, A. D. and Paton, J. C. The crystal structure of pneumococcal surface antigen PsaA reveals a metal-binding site and a novel structure for a putative ABC-type binding protein. *Structure* 6(12):1553-1561 (1998).

123. Lee, H. A. The relation of stocks to mottled leaf of citrus trees. *Philipp J Sci* 18:85-95 (1921).

124. Lee, Y. H., Deka, R. K., Norgard, M. V., Radolf, J. D. and Hasemann, C. A. *Treponema pallidum* TroA is a periplasmic zinc-binding protein with a helical backbone. *Nat Struct Mol Biol* 6(7):628-633 (1999).

125. Lee, Y. H., Dorwart, M. R., Hazlett, K. R., Deka, R. K., Norgard, M. V., Radolf, J. D. and Hasemann, C. A. The crystal structure of Zn (II)-free *Treponema pallidum* TroA, a

periplasmic metal-binding protein, reveals a closed conformation. *J bacteriol* 184(8):2300-2304 (2002).

126. Leonard, M. T., Fagen, J. R., Davis-Richardson, A. G., Davis, M. J. and Triplett, E. W. Complete genome sequence of *Liberibacter* crescens BT-1. *Stand Genomic Sci* 7(2):271-283 (2012).

127. Lewis, V. G., Ween, M. P. and McDevitt, C. A. The role of ATP-binding cassette transporters in bacterial pathogenicity. *Protoplasma* 249(4):919-942 (2012).

128. Li, H. and Jogl, G. Crystal structure of the zinc-binding transport protein ZnuA from *Escherichia coli* reveals an unexpected variation in metal coordination. *J Mol Biol* 368(5):1358-1366 (2007).

129. Li, W., Cong, Q., Pei, J., Kinch, L. N. and Grishin, N. V. The ABC transporters in *Candidatus* Liberibacter asiaticus. *Proteins* 80(11):2614-2628 (2012).

130. Li, W., Hartung, J. S. and Levy, L. Quantitative real-time PCR for detection and identification of *Candidatus* Liberibacter species associated with citrus huanglongbing. *J Microbiol Methods* 66(1):104-115 (2006).

131. Lim, K. H., Jones, C. E., vanden Hoven, R. N., Edwards, J. L., Falsetta, M. L., Apicella, M. A., Jennings, M. P. and McEwan, A. G. Metal binding specificity of the MntABC permease of *Neisseria gonorrhoeae* and its influence on bacterial growth and interaction with cervical epithelial cells. *Infect Immun* 76(8):3569-3576 (2008).

132. Lin, H., Chen, C., Doddapaneni, H., Duan, Y. P., Civerolo, E. L., Bai, X. and Zhao, X. A new diagnostic system for ultra-sensitive and specific detection and quantification of *Candidatus* Liberibacter asiaticus, the bacterium associated with citrus Huanglongbing. *J Microbiol Methods* 81(1):17-25 (2010).

133. Lin, H., Lou, B., Glynn, J. M., Doddapaneni, H., Civerolo, E. L., Chen, C., Duan, Y. P., Zhou, L. and Vahling, C. M. The complete genome sequence of '*Candidatus* Liberibacter solanacearum', the bacterium associated with potato zebra chip disease. *PLoS One* 6(4):e19135 (2011).

134. Linke, C., Caradoc-Davies, T. T., Proft, T. and Baker, E. N. Purification, crystallization and preliminary crystallographic analysis of *Streptococcus pyogenes* laminin-binding protein Lbp. *Acta Crystallogr Sect F Struct Biol Cryst Commun* 64(2):141-143 (2008).

135. Linke, C., Caradoc-Davies, T. T., Young, P. G., Proft, T. and Baker, E. N. The laminin-binding protein Lbp from *Streptococcus pyogenes* is a zinc receptor. *J bacteriol* 191(18):5814-5823 (2009).

136. Liu, R., Zhang, P., Pu, X., Xing, X., Chen, J. and Deng, X. Analysis of a prophage gene frequency revealed population variation of '*Candidatus* Liberibacter asiaticus' from two citrus-growing provinces in China. *Plant Dis* 95(4):431-435 (2011).

137. Locher, K. P. Structure and mechanism of ATP-binding cassette transporters. *Philos Trans R Soc Lond B Biol Sci* 364(1514):239-245 (2009).

138. Loisel, E., Jacquamet, L., Serre, L., Bauvois, C., Ferrer, J. L., Vernet, T., Di Guilmi, A. M. and Durmort, C. AdcAII, a new pneumococcal Zn-binding protein homologous with ABC transporters: biochemical and structural analysis. *J Mol Biol* 381(3):594-606 (2008).

139. Long, F., Vagin, A. A., Young, P. and Murshudov, G. N. BALBES: a molecular-replacement pipeline. *Acta Crystallogr D Biol Crystallogr* 64(1):125-132 (2008).

140. Lopes, S., Frare, G., Camargo, L., Wulff, N., Teixeira, D., Bassanezi, R., Beattie, G. and Ayres, A. Liberibacters associated with orange jasmine in Brazil: incidence in urban areas and relatedness to citrus liberibacters. *Plant Pathol* 59(6):1044-1053 (2010).

141. Lu, G., Westbrooks, J. M., Davidson, A. L. and Chen, J. ATP hydrolysis is required to reset the ATP-binding cassette dimer into the resting-state conformation. *Proc Natl Acad Sci U S A* 102(50):17969-17974 (2005).

142. M Counago, R., A McDevitt, C., P Ween, M. and Kobe, B. Prokaryotic substrate-binding proteins as targets for antimicrobial therapies. *Curr Drug Targets* 13(11):1400-1410 (2012).

143. Mafra, V., Martins, P. K., Francisco, C. S., Ribeiro-Alves, M., Freitas-Astúa, J. and Machado, M. A. *Candidatus* Liberibacter americanus induces significant reprogramming of the transcriptome of the susceptible citrus genotype. *BMC genomics* 14(1):247 (2013).

144. Mao, B., Pear, M., McCammon, J. and Quiocho, F. Hinge-bending in L-arabinose-binding protein. The "Venus's-flytrap" model. *J Biol Chem* 257(3):1131-1133 (1982).

145. Martinez, A. and Wallace, J. Citrus leaf mottle-yellows disease in the Philippines and transmission of the causal virus by a psyllid, *Diaphorina citri*. *Plant Dis Rep* 51(8):692-695 (1967).

146. Martinez, A. and Wallace, J. Studies on leaf-mottle-yellows disease of citrus in the Philippines. *Proc 4th Conf IOCV* 167-176 (1968).

147. McAllister, L. J., Tseng, H. J., Ogunniyi, A. D., Jennings, M. P., McEwan, A. G. and Paton, J. C. Molecular analysis of the psa permease complex of *Streptococcus pneumoniae*. *Mol Microbiol* 53(3):889-901 (2004).

148. McClean, A. and Oberholzer, P. Citrus psylla, a vector of the greening disease of sweet orange. *S Afr J Agr Sci* 8(1):297-298 (1965).

149. McClean, A. and Oberholzer, P. Greening disease of the sweet orange: evidence that it is caused by a transmissible virus. *S Afr J Agr Sci* 8(1):253-275 (1965).

150. McDevitt, C. A., Ogunniyi, A. D., Valkov, E., Lawrence, M. C., Kobe, B., McEwan, A. G. and Paton, J. C. A molecular mechanism for bacterial susceptibility to zinc. *PLoS Pathog* 7(11):e1002357 (2011).

151. Meena, S. R., Gangwar, S. P. and Saxena, A. K. Purification, crystallization and preliminary X-ray crystallographic analysis of the ATPase domain of human TAP in nucleotide-free and ADP-, vanadate-and azide-complexed forms. *Acta Crystallogr Sect F Struct Biol Cryst Commun* 68(6):655-658 (2012).

152. Mohammadi, T., van Dam, V., Sijbrandi, R., Vernet, T., Zapun, A., Bouhss, A., Diepeveen-de Bruin, M., Nguyen-Distèche, M., de Kruijff, B. and Breukink, E. Identification of FtsW as a transporter of lipid-linked cell wall precursors across the membrane. *EMBO J* 30(8):1425-1432 (2011).

153. Moll, J. and Martin, M. Electron microscope evidence that citrus psylla (*Trioza etytreae*) is a vector of greening disease in South Africa. *Phytophylactica* 5:41-44 (1973).

154. Moran, N. A. Microbial minimalism: genome reduction in bacterial pathogens. *Cell* 108(5):583-586 (2002).

155. Moran, N. A., McCutcheon, J. P. and Nakabachi, A. Genomics and evolution of heritable bacterial symbionts. *Annu Rev Genet* 42:165-190 (2008).

156. Morgan, J. K., Zhou, L., Li, W., Shatters, R. G., Keremane, M. and Duan, Y. P. Improved real-time PCR detection of '*Candidatus* Liberibacter asiaticus' from citrus and psyllid hosts by targeting the intragenic tandem-repeats of its prophage genes. *Mol Cell Probes* 26(2):90-98 (2012).

157. Moya, A., Peretó, J., Gil, R. and Latorre, A. Learning how to live together: genomic insights into prokaryote-animal symbioses. *Nat Rev Genet* 9(3):218-229 (2008).

158. Mukherjee, S., Dhar, R. and Das, A. K. Analyzing the catalytic mechanism of protein tyrosine phosphatase PtpB from *Staphylococcus aureus* through site-directed mutagenesis. *Int J Biol Macromol* 45(5):463-469 (2009).

159. Mukherjee, S., Saha, B. and Das, A. K. Differential chemical and thermal unfolding pattern of Rv3588c and Rv1284 of *Mycobacterium tuberculosis*-A comparison by fluorescence and circular dichroism spectroscopy. *Biophys Chem* 141(1):94-104 (2009).

160. Murray, R. and Schleifer, K. Taxonomic notes: a proposal for recording the properties of putative taxa of procaryotes. *Int J Syst Bacteriol* 44(1):174-176 (1994).

161. Murshudov, G. N., Vagin, A. A. and Dodson, E. J. Refinement of macromolecular structures by the maximum-likelihood method. *Acta Crystallogr D Biol Crystallogr* 53(3):240-255 (1997).

162. Nwugo, C. C., Lin, H., Duan, Y. P. and Civerolo, E. L. The effect of '*Candidatus* Liberibacter asiaticus' infection on the proteomic profiles and nutritional status of pre-symptomatic and symptomatic grapefruit (*Citrus paradisi*) plants. *BMC Plant Biol* 13(1):59 (2013).

163. Oberholzer, P., Von Standen, D. and Basson, W. Greening disease of sweet orange in South Africa. *Proc 3rd Conf IOCV* 213-219 (1965).

164. Okuda, M., Matsumoto, M., Tanaka, Y., Subandiyah, S. and Iwanami, T. Characterization of the tuf B-sec E-nus G-rpl KAJL-rpo B gene cluster of the citrus greening organism and detection by loop-mediated isothermal amplification. *Plant Dis* 89(7):705-711 (2005).

165. Oldham, M. L. and Chen, J. Crystal structure of the maltose transporter in a pretranslocation intermediate state. *Science* 332(6034):1202-1205 (2011).

166. Orelle, C., Ayvaz, T., Everly, R. M., Klug, C. S. and Davidson, A. L. Both maltose-binding protein and ATP are required for nucleotide-binding domain closure in the intact maltose ABC transporter. *Proc Natl Acad Sci U S A* 105(35):12837-12842 (2008).

167. Orozco-Cardenas, M. and Ryan, C. A. Hydrogen peroxide is generated systemically in plant leaves by wounding and systemin via the octadecanoid pathway. *Proc Natl Acad Sci U S A* 96(11):6553-6557 (1999).

168. Paik, S., Brown, A., Munro, C. L., Cornelissen, C. N. and Kitten, T. The sloABCR operon of *Streptococcus mutans* encodes an Mn and Fe transport system required for endocarditis virulence and its Mn-dependent repressor. *J bacteriol* 185(20):5967-5975 (2003).

169. Papp-Wallace, K. M. and Maguire, M. E. Manganese transport and the role of manganese in virulence. *Annu Rev Microbiol* 60:187-209 (2006).

170. Pazy, Y., Motaleb, M., Guarnieri, M., Charon, N., Zhao, R. and Silversmith, R. Identical phosphatase mechanisms achieved through distinct modes of binding phosphoprotein substrate. *Proc Natl Acad Sci U S A* 107(5):1924-1929 (2010).

171. Pazy, Y., Wollish, A. C., Thomas, S. A., Miller, P. J., Collins, E. J., Bourret, R. B. and Silversmith, R. E. Matching biochemical reaction kinetics to the timescales of life: structural determinants that influence the autodephosphorylation rate of response regulator proteins. *J Mol Biol* 392(5):1205-1220 (2009).

172. Permyakov, E. Metalloproteomics: John Wiley & Sons (2009).

173. Petersen, T. N., Brunak, S., von Heijne, G. and Nielsen, H. SignalP 4.0: discriminating signal peptides from transmembrane regions. *Nat methods* 8(10):785-786 (2011).

174. Pettersen, E. F., Goddard, T. D., Huang, C. C., Couch, G. S., Greenblatt, D. M., Meng, E. C. and Ferrin, T. E. UCSF Chimera-a visualization system for exploratory research and analysis. *J Comput Chem* 25(13):1605-1612 (2004).

175. Pinkett, H., Lee, A., Lum, P., Locher, K. and Rees, D. An inward-facing conformation of a putative metal-chelate-type ABC transporter. *Science* 315(5810):373-377 (2007).

176. Pugsley, A. P. The complete general secretory pathway in gram-negative bacteria. *Microbiol Rev* 57(1):50-108 (1993).

177. Quiocho, F. A. and Ledvina, P. S. Atomic structure and specificity of bacterial periplasmic receptors for active transport and chemotaxis: variation of common themes. *Mol Microbiol* 20(1):17-25 (1996).

178. Quiocho, F. A., Phillips, G. N., Parsons, R. G. and Hogg, R. W. Crystallographic data of an L-arabinose-binding protein from *Escherichia coli*. *J Mol Biol* 86(2):491-493 (1974).

179. Ramadugu, C., Manjunah, K., Halbert, S., Brlansky, R., Roose, M. and Lee, R. Characterization of huanglongbing associated '*Candidatus* Liberibacter asiaticus' from citrus relatives. *Phytopathology* 100:S107 (2010).

180. Rawal, M. K., Khan, M. F., Kapoor, K., Goyal, N., Sen, S., Saxena, A. K., Lynn, A. M., Tyndall, J. D., Monk, B. C. and Cannon, R. D. Insight into pleiotropic drug resistance ATP-binding cassette pump drug transport through mutagenesis of Cdr1p transmembrane domains. *J Biol Chem* 288(34):24480-24493 (2013).

181. Rice, C. W. and Hempfling, W. P. Oxygen-limited continuous culture and respiratory energy conservation in *Escherichia coli*. *J bacteriol* 134(1):115-124 (1978).

182. Roistacher, C. The economics of living with citrus diseases: huanglongbing (greening) in Thailand. *Proc 13th Conf IOCV* 279-285 (1996).

183. Rosales, R. and Burns, J. K. Phytohormone changes and carbohydrate status in sweet orange fruit from Huanglongbing-infected trees. *J Plant Growth Regul* 30(3):312-321 (2011).

184. Roychowdhury, A., Kundu, A., Bose, M., Gujar, A., Mukherjee, S. and Das, A. K. Complete catalytic cycle of cofactor-independent phosphoglycerate mutase involves a spring-loaded mechanism. *FEBS J* 282(6):1097–1110 (2015).

185. Rukhman, V., Anati, R., Melamed-Frank, M. and Adir, N. The MntC crystal structure suggests that import of Mn^{2+} in cyanobacteria is redox controlled. *J Mol Biol* 348(4):961-969 (2005).

186. Sabri, M., Houle, S. and Dozois, C. M. Roles of the extraintestinal pathogenic *Escherichia coli* ZnuACB and ZupT zinc transporters during urinary tract infection. *Infect Immun* 77(3):1155-1164 (2009).

187. Saglio, P., Lafleche, D., Bonissol, C. and Bove, J. Isolement culture et observation au microscope electronique des structures de type mycoplasme associees a la maladie du Stubborn des agrumes et leur comparaison avec les structures observees dans le cas de la maladie du Greening des agrumes. *Physiologie végétale* 9:569-582 (1971).

188. Saglio, P., Lhospital, M., Lafleche, D., Dupont, G., Bové, J., Tully, J. and Freundt, E. *Spiroplasma citri* gen. and sp. n.: a mycoplasma-like organism associated with “stubborn” disease of citrus. *Int J Syst Bacteriol* 23(3):191-204 (1973).

189. Salibe, A. and Cortez, R. Leaf mottling, a serious virus disease of citrus in the Philippines. *Proc 4th Conf IOCV* 131-136 (1968).

190. Saxena, A. K., Singh, K., Su, H. P., Klein, M. M., Stowers, A. W., Saul, A. J., Long, C. A. and Garboczi, D. N. The essential mosquito-stage P25 and P28 proteins from *Plasmodium* form tile-like triangular prisms. *Nat Struct Mol Biol* 13(1):90-91 (2006).

191. Schmidtchen, A., Frick, I. M., Andersson, E., Tapper, H. and Björck, L. Proteinases of common pathogenic bacteria degrade and inactivate the antibacterial peptide LL-37. *Mol Microbiol* 46(1):157-168 (2002).

192. Schneider, H. Anatomy of greening-diseased sweet orange shoots. *Phytopathology* 58(1):1155-1160 (1968).

193. Schreur, P. J. W., Rebel, J. M., Smits, M. A., van Putten, J. P. and Smith, H. E. TroA of *Streptococcus suis* is required for manganese acquisition and full virulence. *J bacteriol* 193(19):5073-5080 (2011).

194. Schwarz, R., Knorr, L. and Prommintara, M. Presence of citrus greening and its psylla vector in Thailand. *FAO Plant Protect B* 21:132-138 (1973).

195. Selvakumar, P., Gahloth, D., Tomar, P. P. S., Sharma, N. and Sharma, A. K. Molecular evolution of miraculin-like proteins in soybean kunitz super-family. *J Mol Evol* 73(5-6):369-379 (2011).

196. Selvakumar, P., Sharma, N., Tomar, P. P. S., Kumar, P. and Sharma, A. K. Structural insights into the aggregation behavior of *Murraya koenigii* miraculin-like protein below pH 7.5. *Proteins* 82(5):830-840 (2014).

197. Sette, A., Sidney, J., Livingston, B. D., Dzuris, J. L., Crimi, C., Walker, C. M., Southwood, S., Collins, E. J. and Hughes, A. L. Class I molecules with similar peptide-binding specificities are the result of both common ancestry and convergent evolution. *Immunogenetics* 54(12):830-841 (2003).

198. Sharma, N., Selvakumar, P., Bhose, S., Ghosh, D. K., Kumar, P. and Sharma, A. K. Crystal structure of a periplasmic solute binding protein in metal-free, intermediate and metal-bound states from *Candidatus* Liberibacter asiaticus. *J Struct Biol* 189(3):184-194 (2015).

199. Sharma, P., Dube, D., Singh, A., Mishra, B., Singh, N., Sinha, M., Dey, S., Kaur, P., Mitra, D. K. and Sharma, S. Structural basis of recognition of pathogen-associated molecular patterns and inhibition of proinflammatory cytokines by camel peptidoglycan recognition protein. *J Biol Chem* 286(18):16208-16217 (2011).

200. Sharma, P., Dube, D., Sinha, M., Mishra, B., Dey, S., Mal, G., Pathak, K. M., Kaur, P., Sharma, S. and Singh, T. P. Multiligand specificity of pathogen-associated molecular pattern-binding site in peptidoglycan recognition protein. *J Biol Chem* 286(36):31723-31730 (2011).

201. Shee, C., Islam, A., Ahmad, F. and Sharma, A. K. Structure-function studies of *Murraya koenigii* trypsin inhibitor revealed a stable core beta sheet structure surrounded by α-helices with a possible role for α-helix in inhibitory function. *Int J Biol Macromol* 41(4):410-414 (2007).

202. Shee, C. and Sharma, A. K. Purification and characterization of a trypsin inhibitor from seeds of *Murraya koenigii*. *J Enzyme Inhib Med Chem* 22(1):115-120 (2007).

203. Shrivastava, R. and Das, A. K. Temperature and urea induced conformational changes of the histidine kinases from *Mycobacterium tuberculosis*. *Int J Biol Macromol* 41(2):154-161 (2007).

204. Singh, M. K., Dhaked, R. K., Singh, P., Gupta, P. and Singh, L. Characterization of LC-HCC fusion protein of botulinum neurotoxin type A. *Protein Pept Lett* 18(3):295-304 (2011).

205. Slisz, A. M., Breksa III, A. P., Mishchuk, D. O., McCollum, G. and Slupsky, C. M. Metabolomic analysis of citrus infection by '*Candidatus* Liberibacter' reveals insight into pathogenicity. *J Proteome Res* 11(8):4223-4230 (2012).

206. Smith, D. W. Ionic hydration enthalpies. *J Chem Educ* 54(9):540 (1977).

207. Sticher, L., Mauch-Mani, B., Métraux and JP. Systemic acquired resistance. *Annu Rev Phytopathol* 35(1):235-270 (1997).

208. Stoebner, J. A. and Payne, S. M. Iron-regulated hemolysin production and utilization of heme and hemoglobin by *Vibrio cholerae*. *Infect Immun* 56(11):2891-2895 (1988).

209. Sun, X., Baker, H. M., Ge, R., Sun, H., He, Q. Y. and Baker, E. N. Crystal structure and metal binding properties of the lipoprotein MtsA, responsible for iron transport in *Streptococcus pyogenes*. *Biochemistry* 48(26):6184-6190 (2009).

210. Tamura, K., Stecher, G., Peterson, D., Filipski, A. and Kumar, S. MEGA6: molecular evolutionary genetics analysis version 6.0. *Mol Biol Evol* 30(12):2725-2729 (2013).

211. Tang, C., Schwieters, C. D. and Clore, G. M. Open-to-closed transition in apo maltose-binding protein observed by paramagnetic NMR. *Nature* 449(7165):1078-1082 (2007).

212. Tatineni, S., Sagaram, U. S., Gowda, S., Robertson, C. J., Dawson, W. O., Iwanami, T. and Wang, N. In planta distribution of '*Candidatus* Liberibacter asiaticus' as revealed by polymerase chain reaction (PCR) and real-time PCR. *Phytopathology* 98(5):592-599 (2008).

213. Teixeira, D. C., Saillard, C., Couture, C., Martins, E. C., Wulff, N. A., Eveillard-Jagoueix, S., Yamamoto, P. T., Ayres, A. J. and Bove, J. M. Distribution and quantification of *Candidatus* Liberibacter americanus, agent of huanglongbing disease of citrus in Sao Paulo State, Brasil, in leaves of an affected sweet orange tree as determined by PCR. *Mol Cell Probes* 22(3):139-150 (2008).

214. Tian, S., Lu, L., Labavitch, J. M., Webb, S. M., Yang, X., Brown, P. H. and He, Z. Spatial imaging of Zn and other elements in Huanglongbing-affected grapefruit by synchrotron-based micro X-ray fluorescence investigation. *J Exp Bot* 65(4):953-964 (2014).

215. Tirtawidjaja, S., Hadewidjaja, T. and Lasheen, A. Citrus vein phloem degeneration virus, a possible cause of citrus chlorosis in Java. *P Am Soc Hortic Sci* 235-243 (1965).

216. Trakhanov, S., Vyas, N. K., Luecke, H., Kristensen, D. M., Ma, J. and Quiocho, F. A. Ligand-free and-bound structures of the binding protein (LivJ) of the *Escherichia coli* ABC leucine/isoleucine/valine transport system: trajectory and dynamics of the interdomain rotation and ligand specificity. *Biochemistry* 44(17):6597-6608 (2005).

217. Trivedi, P., Sagaram, U. S., Kim, J. S., Brlansky, R. H., Rogers, M. E., Stelinski, L. L., Oswalt, C. and Wang, N. Quantification of viable *Candidatus* Liberibacter asiaticus in hosts using quantitative PCR with the aid of ethidium monoazide (EMA). *Eur J Plant Pathol* 124(4):553-563 (2009).

218. Trivedi, P. and Wang, N. Characterization of salicylate hydroxylase of "*Candidatus* Liberibacter asiaticus" and its role in plant defense suppression. *Phytopathology* 100(6):S127-S127 (2010).

219. Trivedi, P. and Wang, N. Modulation of plant defense responses by salicylate hydroxylase of '*Candidatus* Liberibacter asiaticus' and its implication on canker pathogen *Xanthomonas citri* subsp. citri in huanglongbing-infected plants. *Phytopathology* 102:S4 (2012).

220. Tsai, C. H., Hung, T. H. and Su, H. J. Strain identification and distribution of citrus Huanglongbing bacteria in Taiwan. *Bot Stud* 49:49-56 (2008).

221. Tsai, C. H., Su, H. J., Liao, Y. C. and Hung, T. H. First report of the causal agent of Huanglongbing "*Candidatus* Liberibacter asiaticus" infecting kumquat in Taiwan. *Plant Dis* 90(10):1360-1360 (2006).

222. Tsai, J. H. and Liu, Y. H. Biology of *Diaphorina citri* (Homoptera: Psyllidae) on four host plants. *J Econ Entomol* 93(6):1721-1725 (2000).

223. Tyler, H. L., Roesch, L. F., Gowda, S., Dawson, W. O. and Triplett, E. W. Confirmation of the sequence of '*Candidatus* Liberibacter asiaticus' and assessment of microbial diversity in Huanglongbing-infected citrus phloem using a metagenomic approach. *Mol Plant Microbe Interact* 22(12):1624-1634 (2009).

224. Vagin, A. and Teplyakov, A. MOLREP: an automated program for molecular replacement. *Journal of applied crystallography* 30(6):1022-1025 (1997).

225. Vahling-Armstrong, C. M., Zhou, H., Benyon, L., Morgan, J. K. and Duan, Y. P. Two plant bacteria, *S. meliloti* and *Ca.* Liberibacter asiaticus, share functional *znu*ABC homologues that encode for a high affinity zinc uptake system. *PLoS One* 7(5):e37340 (2012).

226. Vahling, C. M., Duan, Y. P. and Lin, H. Characterization of an ATP translocase identified in the destructive plant pathogen "*Candidatus* Liberibacter asiaticus". *J bacteriol* 192(3):834-840 (2010).

227. Van der Merwe, A. and Andersen, F. Chromium and manganese toxicity. Is it important in Transvaal citrus greening? *Farm S Afr* 12:439-440 (1937).

228. Van Loon, L., Bakker, P. and Pieterse, C. Systemic resistance induced by rhizosphere bacteria. *Annu Rev Phytopathol* 36(1):453-483 (1998).

229. Van Wees, S. and Glazebrook, J. Loss of non-host resistance of *Arabidopsis* NahG to *Pseudomonas syringae* pv. phaseolicola is due to degradation products of salicylic acid. *Plant J* 33(4):733-742 (2003).

230. Varma, A., Ahlawat, Y. S., Chakraborty, N. K., Garnier, M. and Bove, J. M. Detection of greening BLO by electron Microscopy, DNA hybridization in citrus leaves with and without mottle from various regions in India. *Proc 12th Conf IOCV* 280-285 (1993).

231. Vasudeva, R. and Capoor, S. Citrus decline in Bombay States. *FAO Plant Protect B* 6:91 (1958).

232. Walter, A. J., Hall, D. G. and Duan, Y. P. Low Incidence of '*Candidatus* Liberibacter asiaticus' in *Murraya paniculata* and Associated *Diaphorina citri*. *Plant Dis* 96(6):827-832 (2012).

233. Wang, N. and Trivedi, P. Citrus huanglongbing: a newly relevant disease presents unprecedented challenges. *Phytopathology* 103(7):652-665 (2013).

234. Wei, B., Randich, A. M., Bhattacharyya-Pakrasi, M., Pakrasi, H. B. and Smith, T. J. Possible regulatory role for the histidine-rich loop in the zinc transport protein, ZnuA. *Biochemistry* 46(30):8734-8743 (2007).

235. Wernegreen, J. J. Genome evolution in bacterial endosymbionts of insects. *Nat Rev Genet* 3(11):850-861 (2002).

236. Winkler, H. H. Rickettsial permeability. An ADP-ATP transport system. *J Biol Chem* 251(2):389-396 (1976).

237. Winn, M. D., Isupov, M. N. and Murshudov, G. N. Use of TLS parameters to model anisotropic displacements in macromolecular refinement. *Acta Crystallogr D Biol Crystallogr* 57(1):122-133 (2001).

238. Yamniuk, A. P. and Vogel, H. J. Structurally homologous binding of plant calmodulin isoforms to the calmodulin-binding domain of vacuolar calcium-ATPase. *J Biol Chem* 279(9):7698-7707 (2004).

239. Yan, Q., Sreedharan, A., Wei, S., Wang, J., Pelz-Stelinski, K., Folimonova, S. and Wang, N. Global gene expression changes in *Candidatus* Liberibacter asiaticus during the transmission in distinct hosts between plant and insect. *Mol Plant Pathol* 14(4):391-404 (2013).

240. Yatsunyk, L. A., Easton, J. A., Kim, L. R., Sugarbaker, S. A., Bennett, B., Breece, R. M., Vorontsov, I. I., Tierney, D. L., Crowder, M. W. and Rosenzweig, A. C. Structure and metal binding properties of ZnuA, a periplasmic zinc transporter from *Escherichia coli*. *J Biol Inorg Chem* 13(2):271-288 (2008).

241. Young, J. and Holland, I. B. ABC transporters: bacterial exporters-revisited five years on. *BBA-Biomembranes* 1461(2):177-200 (1999).

242. Zhang, M., Duan, Y. P., Zhou, L., Turechek, W. W., Stover, E. and Powell, C. A. Screening molecules for control of citrus huanglongbing using an optimized regeneration system for '*Candidatus* Liberibacter asiaticus'-infected periwinkle (*Catharanthus roseus*) cuttings. *Phytopathology* 100(3):239-245 (2010).

243. Zhang, M., Guo, Y., Powell, C. A., Doud, M. S., Yang, C. and Duan, Y. P. Effective antibiotics against '*Candidatus* Liberibacter asiaticus' in HLB-affected citrus plants identified via the graft-based evaluation. *PLoS One* 9(11):e111032 (2014).

244. Zhang, M., Powell, C. A., Zhou, L., He, Z., Stover, E. and Duan, Y. P. Chemical compounds effective against the citrus huanglongbing bacterium '*Candidatus* Liberibacter asiaticus' in planta. *Phytopathology* 101(9):1097-1103 (2011).

245. Zhang, S., Flores-Cruz, Z., Zhou, L., Kang, B. H., Fleites, L. A., Gooch, M. D., Wulff, N. A., Davis, M. J., Duan, Y. P. and Gabriel, D. W. '*Ca*. Liberibacter asiaticus' carries an excision plasmid prophage and a chromosomally integrated prophage that becomes lytic in plant infections. *Mol Plant Microbe Interact* 24(4):458-468 (2011).

246. Zhao, R., Collins, E. J., Bourret, R. B. and Silversmith, R. E. Structure and catalytic mechanism of the *E. coli* chemotaxis phosphatase CheZ. *Nat Struct Biol* 9(8):570-575 (2002).

247. Zheng, B., Zhang, Q., Gao, J., Han, H., Li, M., Zhang, J., Qi, J., Yan, J. and Gao, G. F. Insight into the interaction of metal ions with TroA from *Streptococcus suis*. *PLoS One* 6(5):e19510 (2011).

248. Zhou, L. J., Gabriel, D. W., Duan, Y. P., Halbert, S. E. and Dixon, W. N. First report of dodder transmission of huanglongbing from naturally infected *Murraya paniculata* to citrus. *Plant Dis* 91(2):227-227 (2007).

249. Zou, H., Gowda, S., Zhou, L., Hajeri, S., Chen, G. and Duan, Y. P. The destructive citrus pathogen, '*Candidatus* Liberibacter asiaticus' encodes a functional flagellin characteristic of a pathogen-associated molecular pattern. *PLoS One* 7(9):e46447 (2012).